

REPORT DOCUMENTATION PAGE				Form Approved OMB No. 0704-0188	
Public reporting burden for this collection of information is estimated to average 1 hour per response, including the time for reviewing instructions, searching existing data sources, gathering and maintaining the data needed, and completing and reviewing this collection of information. Send comments regarding this burden estimate or any other aspect of this collection of information, including suggestions for reducing this burden to Department of Defense, Washington Headquarters Services, Directorate for Information Operations and Reports (0704-0188), 1215 Jefferson Davis Highway, Suite 1204, Arlington, VA 22202-4302. Respondents should be aware that notwithstanding any other provision of law, no person shall be subject to any penalty for failing to comply with a collection of information if it does not display a currently valid OMB control number. PLEASE DO NOT RETURN YOUR FORM TO THE ABOVE ADDRESS.					
1. REPORT DATE (DD-MM-YYYY) 02-03-11		2. REPORT TYPE Technical Paper		3. DATES COVERED (From - To)	
4. TITLE AND SUBTITLE Temperature Effects on Electrospray Performance				5a. CONTRACT NUMBER	
				5b. GRANT NUMBER	
				5c. PROGRAM ELEMENT NUMBER	
6. AUTHOR(S) Nicholas Albert Kreitinger (AFRL/RZSS)				5d. PROJECT NUMBER	
				5f. WORK UNIT NUMBER 33SP0708	
7. PERFORMING ORGANIZATION NAME(S) AND ADDRESS(ES) Air Force Research Laboratory (AFMC) AFRL/RZSS 1 Ara Drive Edwards AFB CA 93524-7013				8. PERFORMING ORGANIZATION REPORT NUMBER AFRL-RZ-ED-TP-2011-051	
9. SPONSORING / MONITORING AGENCY NAME(S) AND ADDRESS(ES) Air Force Research Laboratory (AFMC) AFRL/RZS 5 Pollux Drive Edwards AFB CA 93524-7048				10. SPONSOR/MONITOR'S ACRONYM(S)	
				11. SPONSOR/MONITOR'S NUMBER(S) AFRL-RZ-ED-TP-2011-051	
12. DISTRIBUTION / AVAILABILITY STATEMENT Distribution A: Approved for public release; distribution unlimited (PA #10797).					
13. SUPPLEMENTARY NOTES Master's Thesis for Cal State Polytechnic Pomona. Includes written thesis and presentation.					
14. ABSTRACT Electrospray thrusters have been considered for the past 50 years; however, the low conductivity of and high volatility of liquids that were available resulted in thrusters that required too much power for them to be a viable propulsion option. The lack of micro-fabrication techniques also resulted in electrospray thrusters with a large inert mass fraction. These constraints have changed in recent times with the formulation and development of new, higher conductivity ionic liquids. Manufacturing processes have improved for micromechanical systems which allow wafers to be etched with features compact enough to generate reasonable thrust density. These developments have opened the possibility of having electrospray thrusters moving spacecraft. Electrosprays lend themselves to electric propulsion in two primary ways: Easily throttled thrust /specific impulse and high efficiency without charge accumulation. Ionic liquids have several properties that make them ideal for electrospray. These properties are the electrical conductivity, the surface tension coefficient, density, and dielectric constant. All of these are affected by temperature changes in various magnitudes and need to be studied to determine the effects this can have on a propulsion system. In this paper a model of an ionic liquid's properties vs. temperature is presented and predictions of the effects temperature will have on the performance of an electrospray thruster are calculated. Using literature on the relevant ionic liquids, a file will be read into a MATLAB®* script and a prediction will be generated to validate data collected in an laboratory experiment. This script can then be refined and used to design and optimize a thruster for space operation where the propellant temperature is balanced by the mission and energy requirements.					
15. SUBJECT TERMS					
16. SECURITY CLASSIFICATION OF:			17. LIMITATION OF ABSTRACT	18. NUMBER OF PAGES	19a. NAME OF RESPONSIBLE PERSON
a. REPORT	b. ABSTRACT	c. THIS PAGE			Dr. Daniel Brown
Unclassified	Unclassified	Unclassified	SAR	103	19b. TELEPHONE NUMBER (include area code) N/A

Temperature Effects on Electrospray Performance

An Independent Study Report

Presented to the

Faculty of

California State Polytechnic University, Pomona

In Partial Fulfillment

Of the Requirements for the Degree

Master of Science

In

Engineering

By

Nicholas Albert Kreitinger

March 2011

Aerospace Engineering?

Table of Contents

Abstract	1
List of Figures:	2
Introduction	4
Electrospray Modes	4
Modeling	10
Model Results	12
Experiment Setup	23
Experiment Results	25
Future Work	40
Summary and Conclusion	41
Bibliography	42
Appendices	43

Abstract

Electrospray thrusters have been considered for the past 50 years; however, the low conductivity of and high volatility of liquids that were available resulted in thrusters that required too much power for them to be a viable propulsion option. The lack of micro-fabrication techniques also resulted in electrospray thrusters with a large inert mass fraction. These constraints have changed in recent times with the formulation and development of new, higher conductivity ionic liquids. Manufacturing processes have improved for micromechanical systems which allow wafers to be etched with features compact enough to generate reasonable thrust density. These developments have opened the possibility of having electrospray thrusters moving spacecraft.

Electrosprays lend themselves to electric propulsion in two primary ways: Easily throttled thrust /specific impulse and high efficiency without charge accumulation. Ionic liquids have several properties that make them ideal for electrospray. These properties are the electrical conductivity, the surface tension coefficient, density, and dielectric constant. All of these are affected by temperature changes in various magnitudes and need to be studied to determine the effects this can have on a propulsion system.

In this paper a model of an ionic liquid's properties vs. temperature is presented and predictions of the effects temperature will have on the performance of an electrospray thruster are calculated. Using literature on the relevant ionic liquids, a file will be read into a MATLAB®* script and a prediction will be generated to validate data collected in an laboratory experiment. This script can then be refined and used to design and optimize a thruster for space operation where the propellant temperature is balanced by the mission and energy requirements.

* MATLAB® Version 7.7.0.471 (R2008b) is a registered trademark of The Mathworks, Inc., One Apple Hill, Natick, MA.

List of Figures:

Figure 1: Electrical force starts to exceed gravitational	7
Figure 2: Taylor cone is shorter, no droop visible, spray is scattering green laser light	7
Figure 3: Taylor cone is still shorter, straighter edges, spray scattering green laser light	8
Figure 4: Ion emission is now evident as purple glow	8
Figure 5: Really short cone off axis, ionization glow still visible	9
Figure 6: Surface Tension and Density vs Temperature	12
Figure 7: Electrical Conductivity vs Temperature	13
Figure 8: Isp vs Temperature	14
Figure 9: Thrust vs Temperature	14
Figure 10: Isp vs Flow rate at 500 V	15
Figure 11: Isp vs Flow rate at 10kV	16
Figure 12: Thrust vs Flow rate at 500V	17
Figure 13: Thrust vs Flow rate at 10kV	17
Figure 14: Isp vs Voltage at LQ	18
Figure 15: Isp vs Voltage at MQ	19
Figure 16: Thrust vs Voltage at LQ	20
Figure 17: Thrust vs Voltage at MQ	20
Figure 18: Current vs Temperature	21
Figure 19: Current vs Temperature	22
Figure 20: Current vs Flow rate	22
Figure 21: Electrospray experimental setup with needle, plate, and illumination lamp	24
Figure 22: Close up of needle, lamp, and extractor plate	24
Figure 23: Electrical diagram of experiment	25
Figure 24: 15 nL/min @ 22 °C, Positive Current	26
Figure 25: 15 nL/min @ 49 °C, Positive Current	27
Figure 26: 15 nL/min @ 22 °C, Positive Current Oscillations	27

Figure 27: 15 nL/min @ 22 °C, Negative Current	28
Figure 28: 15 nL/min @ 49 °C, Negative Current	28
Figure 29: 15 nL/min @ 22 °C, Negative Current	29
Figure 30: 15 nL/min @ 49 °C, Negative Current	29
Figure 31: 30 nL/min @ 22 °C, Positive Current	31
Figure 32: 30 nL/min @ 49 °C, Positive Current	31
Figure 33: 30 nL/min @ 22 °C, Negative Current	32
Figure 34: 30 nL/min @ 49 °C, Negative Current	32
Figure 35: 30 nL/min @ 22 °C, All Current	33
Figure 36: 30 nL/min @ 49 °C, All Current	33
Figure 37: 60 nL/min @ 22 °C, Positive Current	34
Figure 38: 60 nL/min @ 49 °C, Positive Current	34
Figure 39: 60 nL/min @ 22 °C, Negative Current	35
Figure 40: 60 nL/min @ 49 °C, Negative Current	35
Figure 41: 60 nL/min @ 22 °C, All Current	36
Figure 42: 60 nL/min @ 49 °C, All Current	36
Figure 43: Current vs Temperature	38
Figure 44: Current vs Temperature	38
Figure 45: Current vs Temperature	39
Figure 46: 15 nL/min @ 49 °C, Lamp turned off	40

Introduction

Electrospray thrusters as a form of propulsion have been theorized for over fifty years. Sir Greogory Ingram Taylor in 1964 first described the electrospray phenomena when a conductive liquid is placed in an electric field (Matthew S. Alexander, September–October 2007). In the 1960's and '70's research was performed and then stalled as an appropriate propellant was not available and the physics were not well understood (James A. Nabity, 2006). The required voltage, 10kV, and low electrical efficiency made other modes of propulsion more appealing (Jijun Xiong, 2006). Recently, ionic liquids with properties favorable to low voltage electrosprays in the range of 500V-5kV have been developed. These liquids have high electrical conductivity and low vapor pressure making space propulsion a possibility. Recent research has accelerated progress on ways to increase the propulsive efficiency means of electrosprays by means of characterizing the electrospray process more thoroughly and miniaturizing the size of each individual thruster. (James A. Nabity, 2006)

Electrospray modes

All materials respond to temperature changes, some go through rapid phase changes, while others transition states more gradually. Surface tension, density, electrical conductivity, and dielectric constant or static relative permittivity all change depending on the temperature. Ionic liquids properties tend to change steadily without sudden phase changes, though sometimes they can experience an order of magnitude change in the properties over the range of temperature of interest. Despite the lack of sudden phase transitions, these continuous changes can influence the electrospray to change modes or quit operating making it crucial to understand the effects of temperature on electrospray operation.

Electrospray operation occurs when a conductive liquid is placed within an electric field; the surface of the liquid deforms as its surface establishes electrical equilibrium with the applied perpendicular electric field. This deformation will form a cone-like structure called a Taylor cone that will vary in length and angle depending on the flow rate through the jet, the applied electric field, surface tension, and conductivity. The local electric field within the cone structure increases as the cone narrows, which results in a very high electric field at the tip of the Taylor cone. When the electric force is stronger than the surface tension charged droplets will separate from the tip and be electrostatically accelerated. Current is carried by these droplets and can be negative or positive depending on the electric field. Droplet emission occurs at lower field strength and when the field strength increases ionic emission can occur when the electric field reaches 1V/nm. (Mora, 2000)

Taylor cones can be formed wherever the liquid forms a bubble or surface features cause a distortion in the liquid surface that sharpens the local electric field. Externally wetted needles, porous emitters, and internally fed needles all can support Taylor cones but the surface geometry dictates how many Taylor cones can form within an area. This is important at higher efficiencies for as the Taylor cones become smaller more charge is carried by each droplet or by ionic emission.

Matching the correct emission material and emitter configuration to specific propulsion missions is very important. Externally wetted needles can perform similarly to capillary needles, but suffer propellant flow restrictions when put in an array. It is not simple for propellant to flow from the outside of an array to the inside with only surface tension forces. As a result, individual needles can stop emitting and the thrust density is degraded. Porous emitters do well covering the spectrum from operating in a single Taylor cone state to multiple cones attached at different

locations on the same surface as propellant can be pushed through the porous material to the emission sites. Internally fed needles can have easily controlled flow rate and with current MEMS technology can be manufactured with thousands in one square inch. Alignment of both externally and internally wetted needles to acceleration grids is sensitive to alignment errors and pressure changes can cause anomalies in the capillary flows. For this project internally fed needles were used in order to control the flow rate and due to the horizontal orientation of our test stand.

There are several modes that the Taylor cone can operate in. These modes are dependent on the flow rate and voltage that the emitter is operating at. Imagine starting a horizontal electrospray needle at a high propellant flow rate. Figures 1 through 5 illustrate how the emission mode changes as propellant flow goes from a high rate to a low or as acceleration potential goes from low to high. At high rate, before a Taylor cone can appear, the surface deforms and forms a knob-like extrusion. The knob will be held together by surface tension and thus resist the electric field. As the flow continues the knob expands until electric forces overcome the surface tension and the knob falls. The force of the applied electric field will still accelerate the drop toward the extractor grid even at higher flow rates. Electrical acceleration still works on a massive droplet with small charge, but it isn't as efficient.

When the flow rate is decreased or the voltage increased a Taylor cone forms although it isn't completely stable. Large droplets become detached in addition to the desired smaller drops, Figure 1.

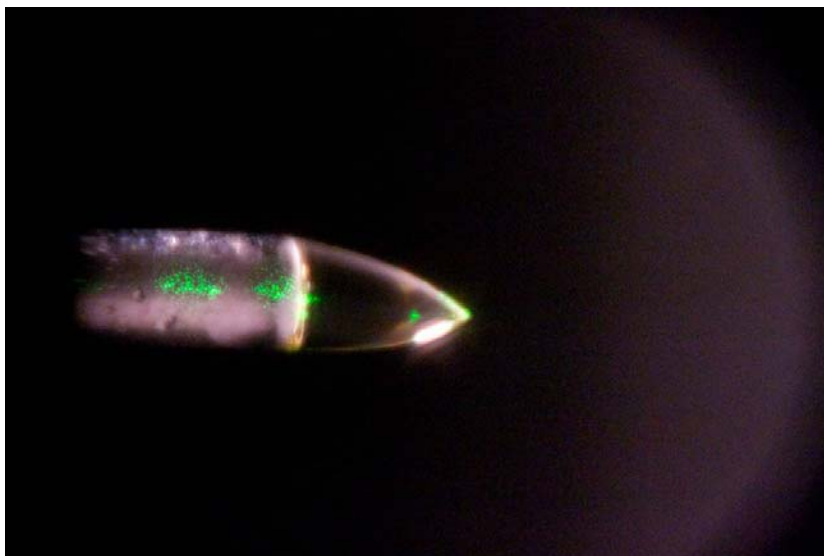


Figure 1: Electrical force starts to exceed gravitational. Note droop of Taylor cone.

As the voltage increases further the Taylor cone shortens and becomes stable. A jet can be seen with enough magnification and this is where the small droplets are generated.

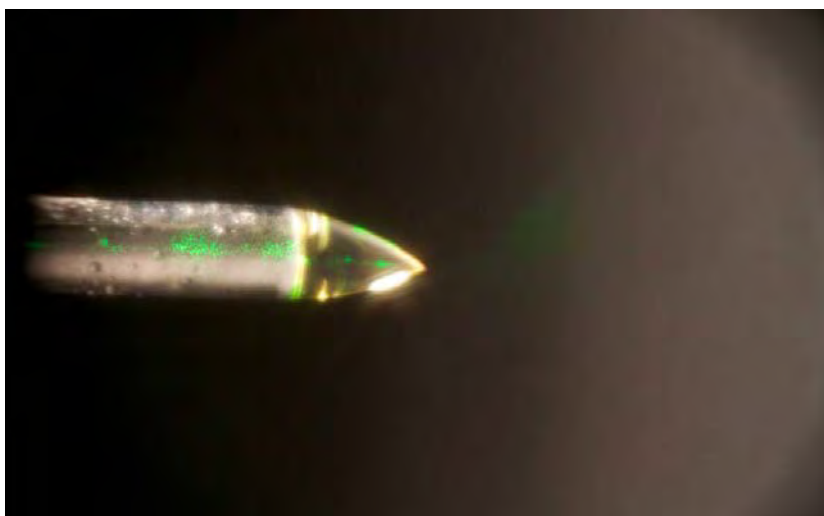


Figure 2: Taylor cone is shorter, no droop visible, spray of droplets is scattering green laser light.

Further increasing the voltage or decreasing the flow rate will cause the Taylor cone to shorten and resemble a right circular cone similar to Figure 3. The droplets should also be smaller than in Figure 2.



Figure 3: Taylor cone is still shorter, straighter edges, spray still visible as scattered green laser light.

An interesting phenomena occurs when the voltage is further increased but before multiple Taylor cones appear. The region in close proximity to the tip of the Taylor cone will begin to glow, Figure 4, which can be seen without illumination. This is believed to be ionization of the surrounding air by ions that are accelerated from the tip of the Taylor cone (Mora, 2000).



Figure 4: Ion emission is now evident as purple glow from ionization of air by energetic electro spray ions. Note that only green laser is on, incandescent illumination is off.

As the voltage is increased further, multiple Taylor cones will appear off the same emitter. In the case of a single needle two cones could form, one in the lower half and a smaller one in the upper, or many more with their bases spread equidistant around the needle's edge. More magnification would be needed to see multiple needles in this series of photos.

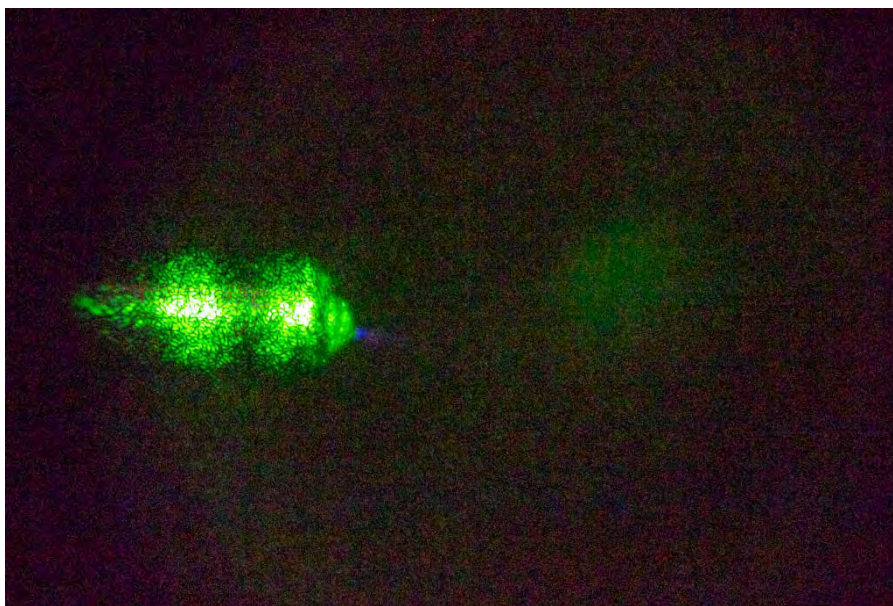


Figure 5: Really short cone off axis, ionization glow still visible.

Rough surface features lend to multiple Taylor cone formations at the rim of the needle or anywhere liquid adheres to the exterior as they cause deformations in the surface of the liquid. Multiple Taylor cones are usually undesirable as they jettison droplets in off-axis directions and may impact the extractor plate if used. If further acceleration is required to keep droplet acceleration vectors aligned then the voltage can be lowered and a second extractor plate or acceleration grid can be used to further accelerate the droplets in the desired direction.

Modeling:

Two performance characteristics that describe a space propulsion system are the specific impulse and thrust which, for an electrospray, are given by the following equations:

$$I_{sp} = \frac{1}{g} \sqrt{2 \frac{q}{m} V_a} \quad \text{Equation 1}$$

$$T = \dot{m} u_e = g \dot{m} I_{sp} \quad (\text{James A. Nabity, 2006}) \quad \text{Equation 2}$$

where g is the acceleration due to gravity at Earth's surface, q/m is the charge-to-mass ratio of the droplets, V_a is the acceleration voltage, \dot{m} is the mass flow rate, and u_e is the exit velocity of the droplets. The droplet charge was assumed to be close to the Rayleigh limit for a spherical droplet:

$$q = 8\pi \sqrt{\epsilon_0 \gamma} R^3 \quad (\text{Cole, 2000}) \quad \text{Equation 3}$$

$$\begin{aligned} m &= \rho V \\ V &= \frac{4}{3} \pi \left(\frac{D}{2} \right)^3 \\ \frac{q}{m} &= \frac{12\sqrt{2}}{\rho} \sqrt{\frac{\epsilon_0 \gamma}{D^3}} \end{aligned} \quad \text{Equation 4}$$

where ϵ_0 is the permittivity of vacuum, γ is the surface tension coefficient of the liquid, V is the volume of a sphere, r the radius of the sphere, and ρ is the density of the liquid. The diameter of the droplets is dependent on the radius of curvature in the region of maximum electric force, R_K as is given in the following equations:

$$\begin{aligned} R_K &= \sqrt[3]{\frac{\epsilon_0 Q}{K}} \quad (\text{W.D. Luedtke, 2008}), (\text{Mora, 2000}) \\ D &\leq 3.3 R_K \end{aligned} \quad \text{Equation 5}$$

where Q is the flow rate through the region of maximum electric force and K is the conductivity of the liquid. There is a physical limit to the flow rate below which a Taylor cone will not form.

The following equation gives us the minimum flow rate:

$$Q_{\min} = \frac{\gamma \kappa \varepsilon_0}{\rho K} \quad (\text{Matthew S. Alexander, September–October 2007}) \quad \text{Equation 6}$$

where κ is the dielectric constant for the liquid.

These equations allow us to predict specific impulse and thrust for an electrospray thruster and were written into several MATLAB® programs and functions which are included in Appendix A.

The model was arranged to run through all data points with respect to temperature, flow rate, and voltage. The only true independent variable was the voltage which could be set apart from the other two variables. Voltage was set to cover the range of 500 V to 20 kV. The minimum flow rate is dependent on all the variables affected by temperature; therefore temperature was set first, then the flow rate calculated. This resulted in a three-loop program that would set the temperature, set a flow rate, and loop through all the voltages last. MATLAB® doesn't allow 3X3 matrix rows or columns to be plotted directly in a command prompt, thus a separate Plot script was used to output the data in graphs.

1-methyl-3-butylimidazolium tetrafluoroborate ([BMIM][BF₄]) was chosen because of its prevalence in the electrospray literature, its high electrical conductivity, and the availability of data (TRC/NIST/Boulder, 2006). This ionic liquid was also readily available from several suppliers. Several sources of property vs. temperature data were referenced and plotted in Excel. Data that fell significantly outside the general curve or had a higher degree of uncertainty were discarded. This resulted in two equations being generated for the behavior of the density and surface tension coefficient over the range of 250–480 K. The electrical conductivity data was

filtered in the same way, but that data was not linear so MATLAB® was used instead to interpolate between all available data points.

Model Results

Figure 6 and Figure 7 show the changes that occur in the surface tension, density, and electrical conductivity for BMIM BF₄. These data sets are normalized with respect to the value at 250 K. The trends seen are consistent with typical liquids; as the temperature increases the density decreases due to expansion. Surface tension also decreases. The same temperature increase also results in an electrical conductivity increase as more ions are free to move and exchange charges. As a result, we will expect a broad range of values for any variable that is dependent on the electrical conductivity and this dependency will drive our model development.

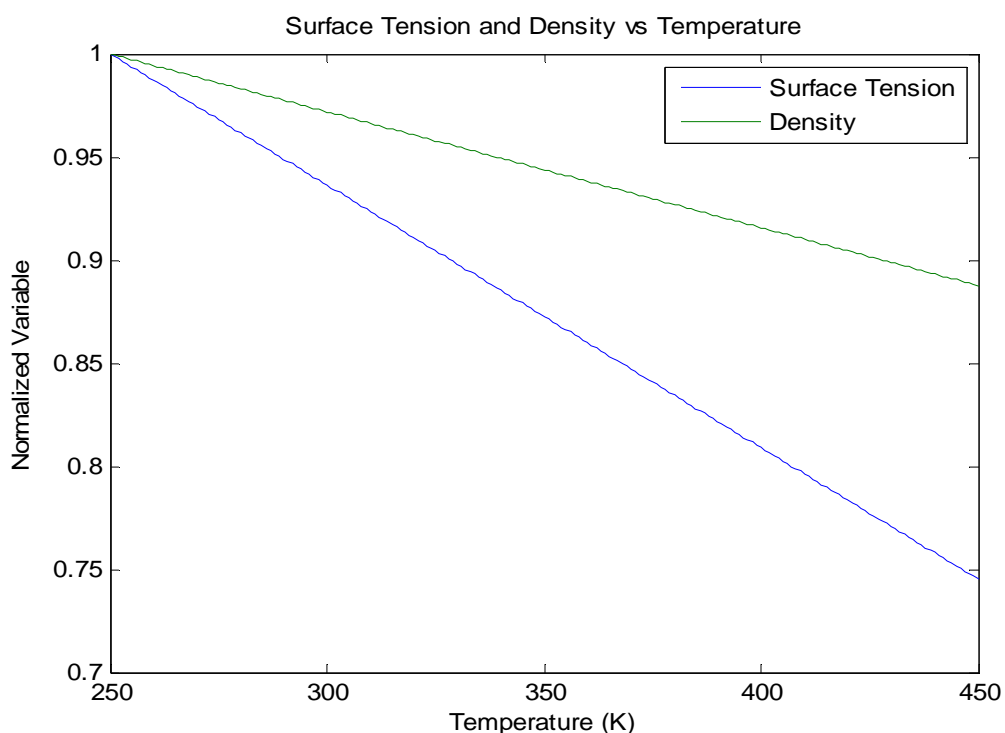


Figure 6

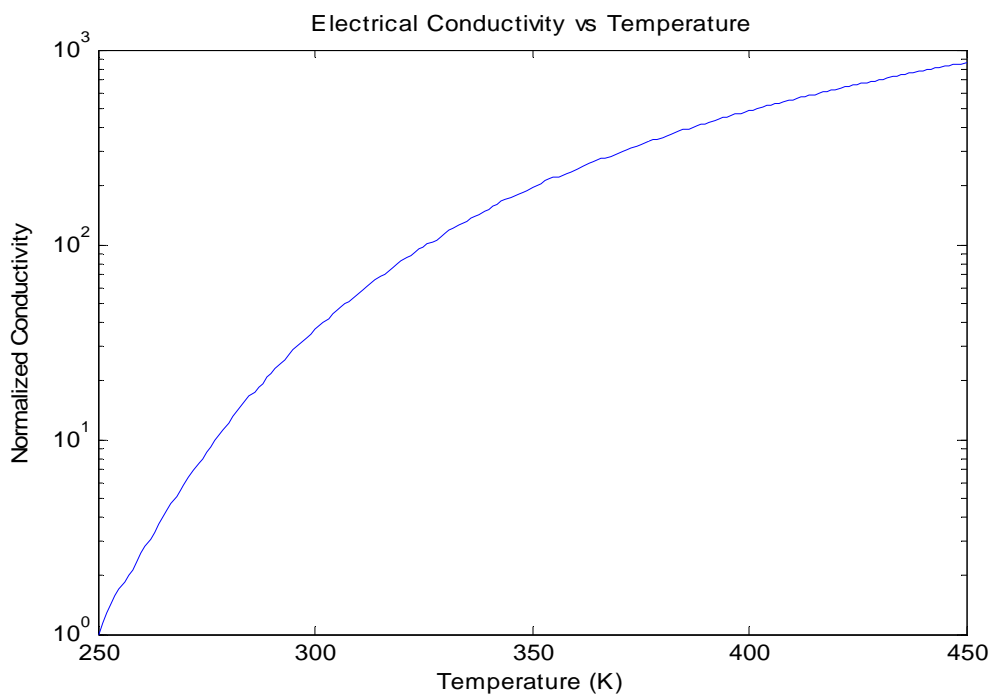


Figure 7

In Figures 8 & 9 we see the broad effect of temperature across the range of thrust and Isp. The traces in Figure 8 intuitively make sense, as temperature increases the efficiency of the electrospray increases due to the increased conductivity. As expected, the low voltage, high flow rate has the lowest specific thrust while the high voltage, low flow rate has the highest. This is consistent with previous comments that acceleration is more efficient for large q/m droplets. The thrust profile in Figure 9 is not quite as straight forward. Two trends are present that are dependent on the flow rate. If the flow rate is high, the increase in temperature also increases thrust. Conversely, as the temperature rises for a fixed low flow rate, the thrust goes down drastically.

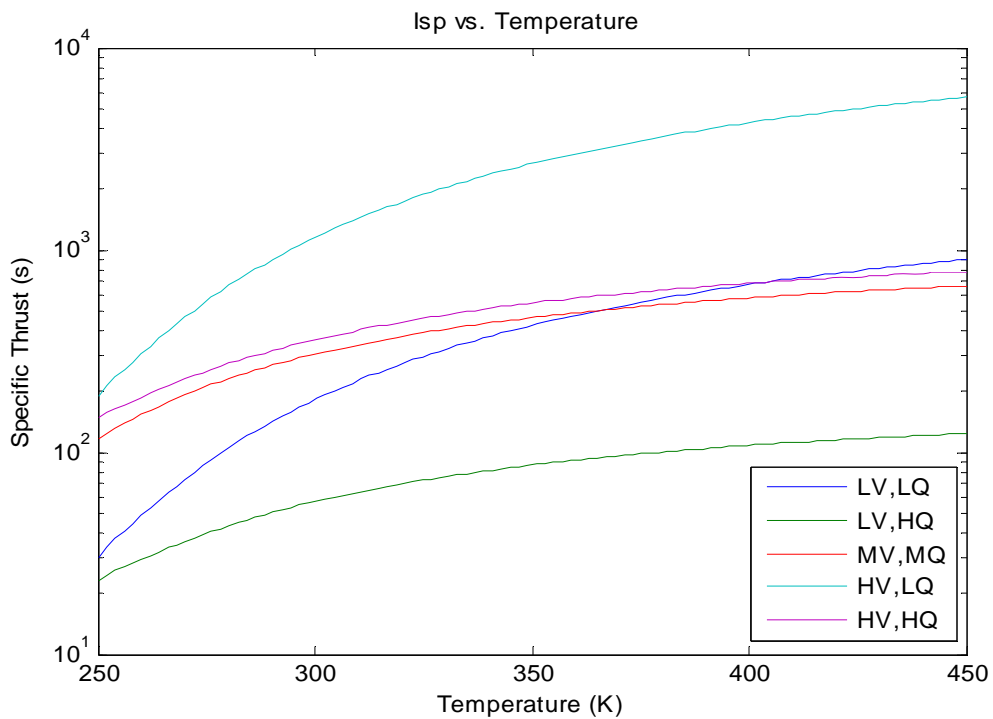


Figure 8

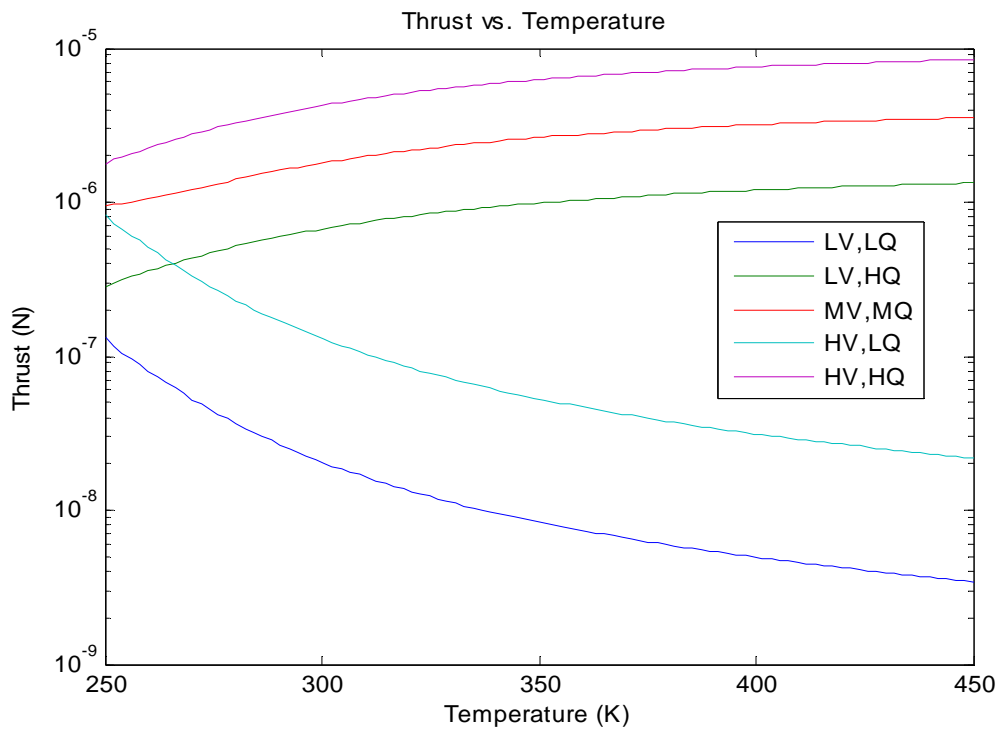


Figure 9

In Figures 10 & 11 we see the specific thrust versus flow rate while holding voltage steady. The graphs appear identical except for the scale of the specific thrust axis. The temperature steps show that we can expect increases in the specific thrust up to an order of magnitude. This agrees with different literature sources that operate in the picoliters per second with very small needles. (Mora, 2000)

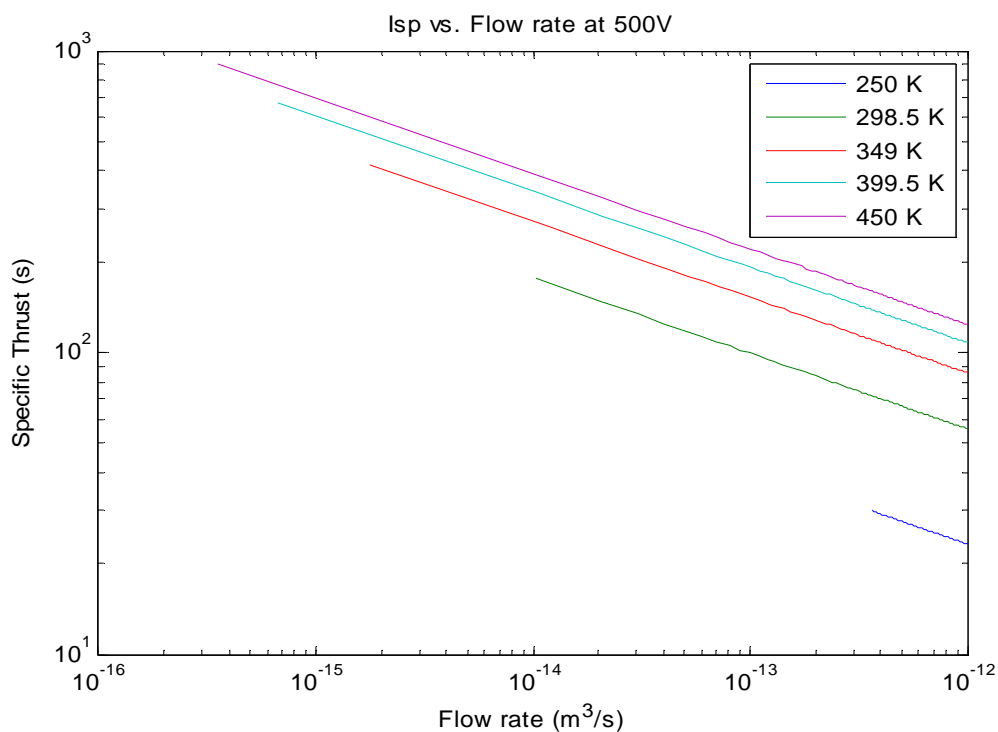


Figure10

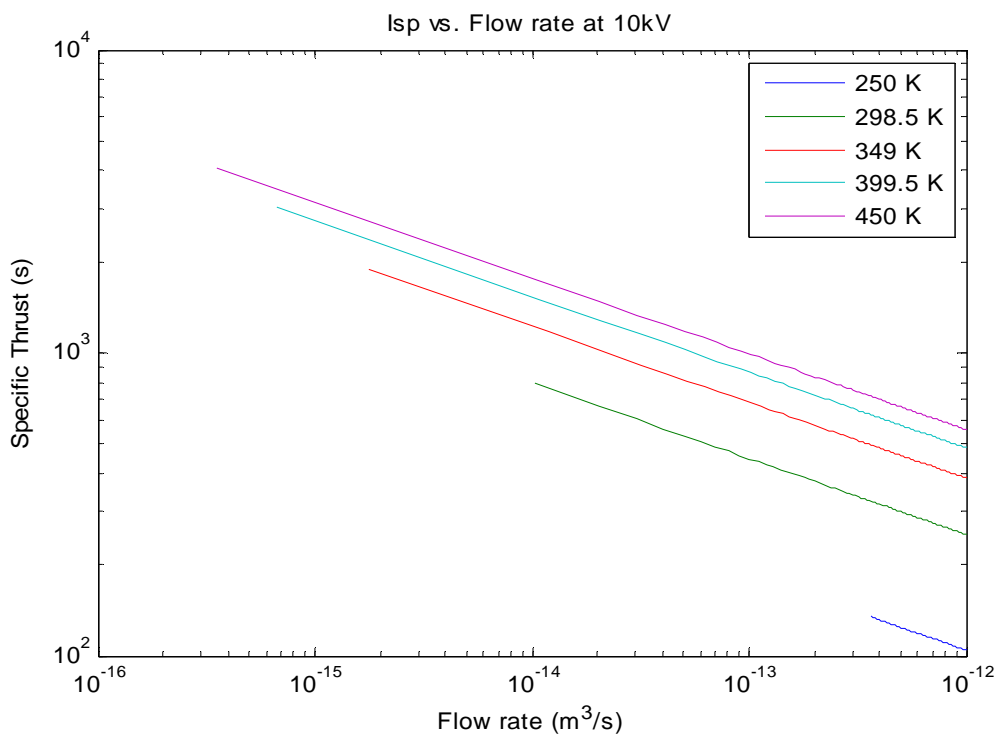


Figure 11

Revisiting our observation from Figure 9 we graph the thrust versus flow rate while holding voltage steady in Figures 12 and 13. As expected the thrust increases as the flow rate increases and the total mass ejected by the electrospray increases. The thrust appears to go down in Figure 9 because the increasing temperature increases the conductivity and lowers the surface tension (Figures 6 & 7), both of which lower the minimum flow rate at which emission can occur. The trend follows the low flow rate limit Q_{min} , thus the appearance of diminishing thrust. Again we see that we can significantly increase the thrust output by increasing the temperature, sometimes by as much as 500% at the higher temperatures.

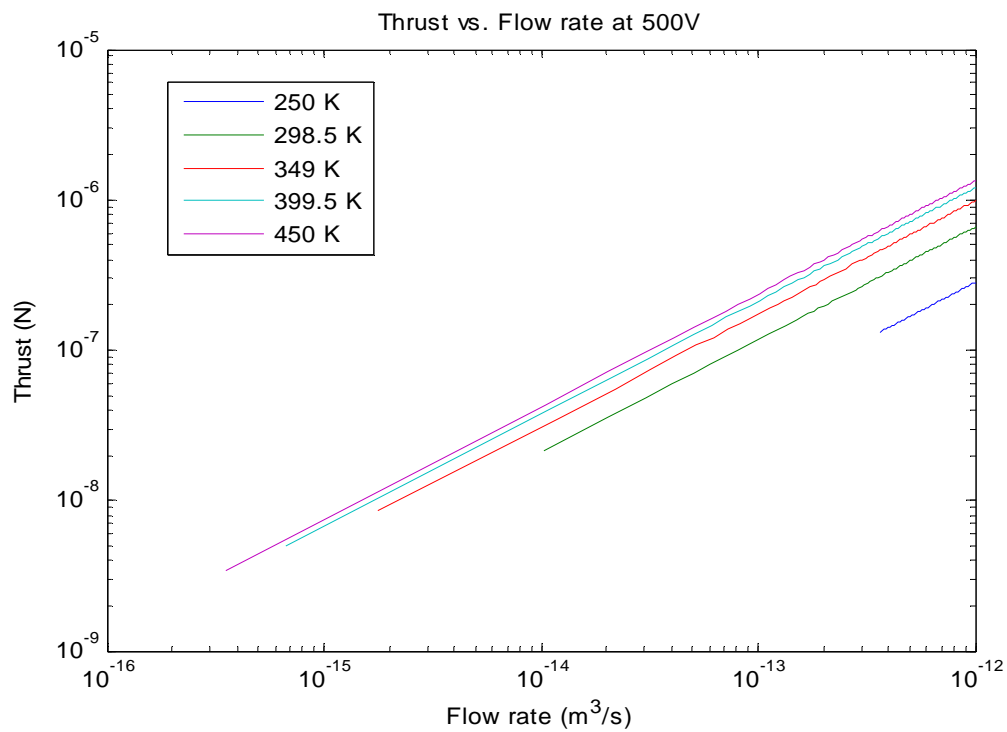


Figure 12

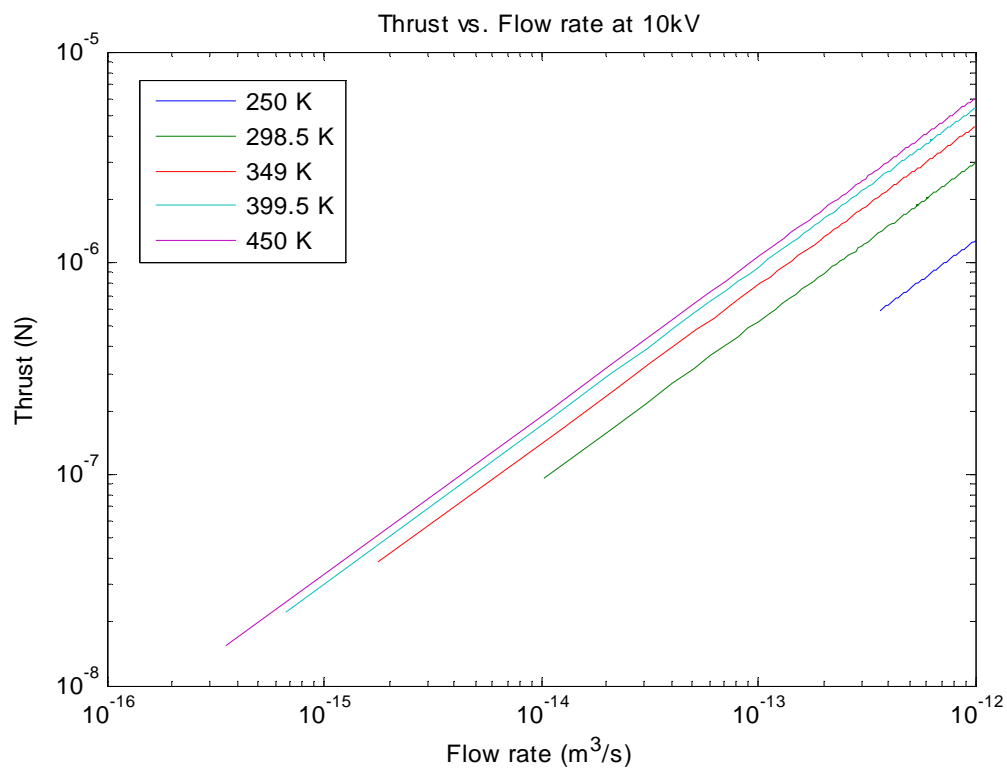


Figure 13

When the flow rate is held constant and the voltage varied, we obtain graphs like Figures 14 and 15 for low flow rate and medium flow rate respectively. Again we see the familiar trend as the temperature increases the performance increases sometimes by as much as a magnitude. An interesting data point is that where the medium flow rate gives the highest specific thrust value of 1000 s, which is the same point that the low flow rate graph starts. This provides a very good cross-section of the performance range of electrosprays. Voltage again has an exponential response for each temperature contour.

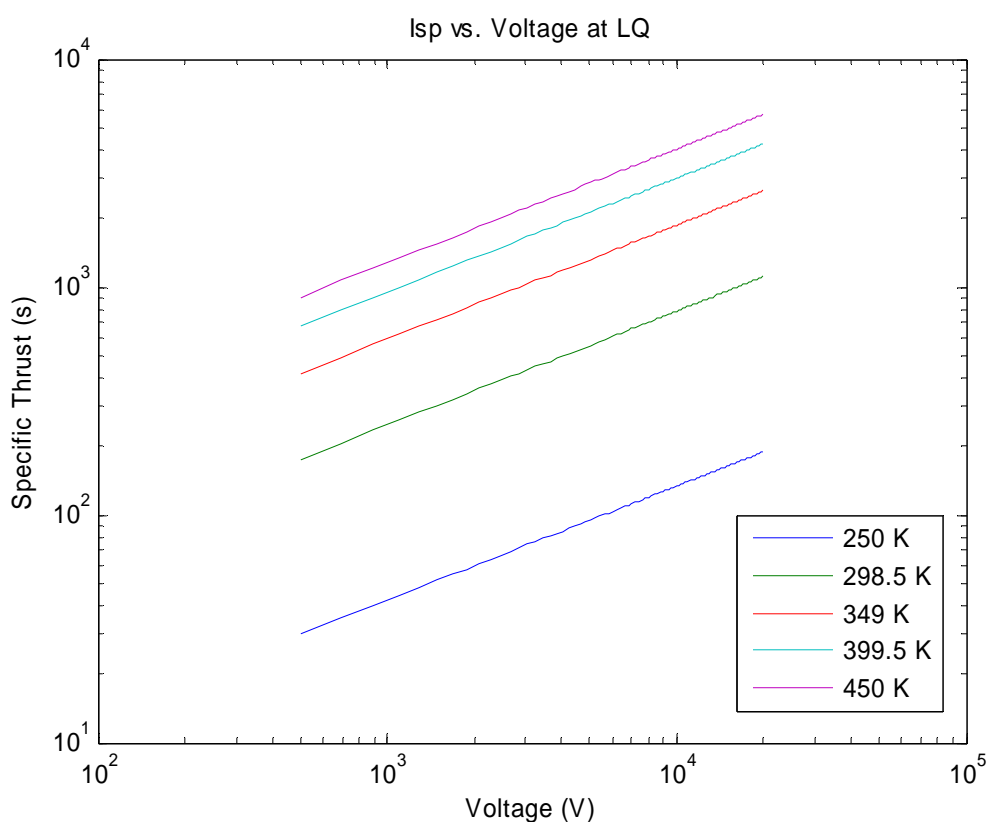


Figure 14

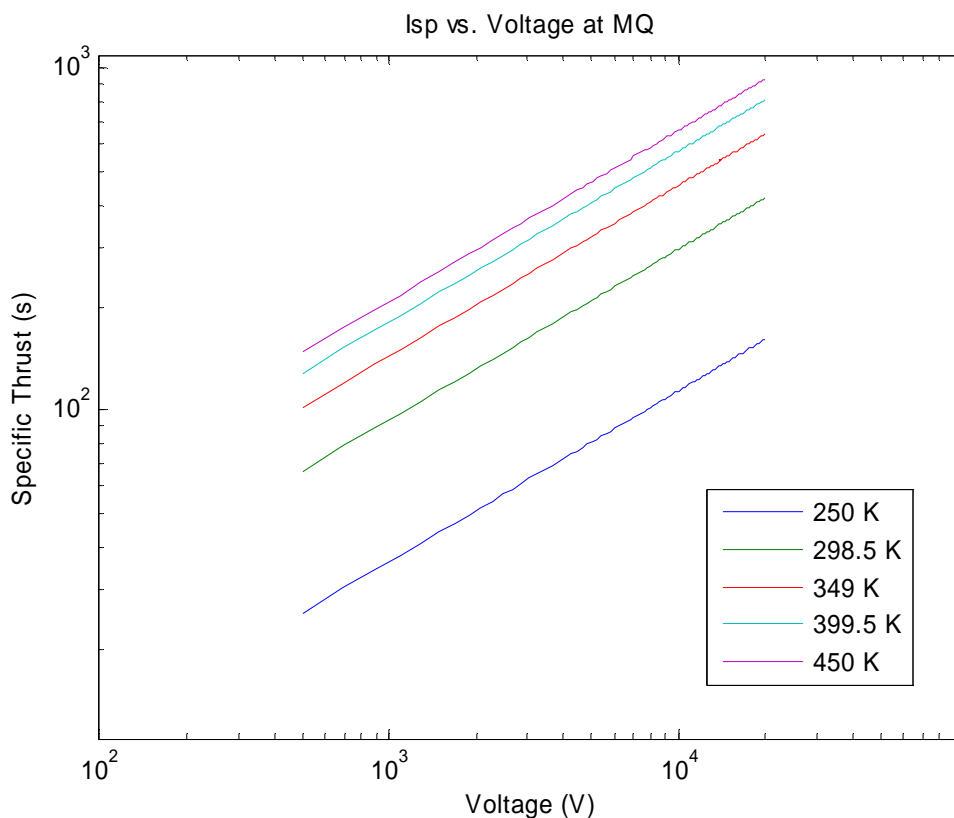


Figure 15

Figure 16 seems to be flipped, but again we see the effect that the temperature has on the minimum flow rate. As the temperature increases the thrust goes down because the flow rate goes down as was discussed previously. Figure 17 shows a very similar trend but not as steep a slope as with respect to the voltage increase. Both figures have an exponential increase as the voltage is increased.

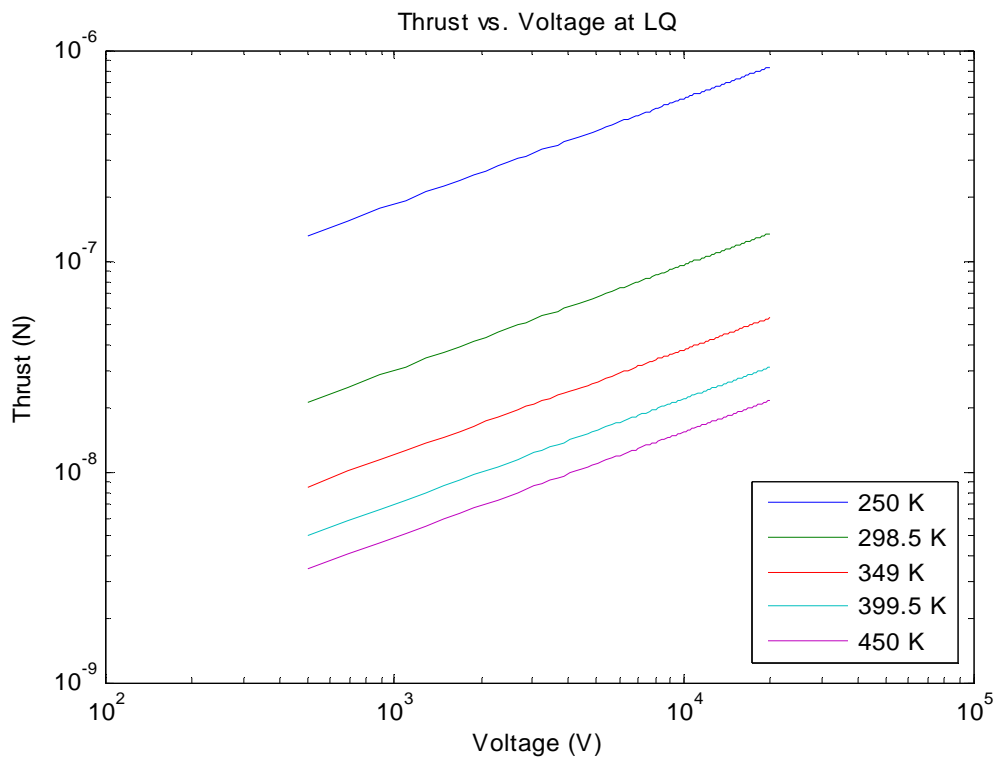


Figure 16

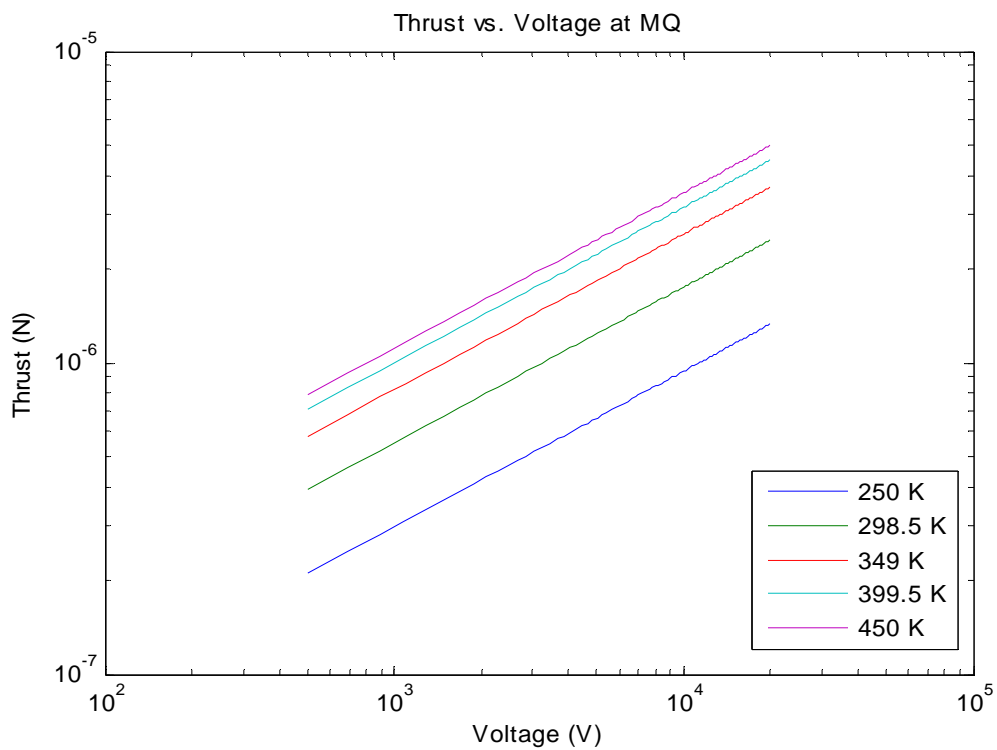


Figure 17

The final figures from the MATLAB® script shows the expected charge the droplets should carry away. Figure 18 shows the expected charge with respect to temperature across all data points. This figure shows the effect that flow rate has on the system.

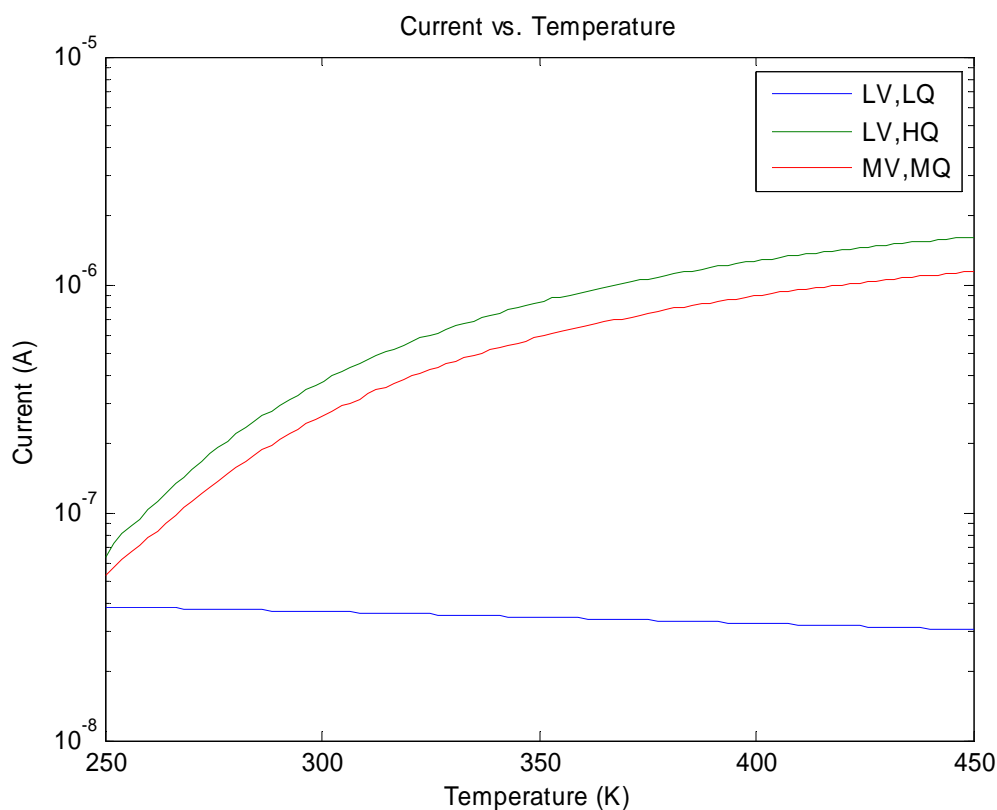


Figure 18

Fixing the voltage as constant a prediction was made as seen in Figure 19. For a given flow rate, holding the voltage constant, an increase in charge will be seen as the temperature increases. The magnitude of the change will be dependent on the flow rate and temperature extremes. A magnification of the range of the flow rates we experimented with is seen in Figure 20.

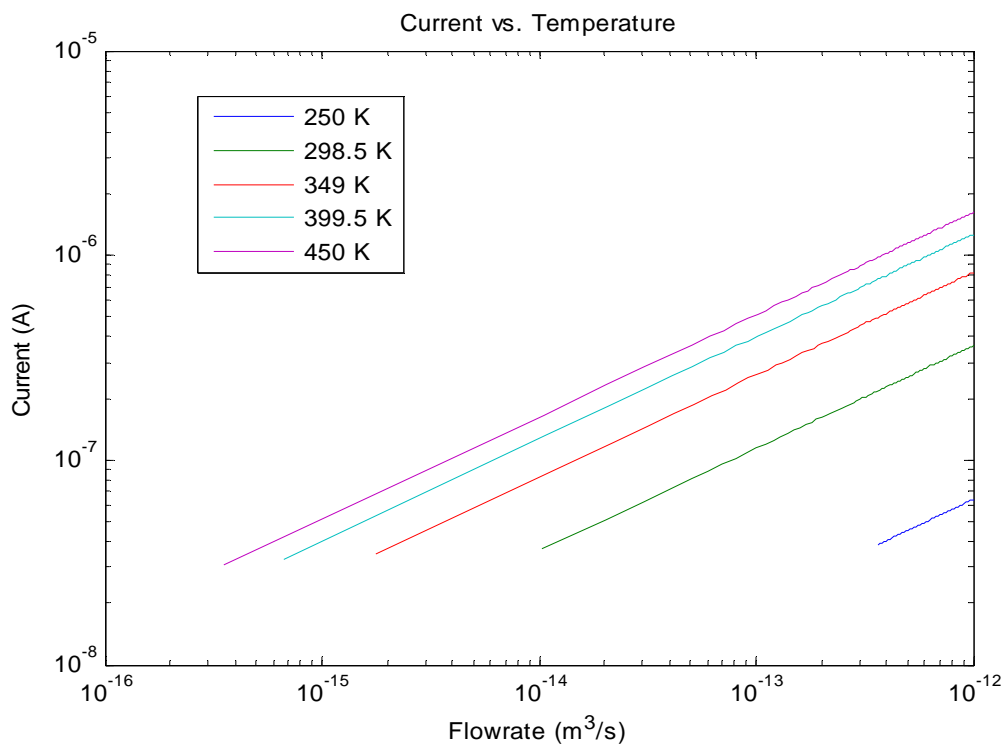


Figure 19

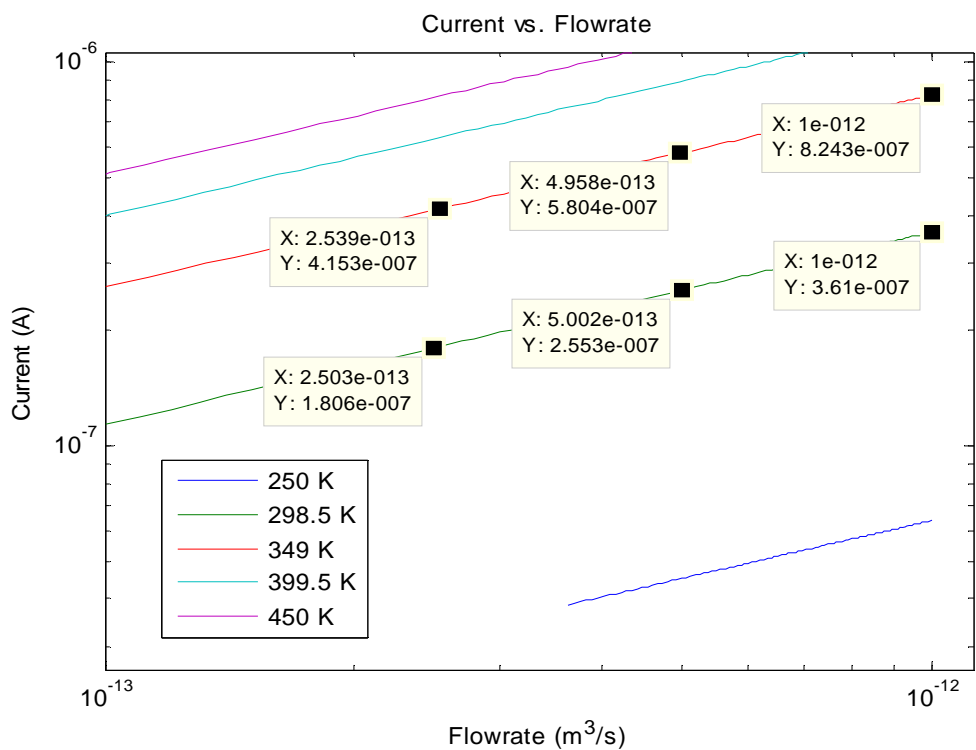


Figure 20

Experiment Setup

An experiment to test the results of the script was constructed in the Electric Propulsion Laboratory at the Air Force Research Laboratory located on Edwards AFB, CA. The experimental apparatus was set up inside a vacuum chamber to enable future testing without moving the experimental setup. A 250 microliter syringe and 22s needle were purchased from the Hamilton Company to serve as the internally fed needle and fuel reservoir. These were mounted on a Harvard Apparatus Pico Pump after the syringe was properly loaded to prevent bubble formation. This experimental setup can be seen in Figure 21. An electrically isolated metal plate was placed 4.6 mm away to serve as the extractor plate and collect the charge from the ejected droplets. A BK Precision 2MHz function generator provided the input voltage to a Trek Model 10/10B High Voltage Amplifier which biased the plate. Two Agilent 6 ½ Digit Multimeters collected outputs of voltage and current from the Trek amplifier while a Keithley Picoammeter/Voltage Source collected the current that left the needle tip seen in Figure 22. To protect the equipment, two resistors were placed in series as can be seen in Figure 23. These inputs were provided to a LabVIEW™ * program that processed and output the data into a text file. A MATLAB® program was created to read these files and plot the data in a useful manner. The orange tape on the needle tip thermally bonds the J type thermocouple to the needle so that needle temperature and also ionic liquid temperature could be measured. This assumes that the liquid can achieve thermal equilibrium by the time it exits the needle and also that the needle temperature is isothermal. Transit time in the high flow case of 60 nL/min is 16.7 minutes. The temperature data was manually recorded from a Tektronix DMM916 True RMS fluke meter.

* LabVIEW™ 8.6, Copyright © 2008 National Instruments. All rights reserved



Figure 21: View of electrospray experimental setup with needle, plate, and illumination lamp

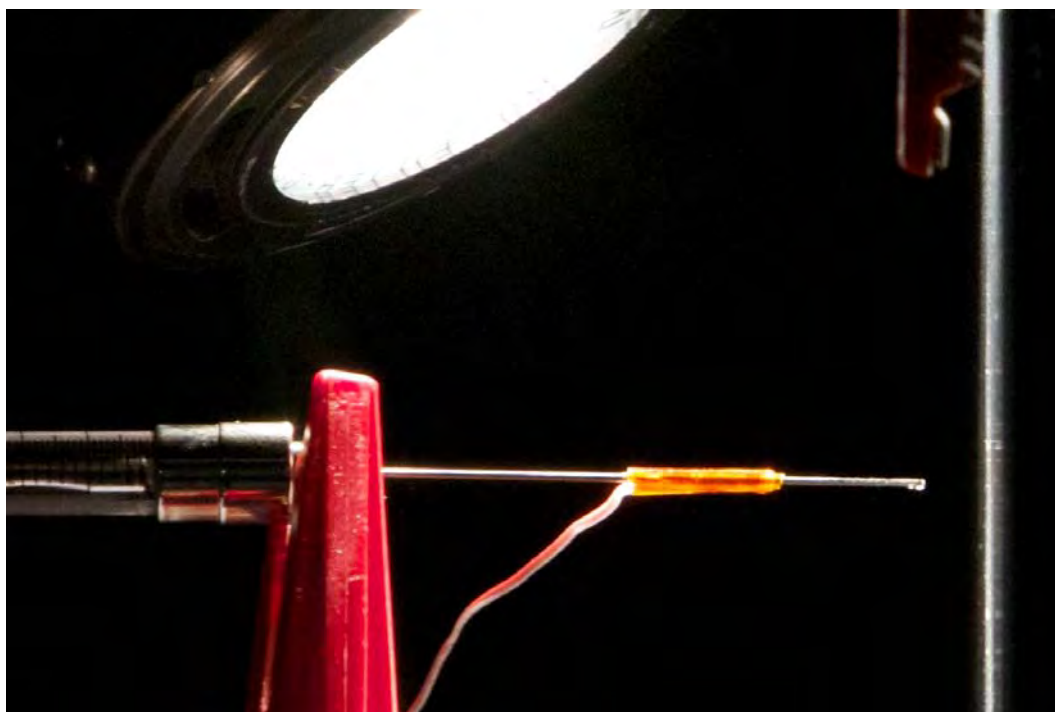


Figure 22: Close up of needle, lamp, and extractor plate

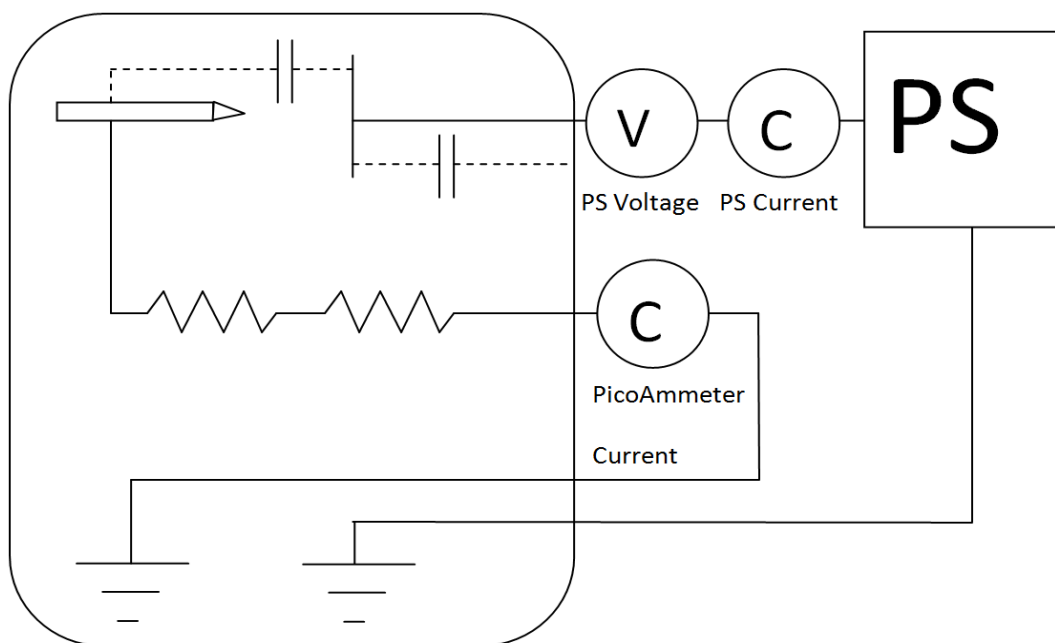


Figure 23: Electrical diagram of experiment

To validate the temperature effect the incandescent lamp shown in Figure 22 was either turned on or off. This gave two temperatures of 22 ° C (295.15 K) and 49 ° C (323.15 K). A few attempts to lower the temperature of the entire syringe and needle were tried but the thermal conduction of the needle and tape allowed for rapid temperature changes.

Experiment Results

For our experiment we ran the syringe at three different flow rates: 15, 30, and 60 nL/min at the same voltage potential. The test cases were run at least half an hour to ensure mass flow equilibrium and in most cases were run for an hour. The figures are arranged with the current traces in the top sub plot and the voltage in the bottom sub-plot. The data collected will be presented with first the positive current traces then the negative current traces and finally a figure with the total data collected for each experimental run.

Figures 24 and 25 show a portion of the results for running at 15 nL/min ($\frac{1}{4}$ nL/sec) at 22 ° C and 49 ° C respectively. Positive current corresponds to current flowing from the needle to

plate in the form of positively charged droplets traveling from the needle to the plate. Negative current corresponds to current flowing from the needle to the plate in the form of negatively charged droplets. The first observation is that the average current measured on the picoameter is lower for the higher temperature case than for the cooler temperature. The glow discharge was also observed during these runs which suggest that we had ionic emission and possible ionization of the air which could contribute to the oscillatory behavior as can be seen in Figure 26. The data suggests that the Taylor cone is stable, there are no visible disturbances of the Taylor cone and the current though oscillatory does have a high average value. However, this mechanism needs to be investigated further. Future operation under vacuum will prove or disprove that air interactions are involved.

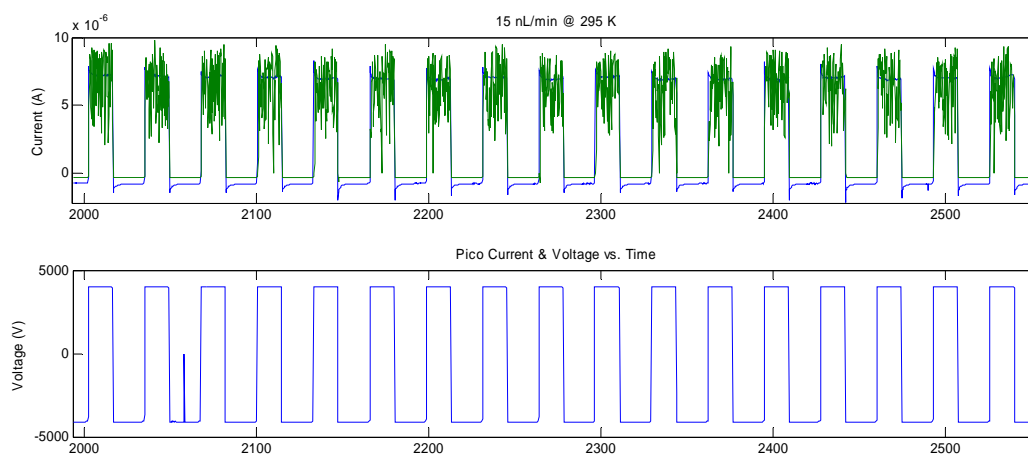


Figure 24: Positive Current

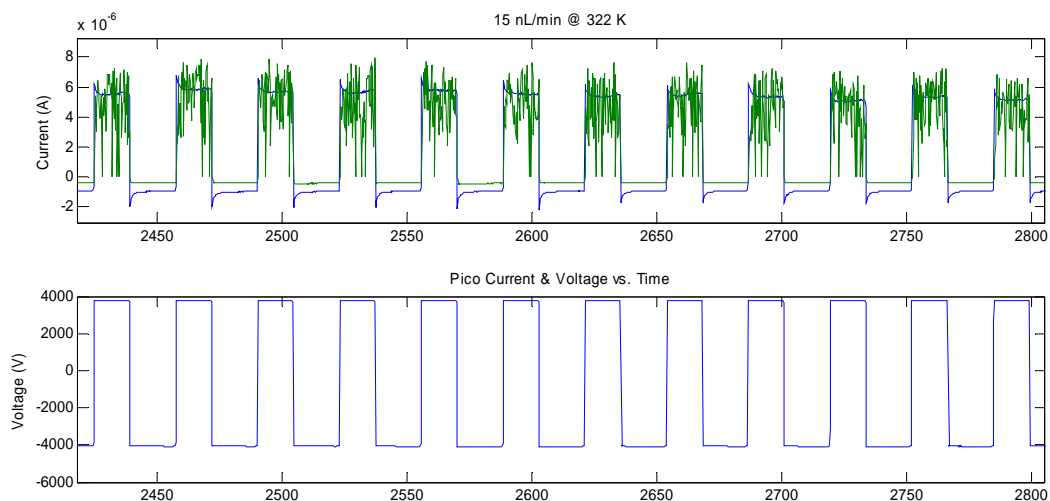


Figure 25: Positive Current

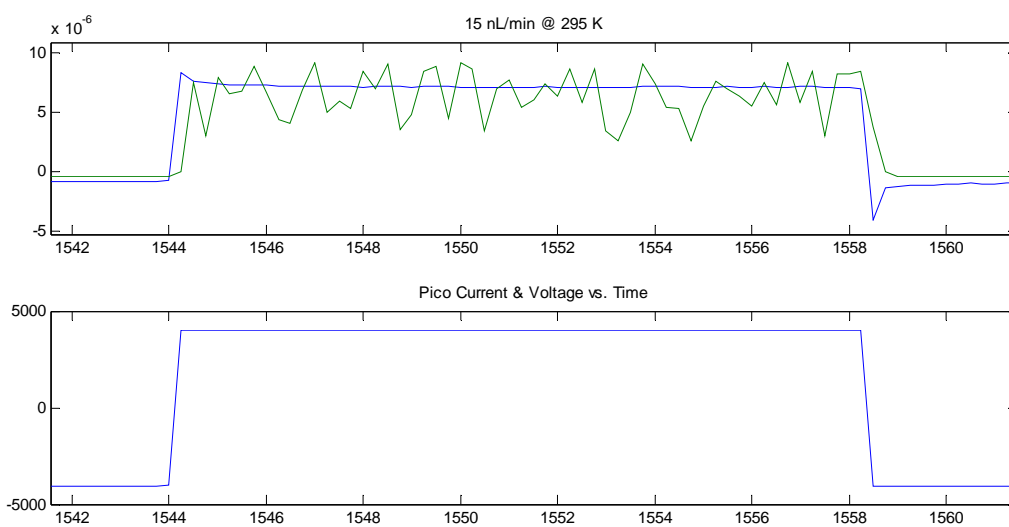


Figure 26: Oscillations

The negative current plot shows only a slight increase in current with temperature, as can be seen in Figures 27 and 28 for 22 ° C and 49 ° C respectively. Overall though, the difference isn't fully apparent as can be seen of all the negative current data in Figures 29 and 30.

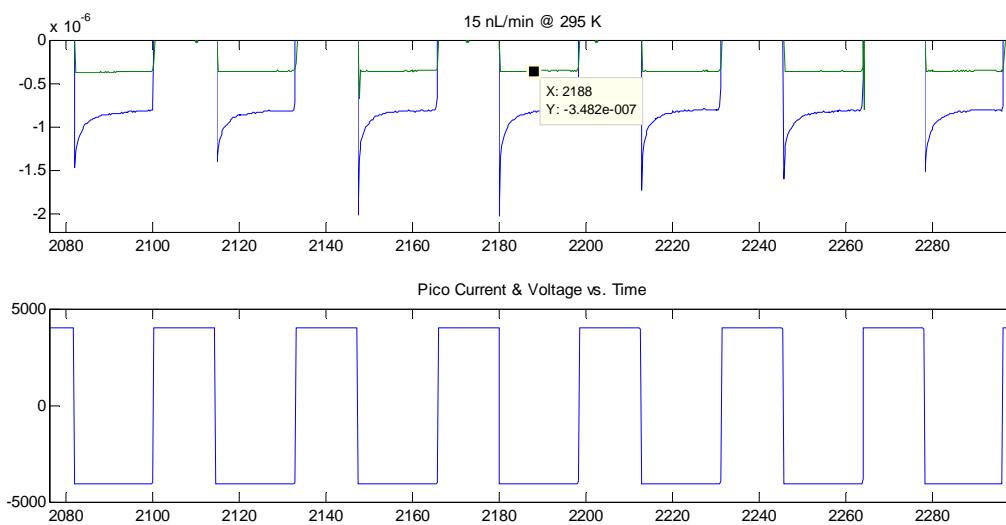


Figure 27: Negative Current

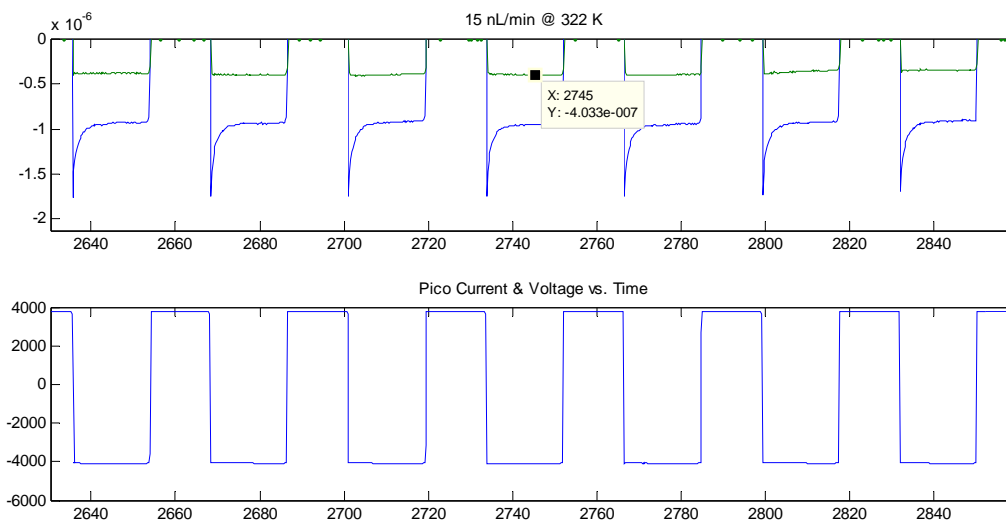


Figure 28: Negative Current

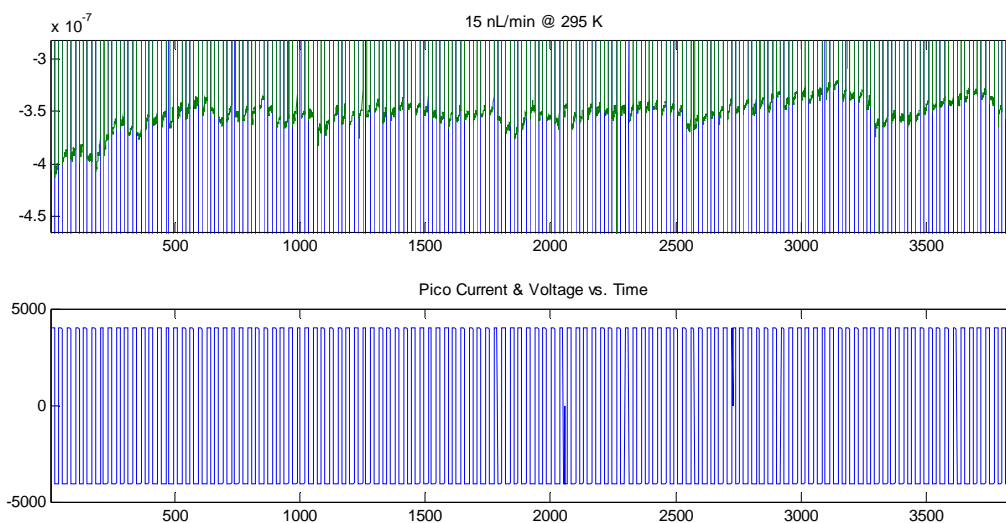


Figure 29: Negative Current

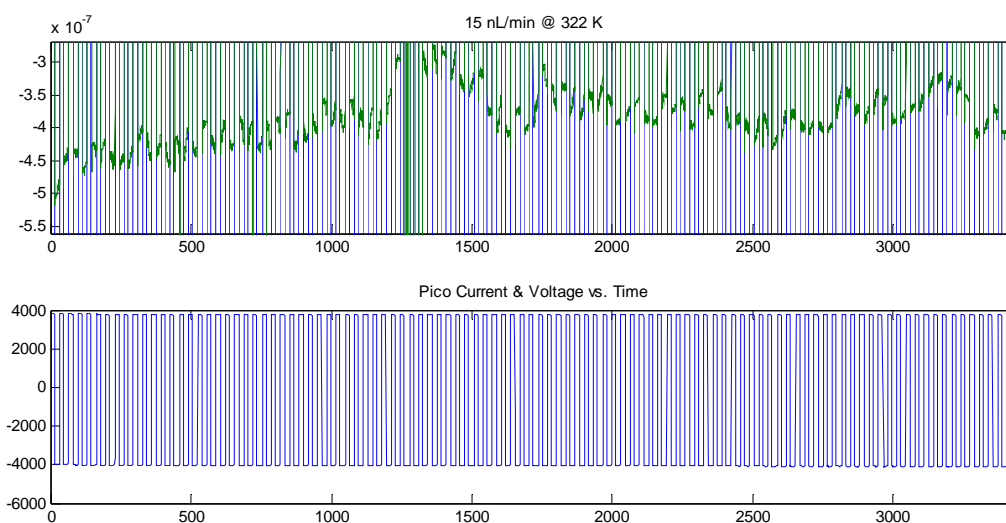


Figure 30: Negative Current

The next two runs double the mass flow rate at 30 nL/min ($\frac{1}{2}$ nL/sec) and show more response to the temperature difference on the positive side of the current. Figure 31 shows an increase of one to two micro amperes over the cooler run in Figure 32. This is very close to what was predicted in Figure 20. Again we have the glow discharge but not as bright as on the shorter

Taylor cone for the 15 nL/min case. The negative current shows a cyclic nature that oscillates between -0.25 micro-amperes to -0.35 micro-amperes for the 22 °C run as is seen in Figure 33. The 49 °C run has some oscillation too but ranges from -0.3 to -0.45 micro-amperes in Figure 34. Figure 35 shows the entire run and the oscillation in the positive current clearly. This wave pattern is a result of macro droplets leaving the Taylor cone as it switches polarity. Larger droplets detach because the Taylor cone collapses during the transition from negative to positive voltage, or vice versa, and as it reforms additional forces are applied. As the Taylor cone grew longer, the electric forces should have become stronger and more charge would have been carried in the droplets. After a large droplet detaches the overall length of the Taylor cone would shorten considerably to make up for the fluid volume lost and the charge carried would decrease on subsequent droplets. Only three large drops were extracted according to the data in Figure 35 while five were extracted in Figure 36. This suggests that the higher temperature allows more stable operation at higher flow rates.

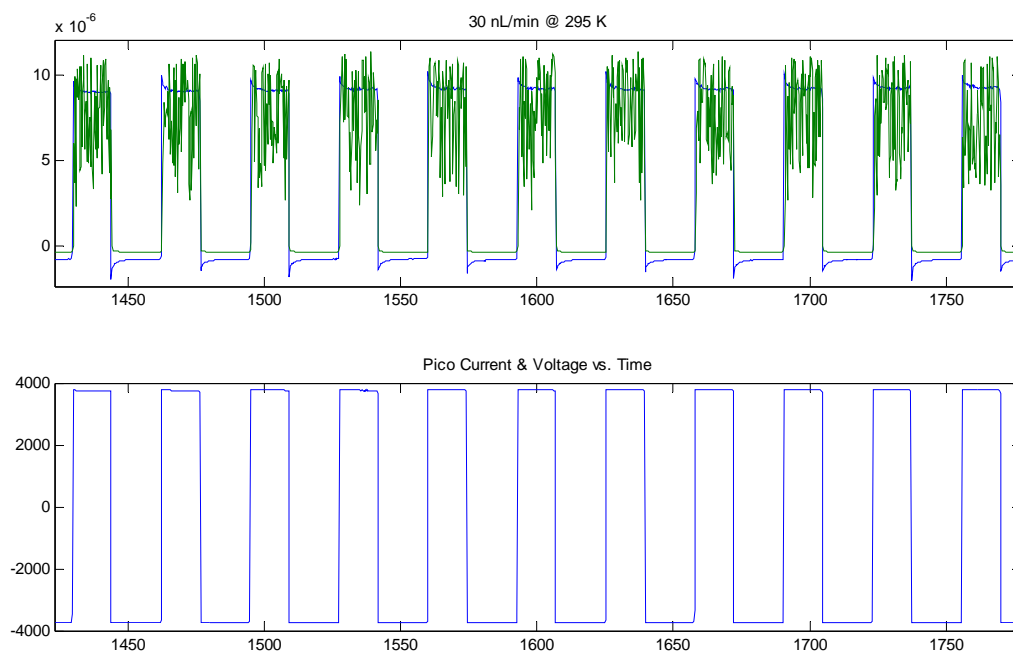


Figure 31: Positive Current

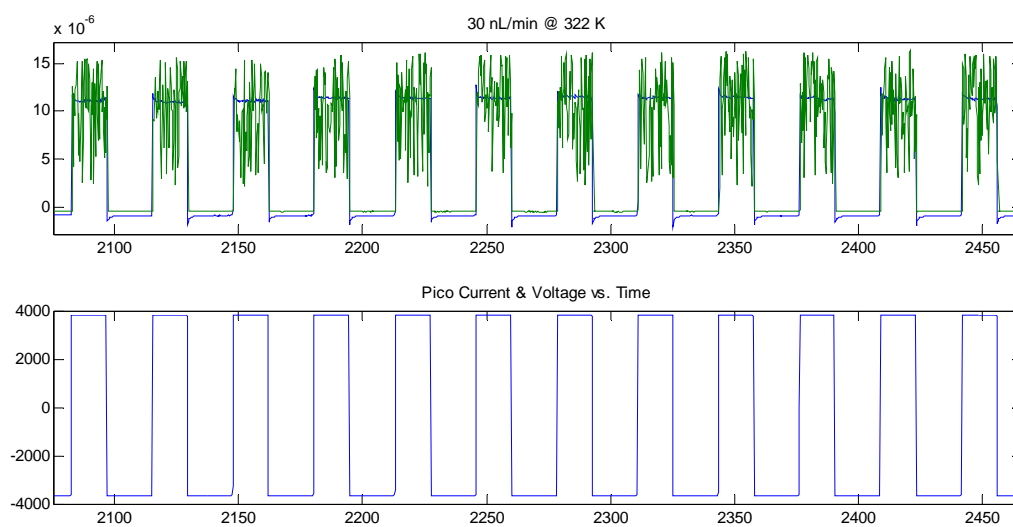


Figure 32: Positive Current

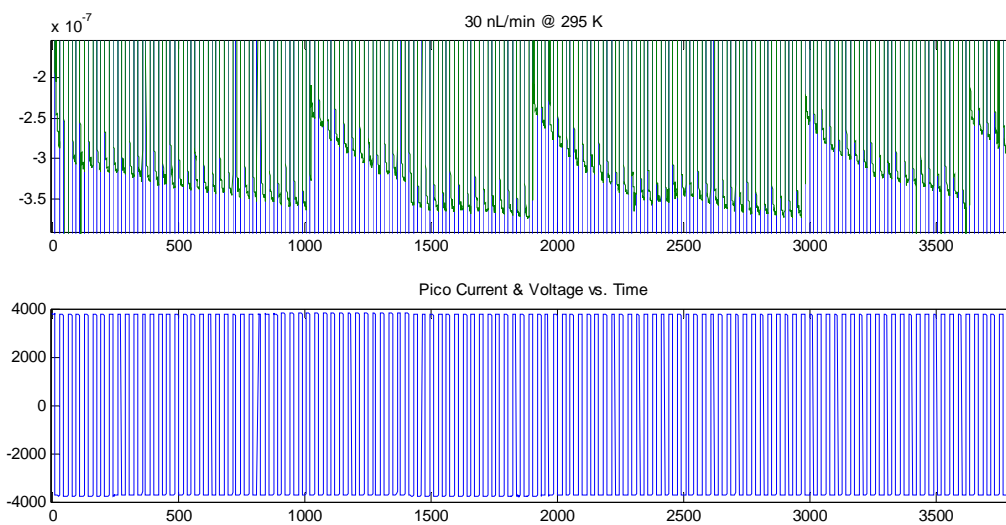


Figure 33: Negative Current

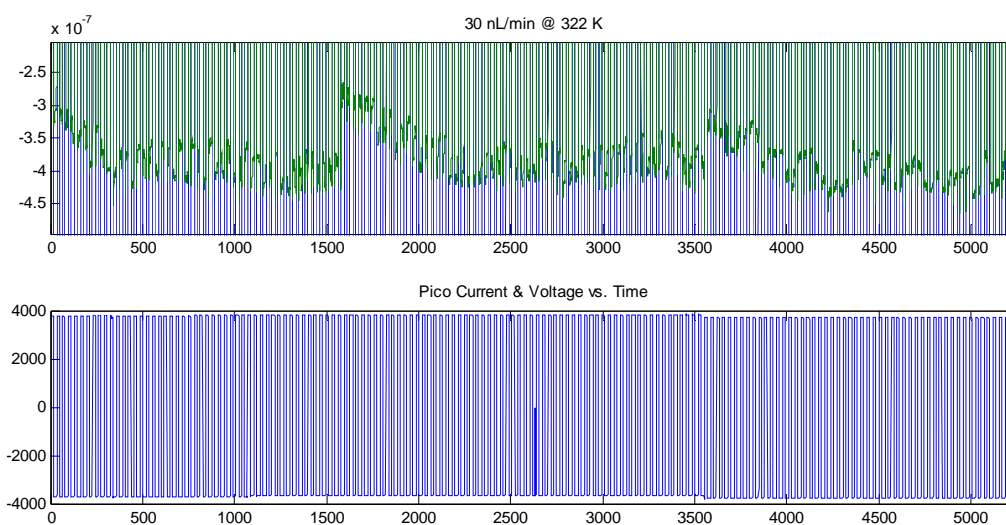


Figure 34: Negative Current

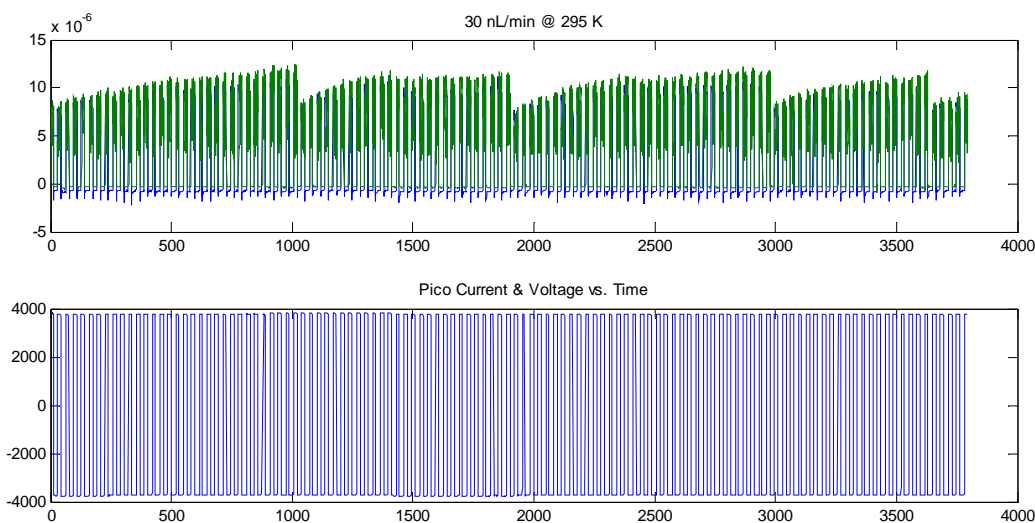


Figure 35: All Current

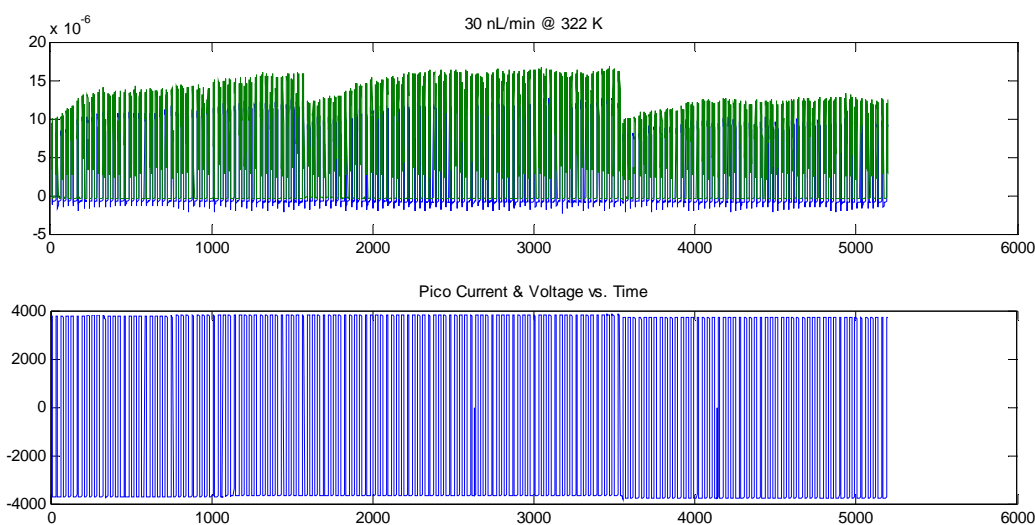


Figure 36: All Current

The last two runs were at 60 nL/min (1 nL/sec) and show higher frequency oscillation and minimal dependence on the positive current shown in Figures 37 and 38 with temperatures of 22 °C and 49 °C respectively. The negative current likewise shows little sensitivity to temperature changes in Figures 39 and 40 for 22 °C and 49 °C respectively. Figure 39 shows a sharp increase in each negative pulse which suggests that the Taylor cone was lengthening and

had an uneven mass flow rate. Figure 40 has very few of these sharp increases and more level current traces. The increase in oscillation frequency can be seen in Figures 41 and 42 which show a factor increase of 7.6 and 4 over their 30 nL/min counterparts respectively.

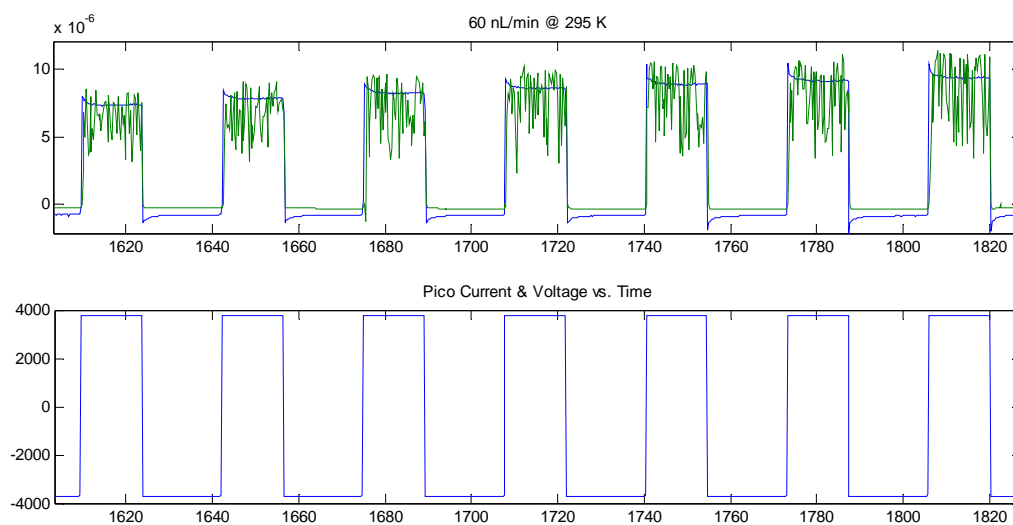


Figure 37: Positive Current

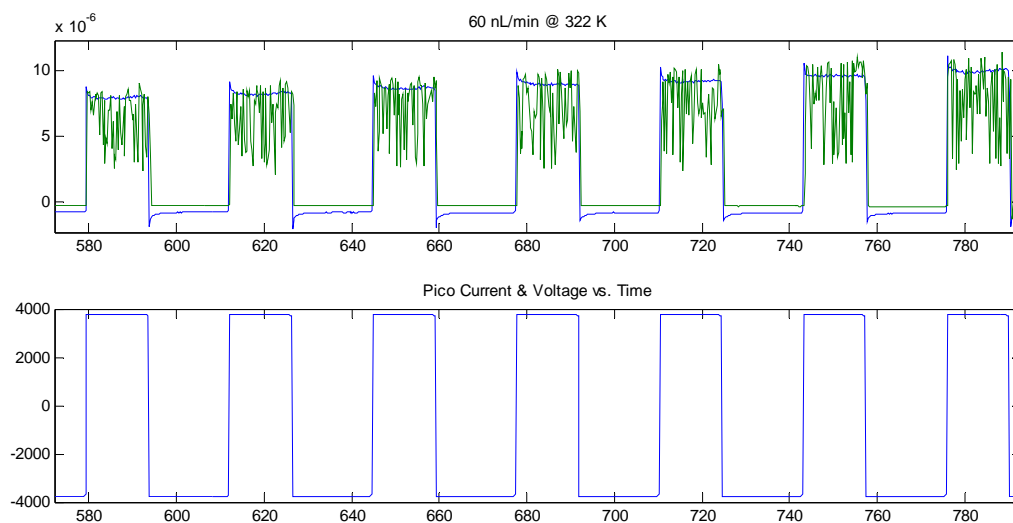


Figure 38: Positive Current

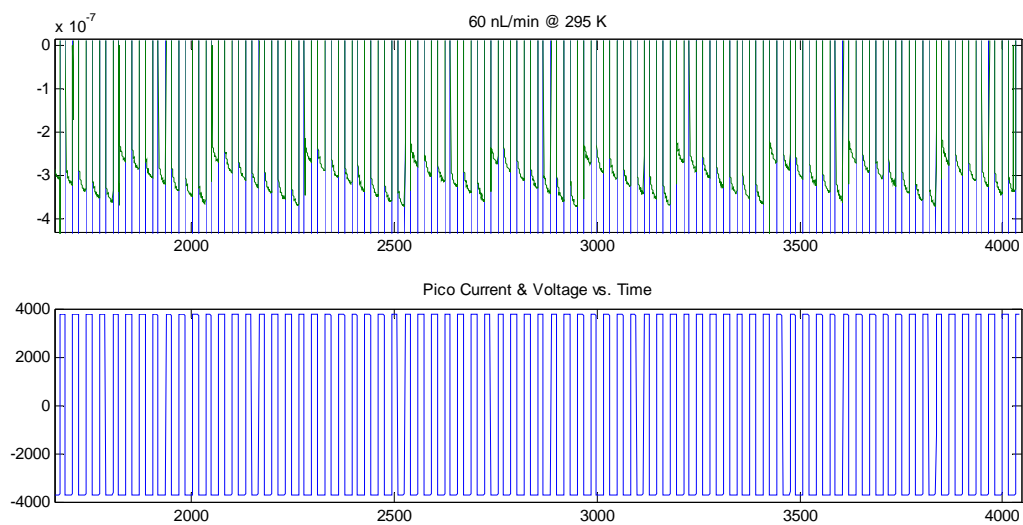


Figure 39: Negative Current

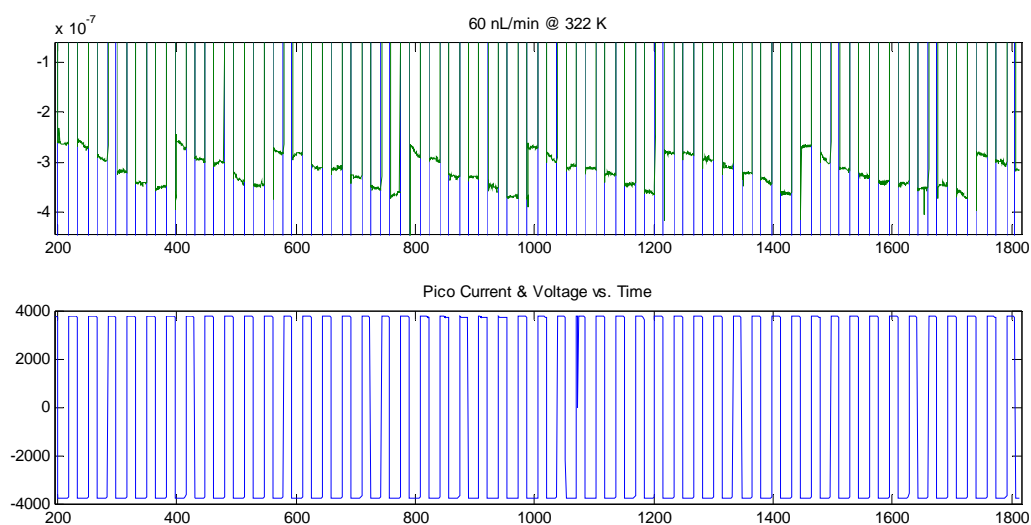


Figure 40: Negative Current

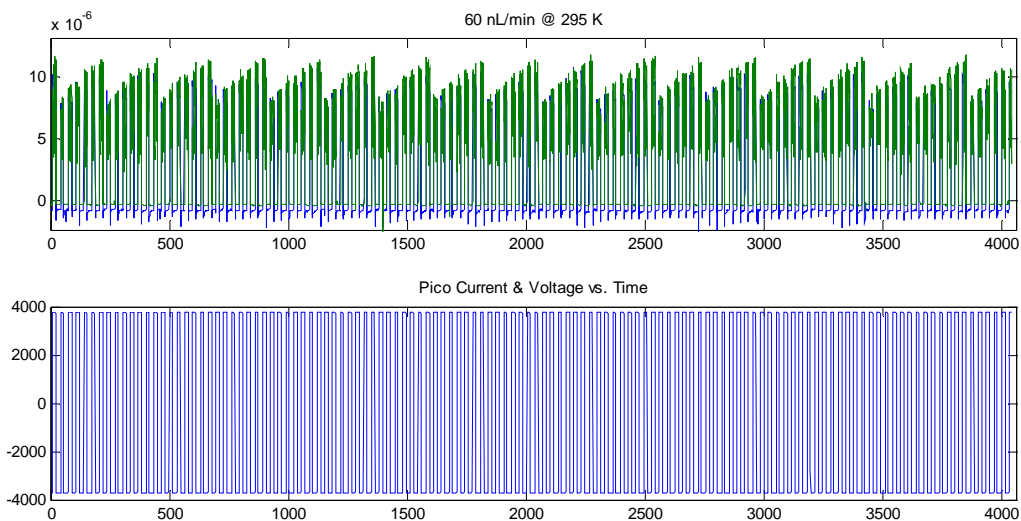


Figure 41: All Current

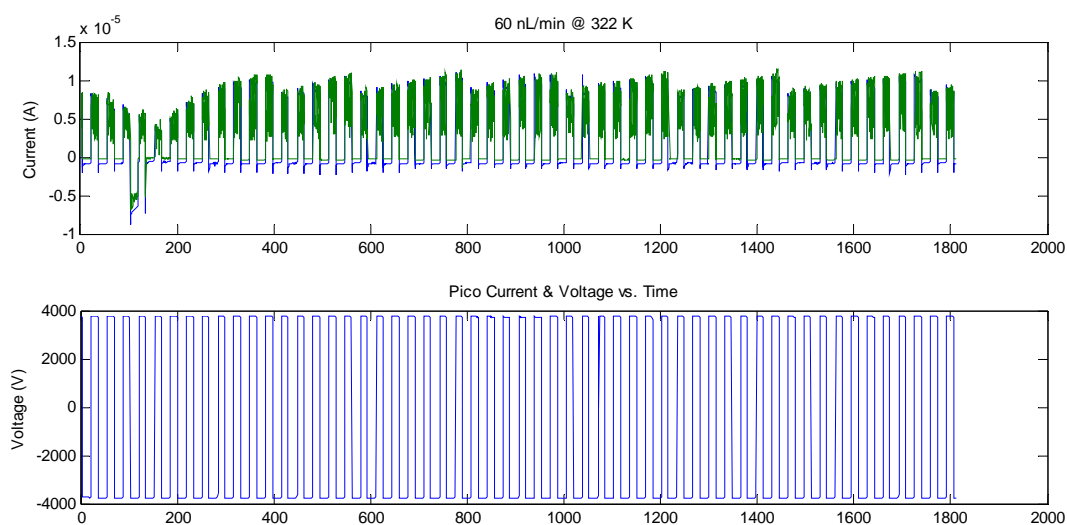


Figure 42: All Current

Visually taking the averages from all cases and plotting while holding voltage steady we get the following, Figure 43. The charge increases in the predicted direction but the different flow rates display a decrease in charge as the flow rate increases. They are near the calculated values but display a lack of response to temperature. On the other side of the axis we see similar

mixed results with two lines increasing proportionally but the lowest flow rate decreasing. The numbers are also an order of magnitude or more above calculated predictions as shown in Figure 44. This although unexpected could partly be explained by ionic emission and decomposition of the BMiM BF₄ liquid. Observation of the pictures taken during these runs also supports ionic emission. Figures 2 and 3 while negatively biased display droplets which Figure 4 lacks. If we take the conductivity for the last segment of the temperature curve and apply a linear trend line we get the following curve in Figure 45 for the charge in relation to temperature. The highest charge predicted would be 6×10^{-6} at 700 K which is 250 K above BMIM BF₄'s thermal decomposition temperature (Michael E. Van Valkenburg, 2003). In order to reach the charge at 300 K a charge-to-mass ratio of 23,320 C/kg would be needed.

Although this is unexpected it does have some major benefits for an electrospray thruster. Operating at 15 nL/min at 295.15 K we have a charge-to-mass ratio of 23,2317.8 C/kg. This gives us a calculated specific thrust of 1392 s and a thrust of 1.018×10^{-6} N an improvement of 1177 s and 3.8395×10^{-7} N or 647.5% and 160.5% improvement respectively. From an operation standpoint if the power is available this would be the preferred mode of operation.

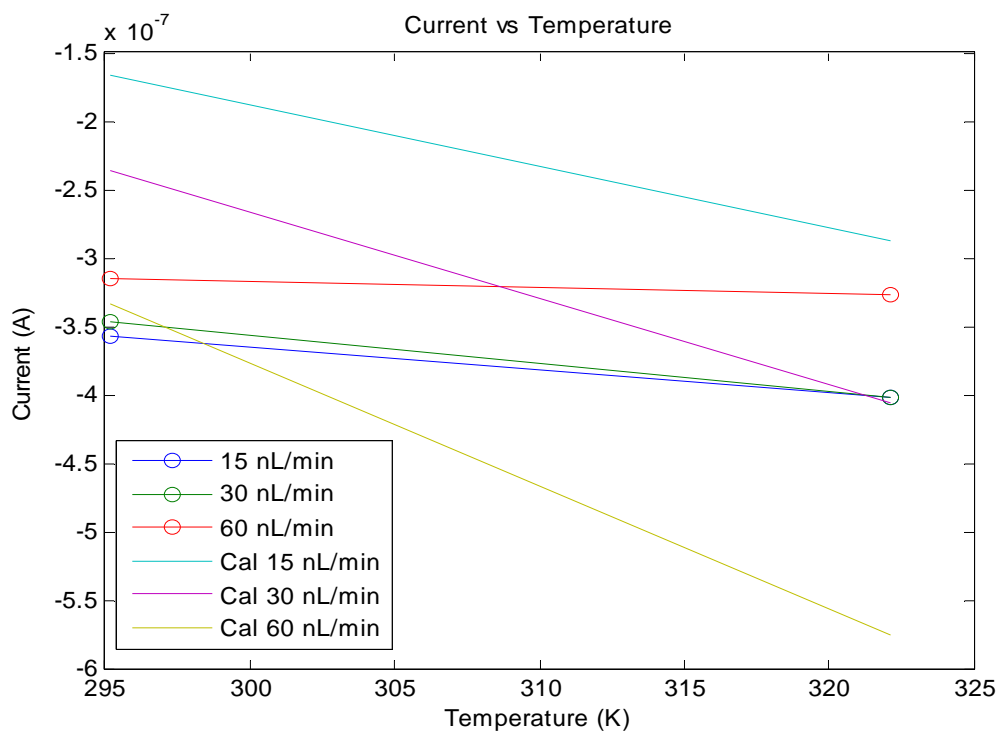


Figure 43

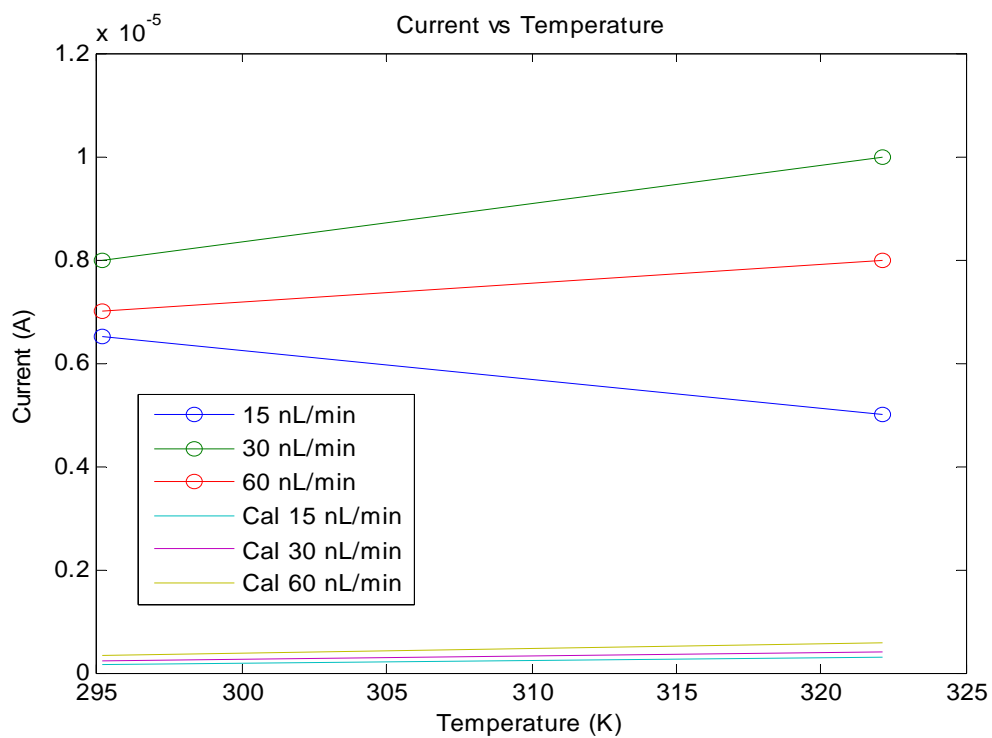


Figure 44

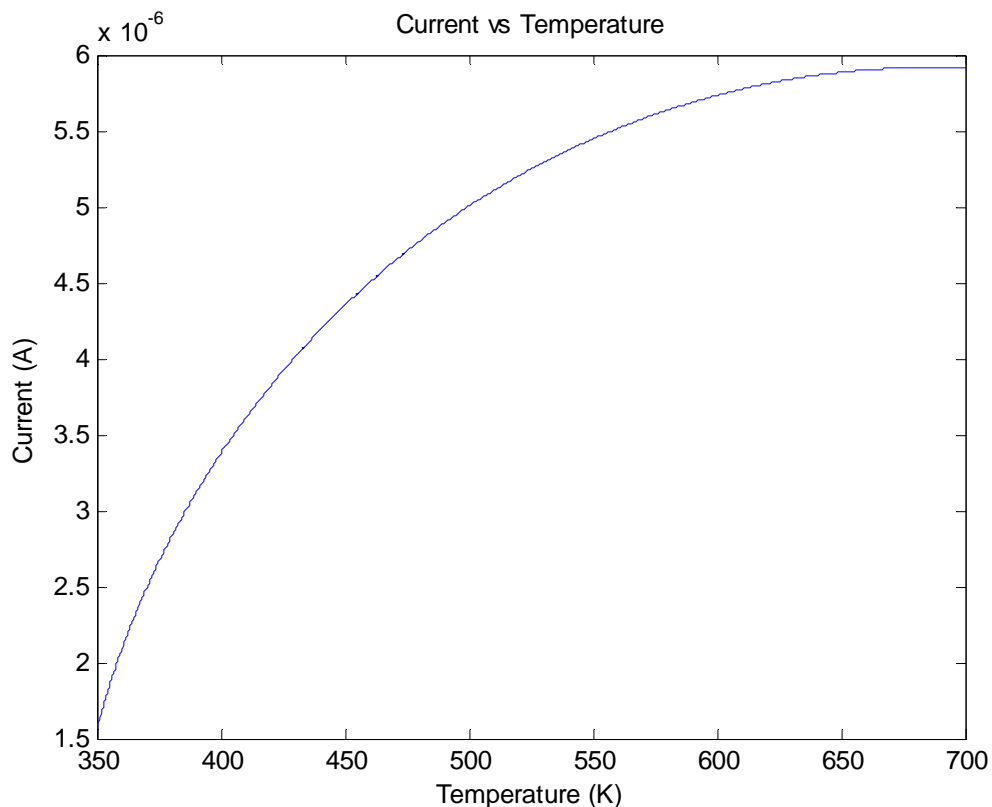


Figure 45

During one of our tests we saw a dramatic response to temperature. Figure 46 has a sharp decrease in the positive current at 1200 s. This was a result of turning off the lamp in our test setup to adjust the optics. The response was immediate with a steady decline in the positive current till the positive current went to zero with the failure to form a Taylor cone at 1275 s. Around 1300 s the lamp was turned back on and normal patterns returned. For two cycles the negative current displays the same behavior as the positive current with highly oscillatory waveform.

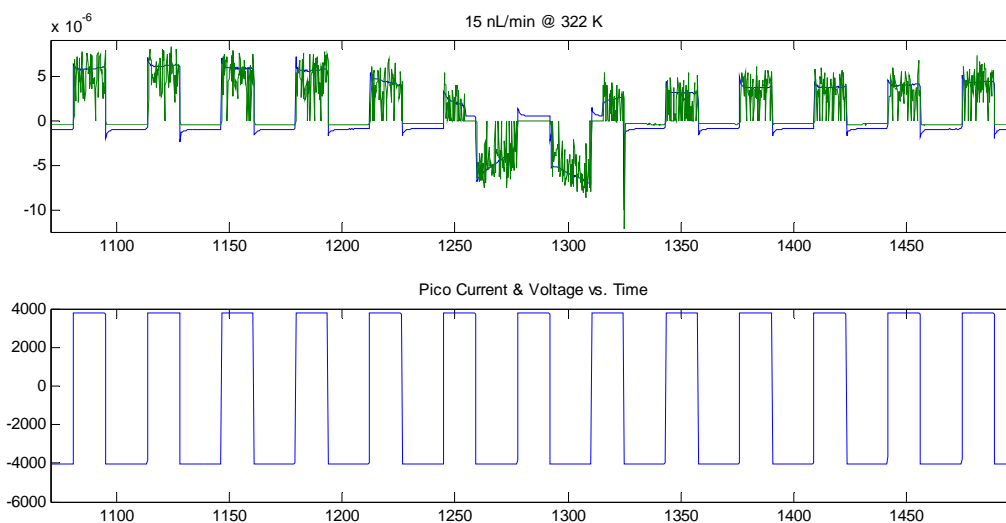


Figure 46: Lamp turned off at 1200 s, back on at 1290

Future Work

More predictive tools need to be researched and developed into the script. The current script has the size of the droplets dependent only on the flow rate, Equation 5, but voltage has some effect. Better prediction and understanding of the different Taylor cone modes needs to be implemented. This may help us predict more accurately the expected performance. Temperature was severely restricted with the conductive tape and needle. The use of an electrothermal cooling device to heat and cool the needle will be implemented in the next round of testing to better control this factor. The tests will also be repeated under vacuum to determine if the glow discharge is indeed ionization of the air or breakdown of the ionic liquid. The glow discharge effect calls for faster sampling of the test data to better understand this phenomenon. Different ionic liquids will be tested to see if they have similar responses to temperature and voltage.

Summary and Conclusion

In summary, we presented an introduction of electrosprays and our findings for the numerical and experimental studies of an electrospray thruster. We were able to form a stable Taylor cone at all test points and collect data; however our current data does not agree with the model calculations. It is evident from the data collected that temperature plays a major role and needs to be studied further; especially its interactions with flow rate and voltage. The model matched the experimental data only for the case of 30 nL/min at 49 deg C on the negative bias side, but as 60 nL/min also was recorded at this point it is more coincidence than accurate prediction. The rest of the negative data holds steady at the roughly same current. For the positive bias, we clearly have some sort of ionic emission because of the charge-to-mass ratio. The results for the positive current follow the general trends we modeled but are an order of magnitude above calculated values. The temperature would have to be 300 K higher in order to account for this kind of difference. As shown in the Figure 46, we can control the mode by controlling the temperature. This allows us to increase the specific impulse and thrust substantially by at least 100%. An ionic liquid could be manufactured that with a simple temperature change switch from one mode to another and leave the voltage and flow rate the same. The flow rate and voltage can be adjusted to the desired level but temperature control will allow operations in conditions outside of the normal electrospray startup environment. This is important for the eventual miniaturization and scaling of electrosprays. Smaller needles will lead to smaller flow rates and temperature plays a larger role at smaller flow rates making control of temperature very important. Equal thermal conduction to all the emitter tips will also be important to have uniform thrust.

Bibliography

Bibliography

Cole, R. B. (2000). Some tenets pertaining to electrospray. *JOURNAL OF MASS SPECTROMETRY* , 763-772.

James A. Nabity, G. M. (2006). *Studies of MEMS Colloid Thrusters*. Boulder, CO: American Institute of Aeronautics and Astronautics.

Jijun Xiong, D. S. (2006). Investigation of the Onset Voltage for the Design of a. *IEEE/ASME TRANSACTIONS ON MECHATRONICS* , 66-74.

Matthew S. Alexander, K. L. (September–October 2007). Voltage-Modulated Flow Rate for Precise Thrust Control. *JOURNAL OF PROPULSION AND POWER* , 1042-1048.

Michael E. Van Valkenburg, R. L. (2003). Ionic Liquid Heat Transfer Fluids. *Fifteenth Symposium on Thermophysical Properties* .

Mora, M. G.-C. (2000). Direct measurement of ion evaporation kinetics. *JOURNAL OF CHEMICAL PHYSICS* , 815-832.

TRC/NIST/Boulder. (2006). *Ionic Liquids Database- IL Thermo*. Retrieved December 1, 2010, from Ionic Liquids Database: <http://ilthermo.boulder.nist.gov/ILThermo/pureprp.uix.do>

W.D. Luedtke, U. L.-H. (2008). Nanojets, Electrospray, and Ion Field Evaporation: Molecular Dynamics Simulations and Laboratory Experiments. *J. Phys. Chem.* , 9628-9648.

Appendix: MATLAB® Script

```

clear;clc;close all;
%Main program to intake Voltage and Flow rate and return Thrust and Isp for
%colloid thruster with regards to temperature. References geometry, liquid
properties and constants
liquid3
constants
Va= linspace(0.5e3,20e3,x); %Voltage potential (V)
for k=1:x
    [gamma, rho, K]= Temp(Tk(k));
    for i=1:x
        Qmin(k)=(gamma.*kappa.*eps0)./(rho.*K) ; %Lowest Flow rate
        Q= linspace(Qmin(k),1.e-12,x); %Flow rate (m^3/s) (1
        picoliter/s=1e-15 m^3/s)
        Qplot(1:x,k)=Q;
        %Droplet size
        Rk=(eps0.*Q./K).^(1/3); %Jet Radius (m)
        Dd=3.3*Rk; %Droplet diameter (m)
        qdm=12.*sqrt(2)./rho*(eps0*gamma./Dd.^3).^0.5; %Charge per
        mass ratio (C/kg)
        mdot=Q.*rho; %Mass flow rate (kg/s)
        %Outputs
        for j=1:x
            Isp(i,j,k)=1/g*(2*qdm(j).*Va(i)).^0.5; %Specific Impulse (s)
            T(i,j,k)=mdot(j)*g.*Isp(i,j,k); %Thrust (N)
            C(i,j,k)=mdot(j)*qdm(j);
        end
    end
end
end
Plot

%Liquid properties input file for colloid thruster for BMI BF4
kappa=[11.7]; %Dielectric constant
x=100; %determines size of end matrix, needs to be multiple of four to avoid
errors while plotting
Tk= linspace(250,450,x); %Temperature array (Kelvin)

%Constants for colloid thruster
eps0=8.8541878e-12; %Permittivity of vacuum (C^2/(N*m^2)
g=9.80665; %Local gravity constant (m/s^2)

function [gamma,rho,K]= Temp(T)
%Script to return values based on Temperature

rho=rhoft(T);
K=Kft(T);
gamma=gammaft(T);

function rho=rhoft(T)
rho=-0.694*T+1408;
%function to return density as function of temperature in Kelvin for BMIM BF4

function K=Kft(T)
Kp=[238 0.00212; 248 0.00778; 258 0.02318; 263 0.036; 268 0.05477; 273 0.08;
278 0.1132; 283 0.16; 288 0.211; 293 0.28; 298 0.3587; 303 0.45427; 308
0.556; 313 0.69129; 318 0.821; 323 0.99417; 328 1.15; 333 1.364; 338 1.545;

```

```

343 1.7999; 348 2; 353 2.3015; 358 2.52; 368 3.1; 373 3.4; 378 3.73; 388
4.41; 398 5.13; 408 5.88; 418 6.64; 428 7.45; 438 8.29; 448 9.15; 458 10.04;
468 10.94];
K=interp1(Kp(:,1),Kp(:,2),T);

```

```

%function to return conductivity as function of temperature in Kelvin for
BMIM
%BF4

```

```

function gamma=gammaft(T)
gamma=-6e-5*T+0.0621;
%function to return the surface tension of BMIM BF4 as function of
%temperature in Kelvin

```

```

%Extracting data from the 3D grids
Ip1(1:x)=Isp(1,1,1:x);           %Temperature Isp(V,Q,K)
Ip2(1:x)=Isp(1,x,1:x);
Ip3(1:x)=Isp(x/2,x/2,1:x);
Ip4(1:x)=Isp(x,1,1:x);
Ip5(1:x)=Isp(x,x,1:x);
T1(1:x)=T(1,1,1:x);
T2(1:x)=T(1,x,1:x);
T3(1:x)=T(x/2,x/2,1:x);
T4(1:x)=T(x,1,1:x);
T5(1:x)=T(x,x,1:x);
Ip6(1:x)=Isp(1,1:x,1);           %Flowrate Isp(V,Q,K)
Ip7(1:x)=Isp(1,1:x,x/4);
Ip8(1:x)=Isp(1,1:x,x/2);
Ip9(1:x)=Isp(1,1:x,x*3/4);
Ip10(1:x)=Isp(1,1:x,x);
T6(1:x)=T(1,1:x,1);
T7(1:x)=T(1,1:x,x/4);
T8(1:x)=T(1,1:x,x/2);
T9(1:x)=T(1,1:x,x*3/4);
T10(1:x)=T(1,1:x,x);
Ip11(1:x)=Isp(x/2,1:x,1);
Ip12(1:x)=Isp(x/2,1:x,x/4);
Ip13(1:x)=Isp(x/2,1:x,x/2);
Ip14(1:x)=Isp(x/2,1:x,x*3/4);
Ip15(1:x)=Isp(x/2,1:x,x);
T11(1:x)=T(x/2,1:x,1);
T12(1:x)=T(x/2,1:x,x/4);
T13(1:x)=T(x/2,1:x,x/2);
T14(1:x)=T(x/2,1:x,x*3/4);
T15(1:x)=T(x/2,1:x,x);
Ip16(1:x)=Isp(1:x,1,1);           %Voltage Isp(V,Q,K)
Ip17(1:x)=Isp(1:x,1,x/4);
Ip18(1:x)=Isp(1:x,1,x/2);
Ip19(1:x)=Isp(1:x,1,x*3/4);
Ip20(1:x)=Isp(1:x,1,x);
Ip21(1:x)=Isp(1:x,x/2,1);
Ip22(1:x)=Isp(1:x,x/2,x/4);
Ip23(1:x)=Isp(1:x,x/2,x/2);
Ip24(1:x)=Isp(1:x,x/2,x*3/4);
Ip25(1:x)=Isp(1:x,x/2,x);
T16(1:x)=T(1:x,1,1);

```

```

T17(1:x)=T(1:x,1,x/4);
T18(1:x)=T(1:x,1,x/2);
T19(1:x)=T(1:x,1,x*3/4);
T20(1:x)=T(1:x,1,x);
T21(1:x)=T(1:x,x/2,1);
T22(1:x)=T(1:x,x/2,x/4);
T23(1:x)=T(1:x,x/2,x/2);
T24(1:x)=T(1:x,x/2,x*3/4);
T25(1:x)=T(1:x,x/2,x);
C1(1:x)=C(1,1,1:x); %Charge(V,Q,K)
C2(1:x)=C(1,x,1:x);
C3(1:x)=C(x/2,x/2,1:x);
C4(1:x)=C(x,1,1:x);
C5(1:x)=C(x,x,1:x);
C6(1:x)=C(1,1:x,1);
C7(1:x)=C(1,1:x,x/4);
C8(1:x)=C(1,1:x,x/2);
C9(1:x)=C(1,1:x,x*3/4);
C10(1:x)=C(1,1:x,x);
C11(1:x)=C(x/5,1:x,1);
C12(1:x)=C(x/5,1:x,x/4);
C13(1:x)=C(x/5,1:x,x/2);
C14(1:x)=C(x/5,1:x,x*3/4);
C15(1:x)=C(x/5,1:x,x);
Csurf1(1:x,1:x)=C(1:x,1:x,1);
Csurf2(1:x,1:x)=C(1:x,1:x,x/2);
Csurf3(1:x,1:x)=C(1:x,1:x,x);

figure
semilogy(Tk,Ip1,Tk,Ip2,Tk,Ip3,Tk,Ip4,Tk,Ip5)
xlabel('Temperature (K)')
ylabel('Specific Thrust (s)')
title('Isp vs. Temperature ')
legend('LV,LQ','LV,HQ','MV,MQ','HV,LQ','HV,HQ')
figure
semilogy(Tk,T1,Tk,T2,Tk,T3,Tk,T4,Tk,T5)
xlabel('Temperature (K)')
ylabel('Thrust (N)')
title('Thrust vs. Temperature ')
legend('LV,LQ','LV,HQ','MV,MQ','HV,LQ','HV,HQ')
figure
loglog(Qplot(1:x,1),Ip6,Qplot(1:x,x/4),Ip7,Qplot(1:x,x/2),Ip8,Qplot(1:x,x*3/4),Ip9,Qplot(1:x,x),Ip10)
xlabel('Flow rate (m^3/s)')
ylabel('Specific Thrust (s)')
title('Isp vs. Flow rate at 500V')
legend('250 K','298.5 K','349 K','399.5 K','450 K')
figure
loglog(Qplot(1:x,1),T6,Qplot(1:x,x/4),T7,Qplot(1:x,x/2),T8,Qplot(1:x,x*3/4),T9,Qplot(1:x,x),T10)
xlabel('Flow rate (m^3/s)')
ylabel('Thrust (N)')
title('Thrust vs. Flow rate at 500V')
legend('250 K','298.5 K','349 K','399.5 K','450 K')
figure
loglog(Qplot(1:x,1),Ip11,Qplot(1:x,x/4),Ip12,Qplot(1:x,x/2),Ip13,Qplot(1:x,x*3/4),Ip14,Qplot(1:x,x),Ip15)

```

```

xlabel('Flow rate (m^3/s)')
ylabel('Specific Thrust (s)')
title('Isp vs. Flow rate at 10kV')
legend('250 K', '298.5 K', '349 K', '399.5 K', '450 K')

figure
loglog(Qplot(1:x,1),T11,Qplot(1:x,x/4),T12,Qplot(1:x,x/2),T13,Qplot(1:x,x*3/4),T14,Qplot(1:x,x),T15)
xlabel('Flow rate (m^3/s)')
ylabel('Thrust (N)')
title('Thrust vs. Flow rate at 10kV')
legend('250 K', '298.5 K', '349 K', '399.5 K', '450 K')
figure
loglog(Va,Ipl6,Va,Ipl7,Va,Ipl8,Va,Ipl9,Va,Ip20)
xlabel('Voltage (V)')
ylabel('Specific Thrust (s)')
title('Isp vs. Voltage at LQ')
legend('250 K', '298.5 K', '349 K', '399.5 K', '450 K')
figure
loglog(Va,Ip21,Va,Ip22,Va,Ip23,Va,Ip24,Va,Ip25)
xlabel('Voltage (V)')
ylabel('Specific Thrust (s)')
title('Isp vs. Voltage at MQ')
legend('250 K', '298.5 K', '349 K', '399.5 K', '450 K')
figure
loglog(Va,T16,Va,T17,Va,T18,Va,T19,Va,T20)
xlabel('Voltage (V)')
ylabel('Thrust (N)')
title('Thrust vs. Voltage at LQ')
legend('250 K', '298.5 K', '349 K', '399.5 K', '450 K')
figure
loglog(Va,T21,Va,T22,Va,T23,Va,T24,Va,T25)
xlabel('Voltage (V)')
ylabel('Thrust (N)')
title('Thrust vs. Voltage at MQ')
legend('250 K', '298.5 K', '349 K', '399.5 K', '450 K')
figure
semilogy(Tk,C1,Tk,C2,Tk,C3)
xlabel('Temperature (K)')
ylabel('Current (A)')
title('Current vs. Temperature')
legend('LV,LQ', 'LV,HQ', 'MV,MQ')
figure
loglog(Qplot(1:x,1),C6,Qplot(1:x,x/4),C7,Qplot(1:x,x/2),C8,Qplot(1:x,x*3/4),C9,Qplot(1:x,x),C10)
xlabel('Flowrate (m^3/s)')
ylabel('Current (A)')
title('Current vs. Flowrate')
legend('250 K', '298.5 K', '349 K', '399.5 K', '450 K')
figure
plot(Qplot(1:x,1),C11,Qplot(1:x,x/4),C12,Qplot(1:x,x/2),C13,Qplot(1:x,x*3/4),C14,Qplot(1:x,x),C15)
xlabel('Flowrate (m^3/s)')
ylabel('Current (A)')
title('Current vs. Flowrate')
legend('250 K', '298.5 K', '349 K', '399.5 K', '450 K')
%script is for opening and handling the data output from DAQ for

```

```

%Electrospray.
clear;clc;
Tryopen
f=6;
scrsz=get(0,'ScreenSize');
BN={'15 nL/min @ 295 K'; '15 nL/min @ 322 K';
    '30 nL/min @ 295 K'; '30 nL/min @ 322 K';
    '60 nL/min @ 295 K'; '60 nL/min @ 322 K'};
for k=1:f

    R=dlmread(B{k});

    if i < 1; i=1;end;
    Time=R(:,1);
    Voltage=R(:,2);
    Current=R(:,3);
    Pico=R(:,4);
    [row,col]=size(R);
    figure
    plot(Time,Voltage)
    tbeg=input('Starting Index ');close;
    [mindif,beg]=min(abs(Time-tbeg));
    Current2=Current-4.34e-9;
    Current2=Current2*1.e3;
    figure('Position',[1 scrsz(4)/4 scrsz(3)*.85 455]);
    NCax=subplot(2,1,1);
    plot(Time(beg:row),Current2(beg:row),Time(beg:row),Pico(beg:row)
    title(BN{k});ylabel('Current (A)');
    Vax=subplot(2,1,2); plot(Time(beg:row),Voltage(beg:row))
    title('Pico Current & Voltage vs. Time'); ylabel('Voltage (V)');
    linkaxes([NCax Vax], 'x');
    CM(k)=mean(Current2);
    PM(k)=mean(Pico);
end

fid=fopen('Files.txt','r');
A=textscan(fid, '%s', 'whitespace');
B(1,:)=A{1};
fclose(fid);

HAC=[-3.577e-7;      %Average negative current recorded, (C/s)
     -4.025e-7;
     -3.468e-7;
     -4.018e-7;
     -3.156e-7;
     -3.27e-7];
HAC2=[6.5e-6; 5e-6;
      8e-6; 1e-5;
      7e-6; 8e-6];

Thac=[295.15; 322.15]; %Temperture HAC was taken at

HACcal=1e-7*[-1.6707; -2.8752;
             -2.3627; -4.0602;
             -3.3414; -5.7505]; %Calcualtion from script, (C/s)

```

```

Tplot=(250:450);
Gplot=gammaft(Tplot); Rplot=rhoft(Tplot); Kplot=Kft(Tplot);
figure
plot(Tplot,Gplot./Gplot(1),Tplot,Rplot./Rplot(1));
title('Surface Tension and Density vs Temperature');
xlabel('Temperature (K)'); ylabel('Normalized Variable');
legend('Surface Tension', 'Density');
figure
plot(Tplot,Kplot./Kplot(1));
title('Electrical Conductivity vs Temperature');
xlabel('Temperature (K)'); ylabel('Normalized Conductivity');

figure
plot(Thac,HAC(1:2,1),'-o',Thac,HAC(3:4,1),'-o',Thac,HAC(5:6,1),'-
o',Thac,HACcal(1:2,1),Thac,HACcal(3:4,1),Thac,HACcal(5:6,1))
title('Current vs Temperature');
xlabel('Temperature (K)');
ylabel('Current (A)');
legend('15 nL/min', '30 nL/min', '60 nL/min', 'Cal 15 nL/min', 'Cal 30
nL/min', 'Cal 60 nL/min');
figure
plot(Thac,HAC2(1:2,1),'-o',Thac,HAC2(3:4,1),'-o',Thac,HAC2(5:6,1),'-o',Thac,-
HACcal(1:2,1),Thac,-HACcal(3:4,1),Thac,-HACcal(5:6,1))
title('Current vs Temperature');
xlabel('Temperature (K)');
ylabel('Current (A)');
legend('15 nL/min', '30 nL/min', '60 nL/min', 'Cal 15 nL/min', 'Cal 30
nL/min', 'Cal 60 nL/min');

clear;close all; clc;
x=1000;
T=linspace(350,700,x);Q=5e-13;
for i=1:x;
    P(i)=HT(T(i),Q);
    CT(i)=Q*rhoft(T(i)).*P(i);
end

figure
plot(T,P); title('Current to Mass Ratio vs Temperature')
figure
plot(T,CT);
title('Current vs Temperature'); xlabel('Temperature (K)');ylabel('Current
(A)')

```



Temperature Effects on Electrospray Performance

16 Mar '11

1st Lt Nicholas Kreitingner
Space Propulsion Branch
Air Force Research Laboratory



DISTRIBUTION STATEMENT A. Approved for public release; distribution unlimited.



Overview



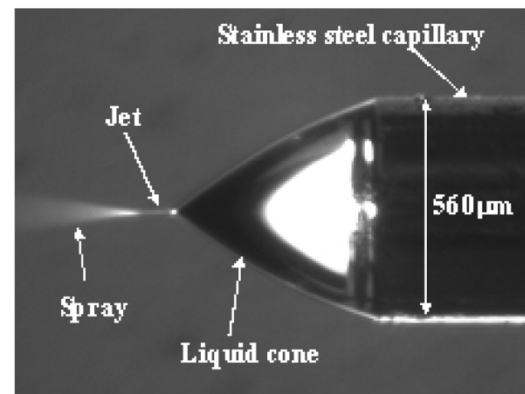
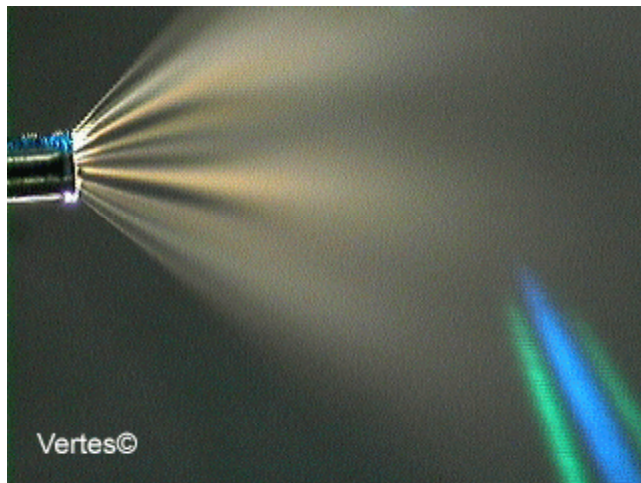
- **Introduction to Electrospray Thrusters**
- **Model Development**
- **Code Results**
- **Experiment Setup**
- **Experiment Results**
- **Future work**
- **Conclusion**



Electrospray



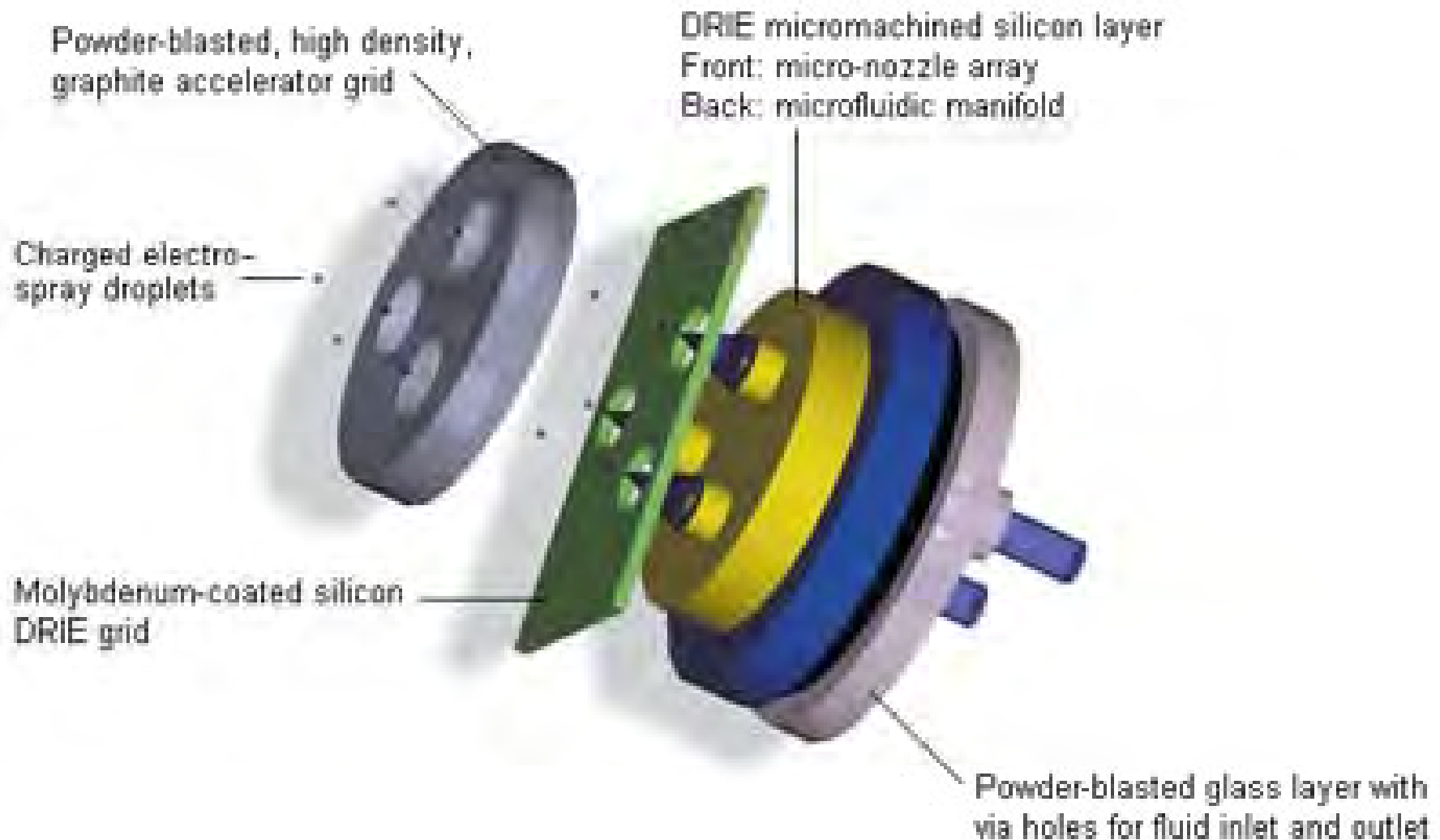
- Taylor Cones
 - Electric field stresses liquid
 - Jet formation
 - Ion vs. Droplets



Taylor Cone; Left colored by electric potential, Right colored by electric field magnitude



Electrospray Thrusters





Equations

- Rayleigh limit

$$q = 8\pi\sqrt{\epsilon_0\gamma}R^3$$

$$m = \rho V$$

$$V = \frac{4}{3}\pi\left(\frac{D}{2}\right)^3$$

- Charge to mass ratio

$$\frac{q}{m} = \frac{12\sqrt{2}}{\rho} \sqrt{\frac{\epsilon_0\gamma}{D^3}}$$

- Minimum Flow rate

$$Q_{\min} = \frac{\gamma K \epsilon_0}{\rho K}$$

- Droplet Diameter

$$R_K = \sqrt[3]{\frac{\epsilon_0 Q}{K}}$$

$$D \leq 3.3R_K$$

- Specific Thrust

$$I_{sp} = \frac{1}{g} \sqrt{2 \frac{q}{m} V_a}$$

- Thrust

$$T = \dot{m}u_e = g\dot{m}I_{sp}$$



MATLAB Code



➤ Temperature

➤ $\gamma(T)$

➤ $k(T)$

➤ $\rho(T)$

➤ Q_{min}

➤ $K(T)$

➤ R_k

➤ D_d

➤ Voltage

➤ I_{sp}

➤ T



BMiM BF₄ Properties

- 1-butyl-3-methylimidazolium tetrafluoroborate
- Density: 1215.43-1163.6 kg/m³
(278-353 K)
- Surface Tension Coefficient: 0.04529-0.0403 N/m
(284-360 K)
- Electrical conductivity: 0.00212-10.94 1/(Ohm m)
(238-463 K)
- Electrical permittivity: 11.7



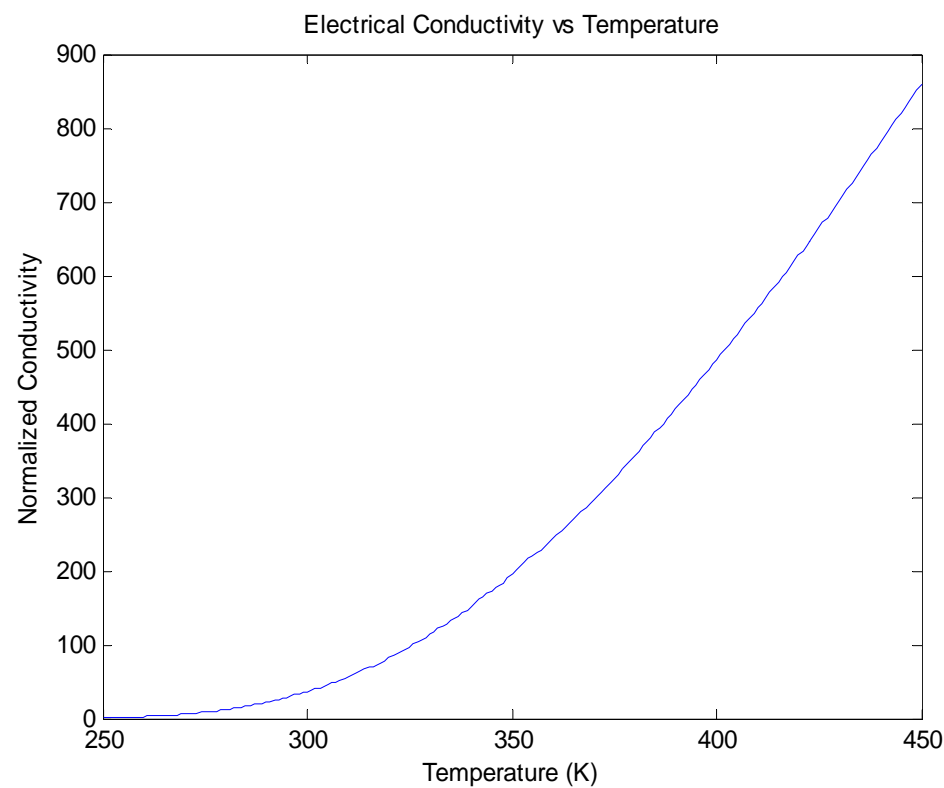
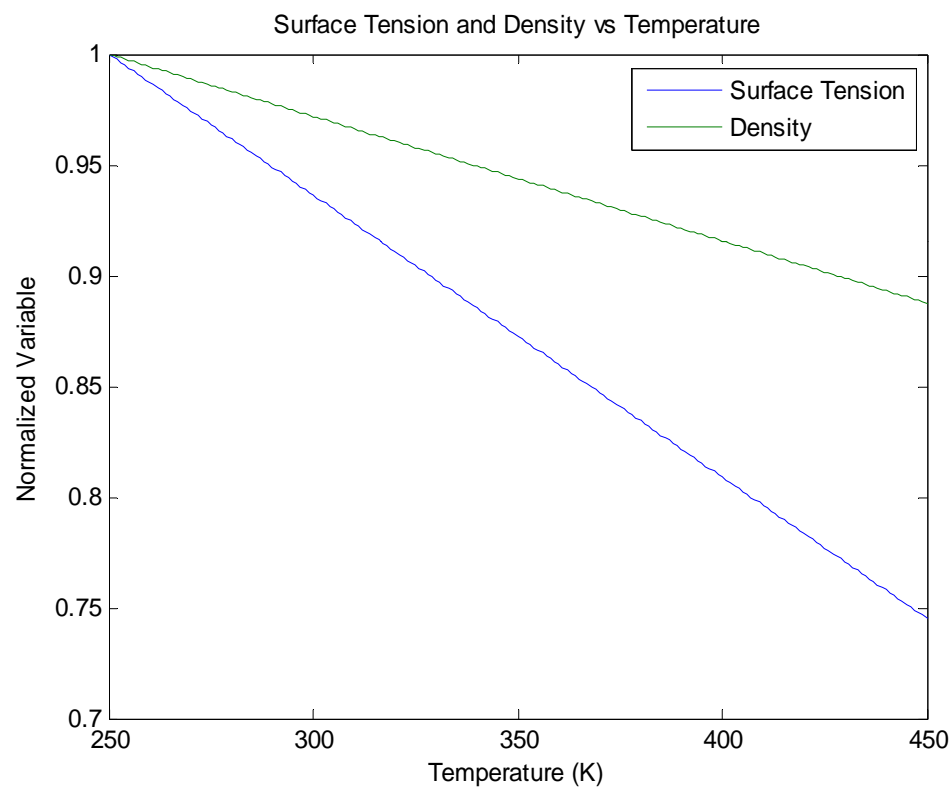
Code Results



- **MATLAB program, estimate**
 - **Thrust**
 - **Specific Thrust**
 - **Current**

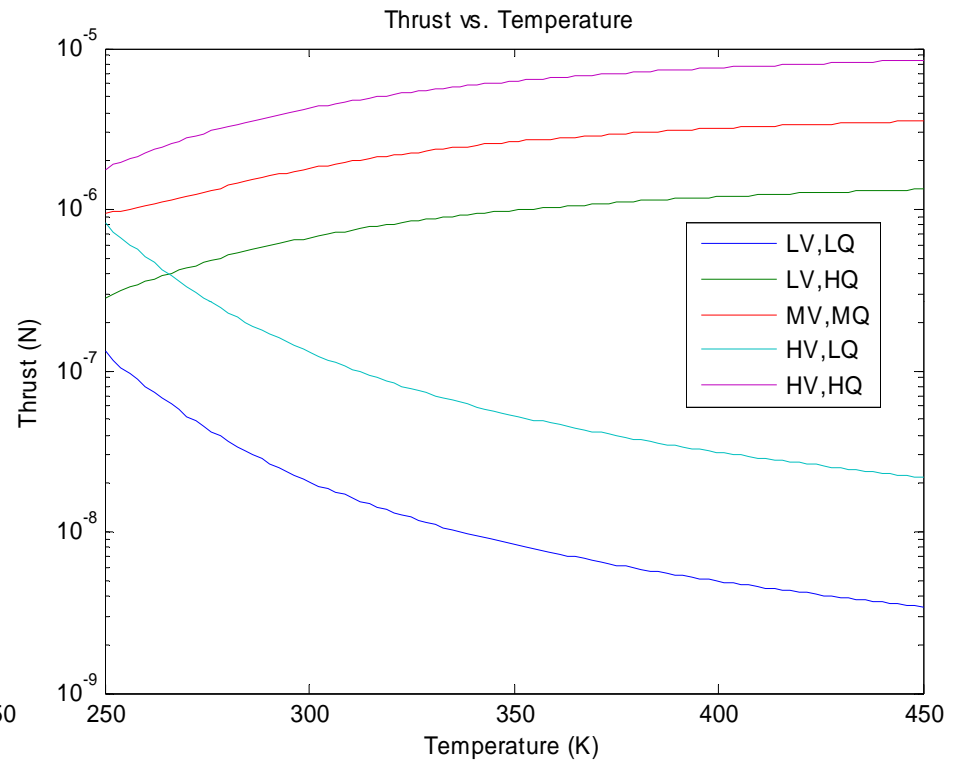
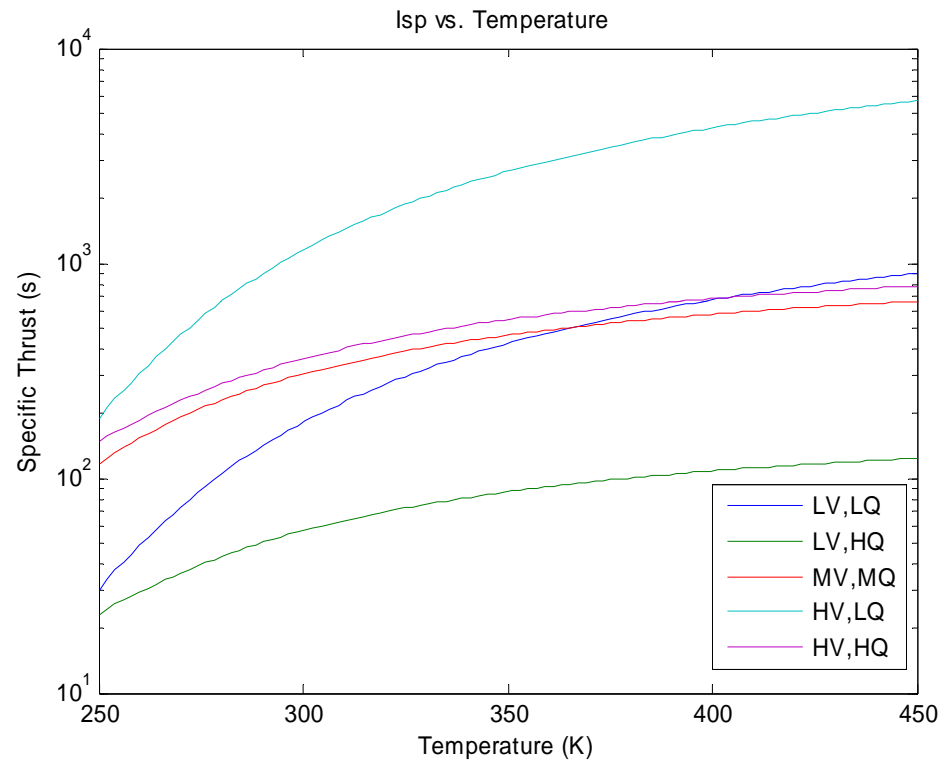


Physical Property Thermal Response



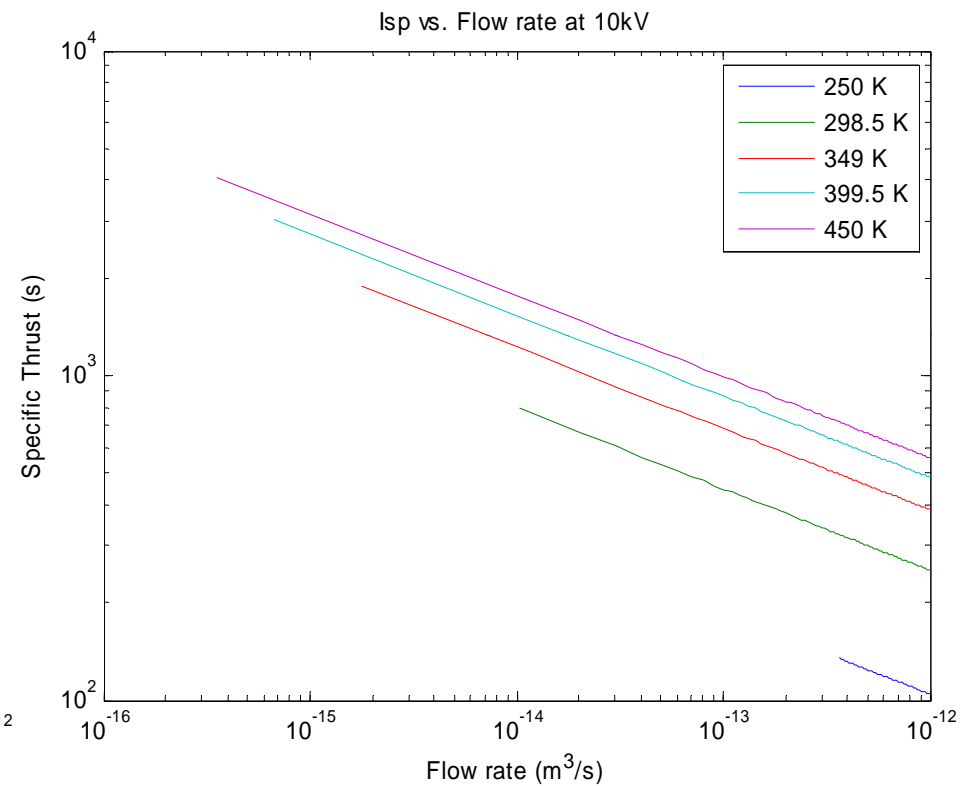
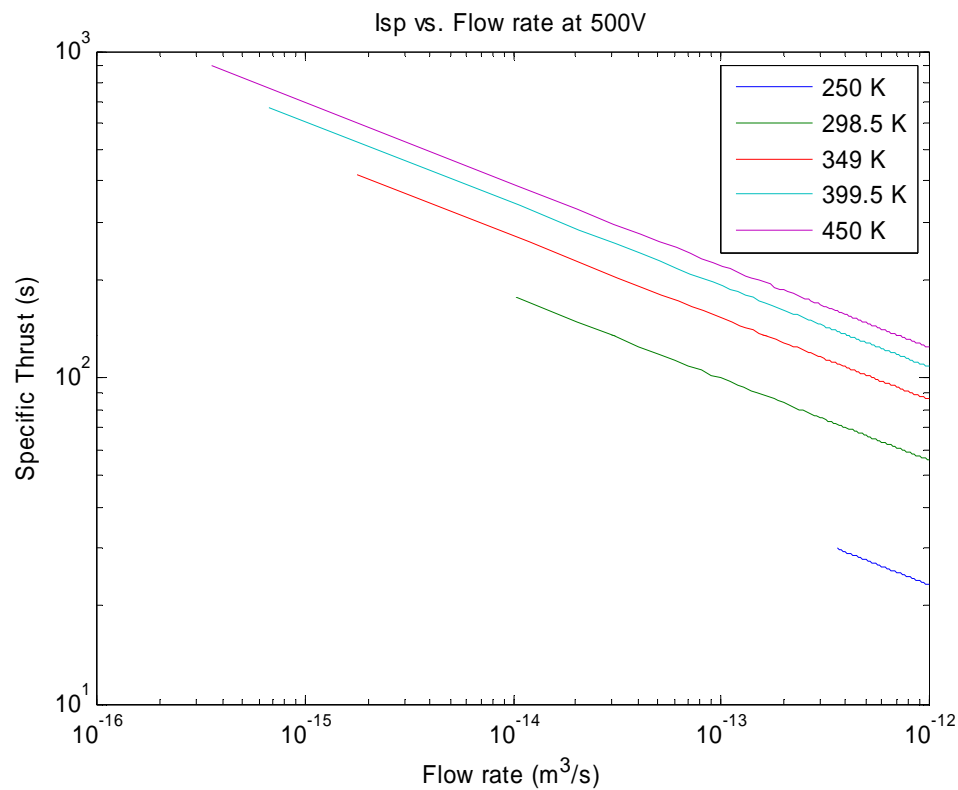


Performance Thermal Response



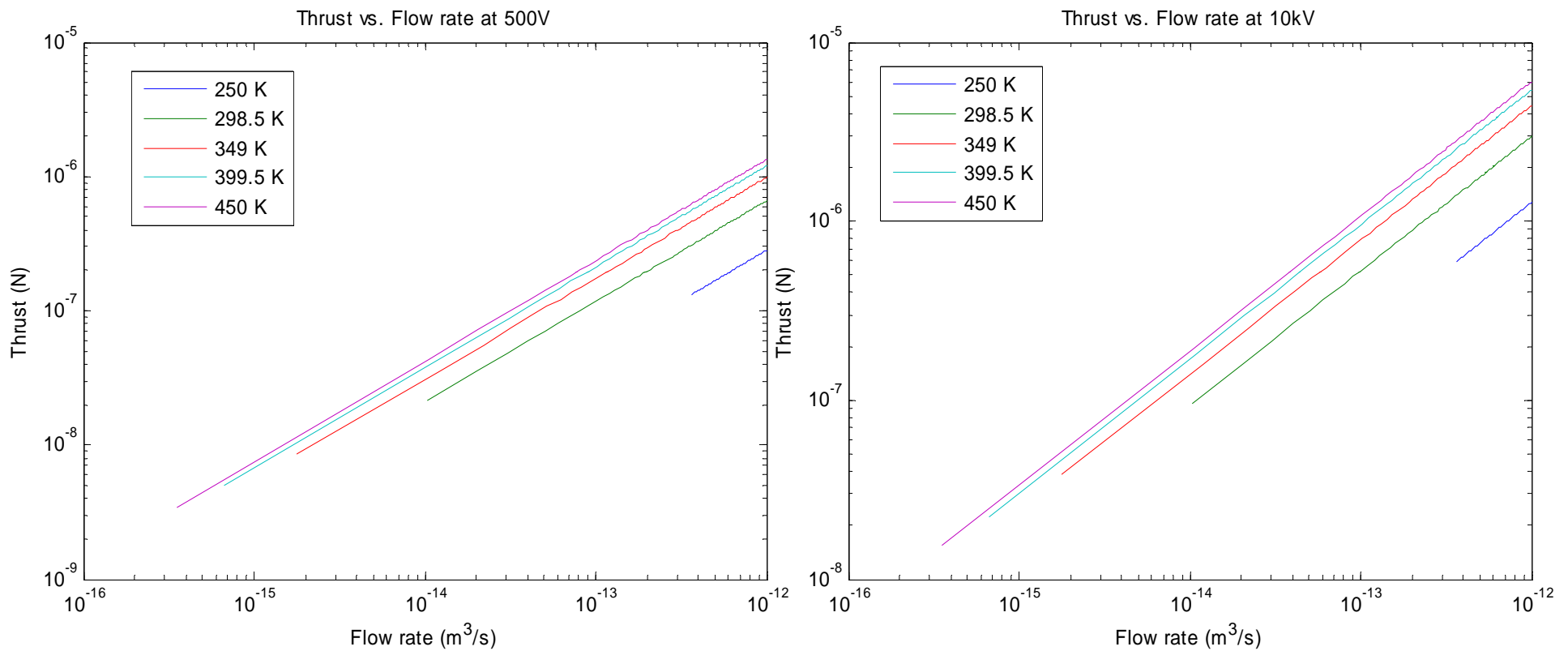


Specific Thrust Thermal Response



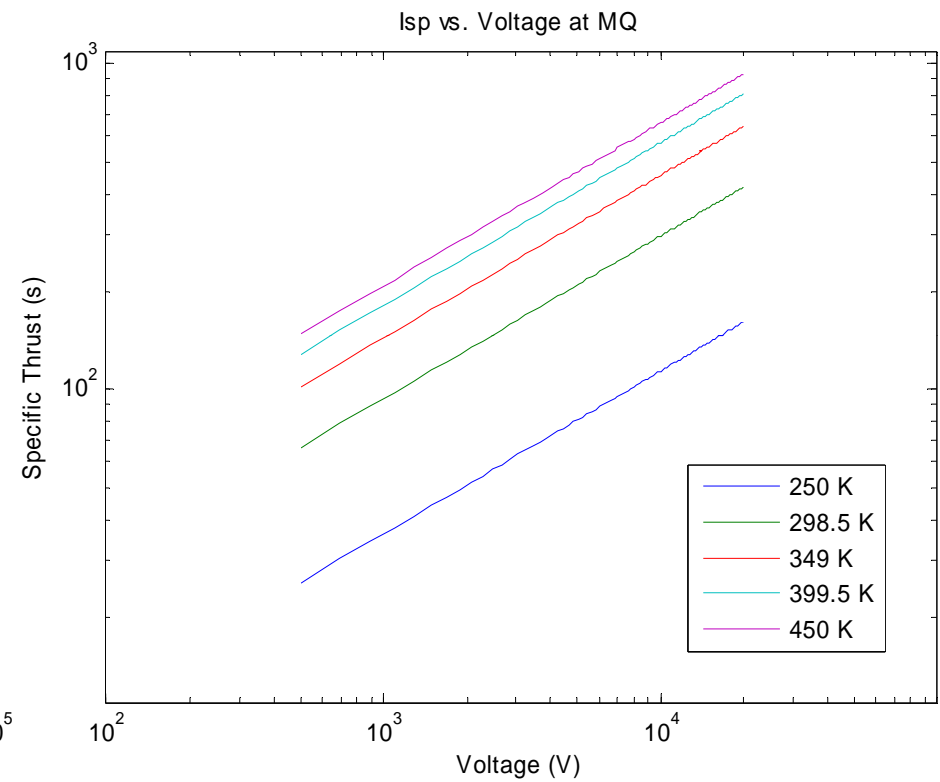
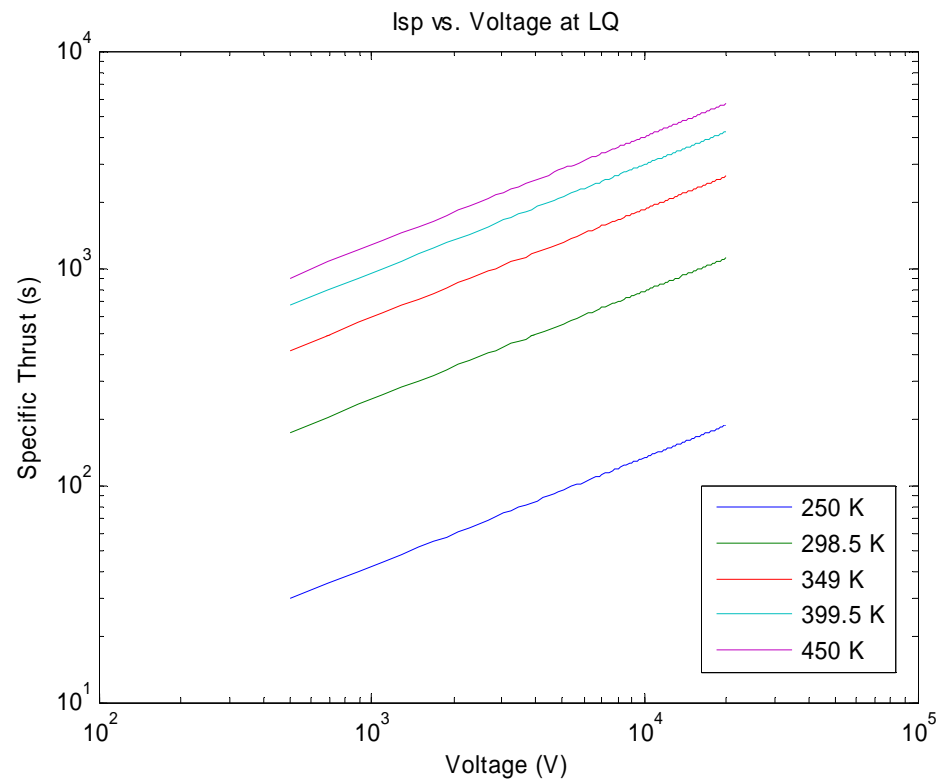


Thrust's Thermal Response



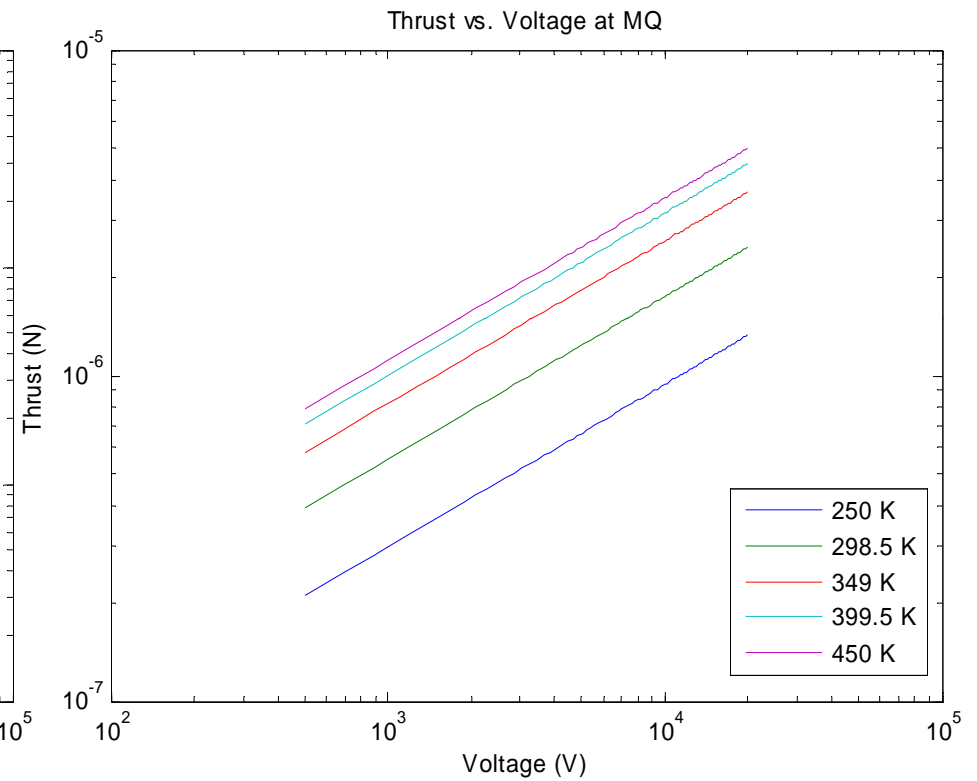
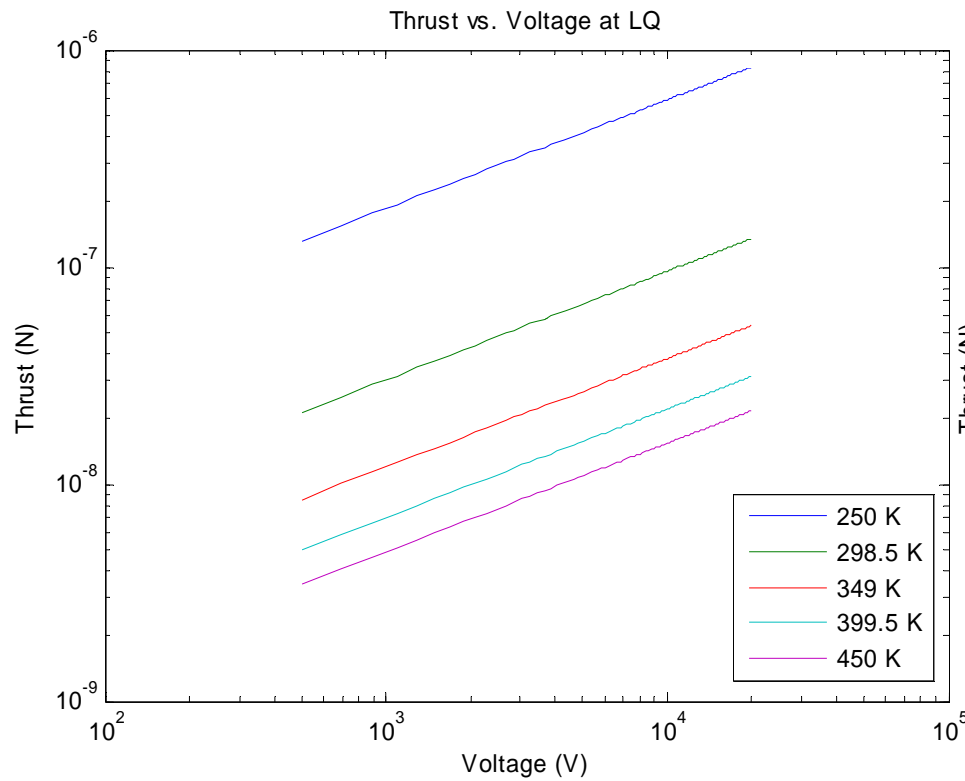


Isp vs. Voltage



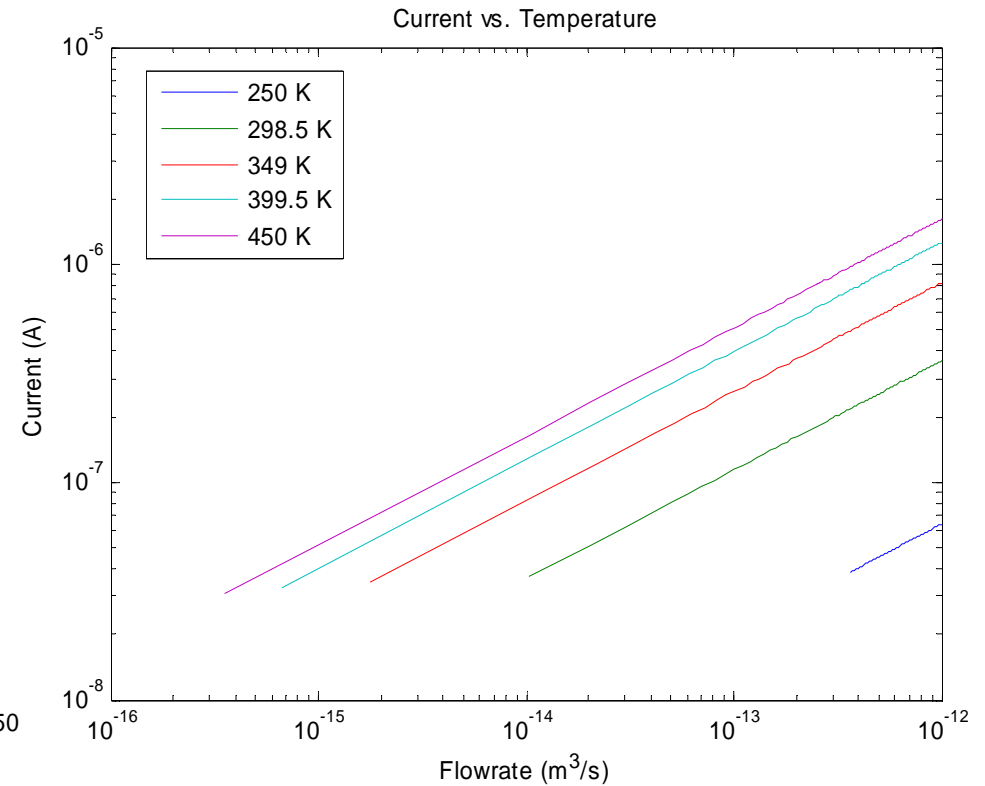
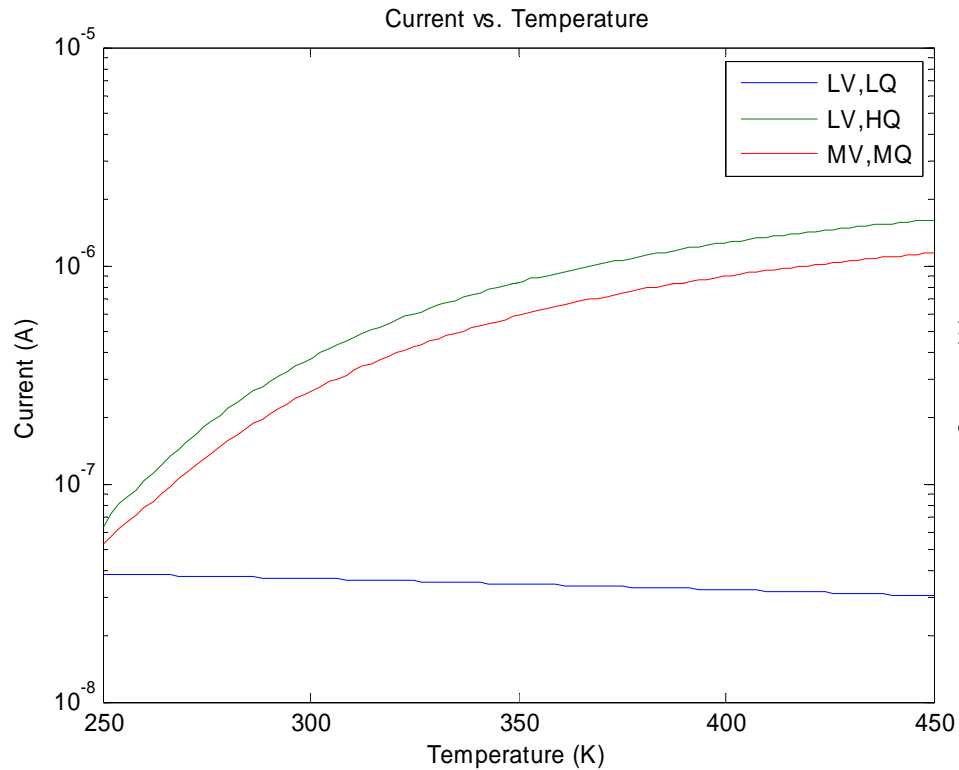


Thrust vs. Voltage



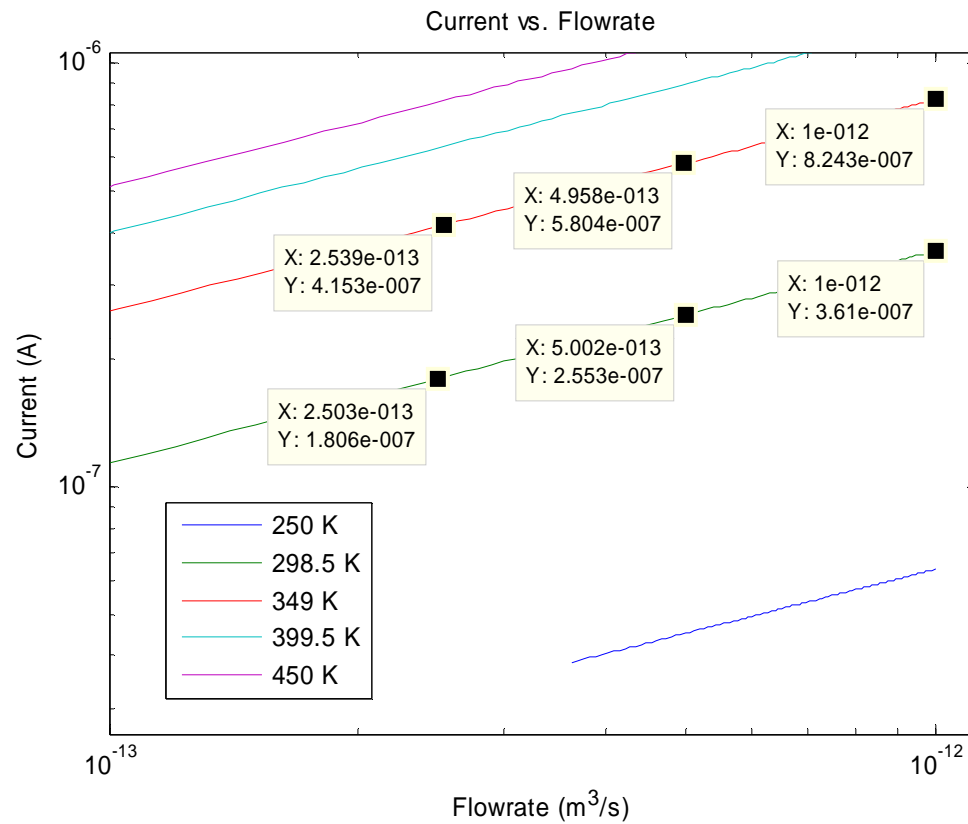


Current Thermal Response



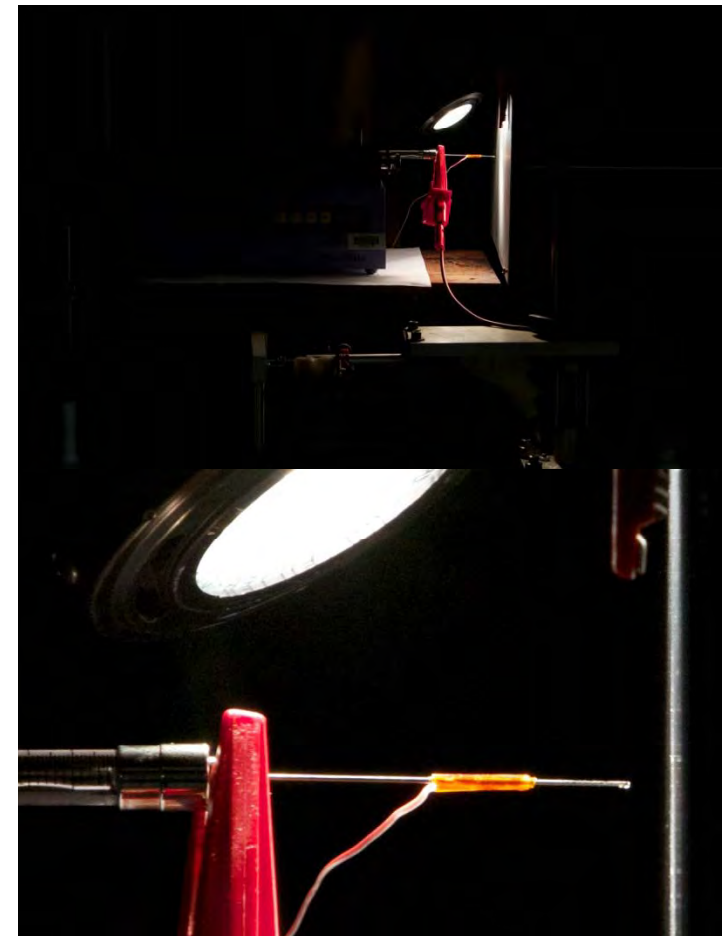
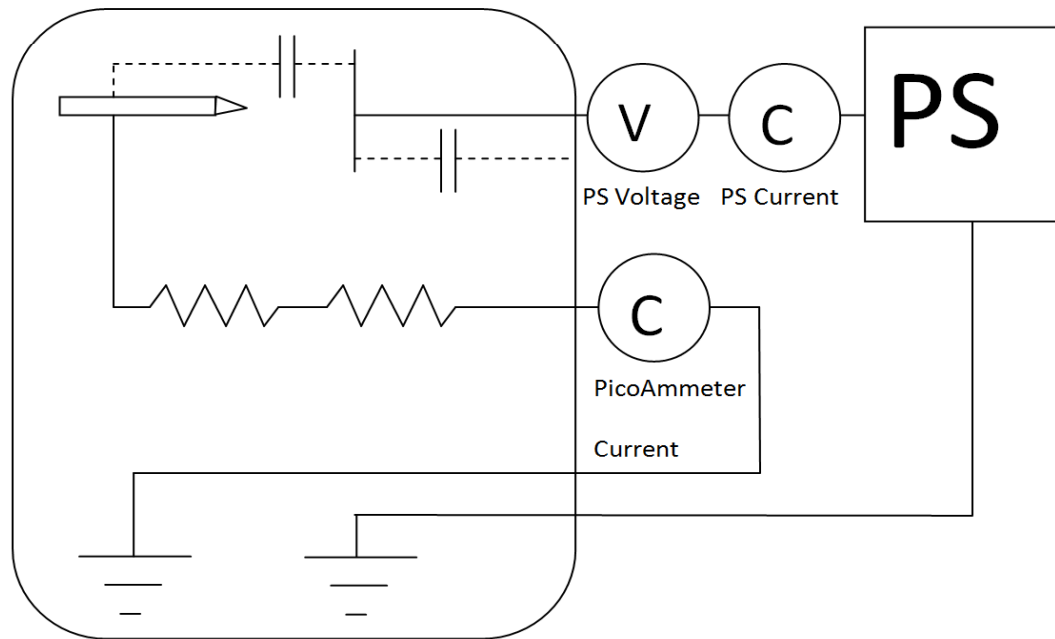


Test Matrix





Experiment Setup





Equipment



- 250 microliter syringe and 22s needle (Hamilton Company)
- Harvard Apparatus Pico Pump
- BK Precision 2MHz function generator
- Trek Model 10/10B High Voltage Amplifier
- Agilent 6 ½ Digit Multimeters
- Keithley Picoammeter/Voltage Source
- Tektronix DMM916 True RMS fluke meter
- J Type Thermocouple
- LabView
- Incandescent Lamp



Electrospray Movie

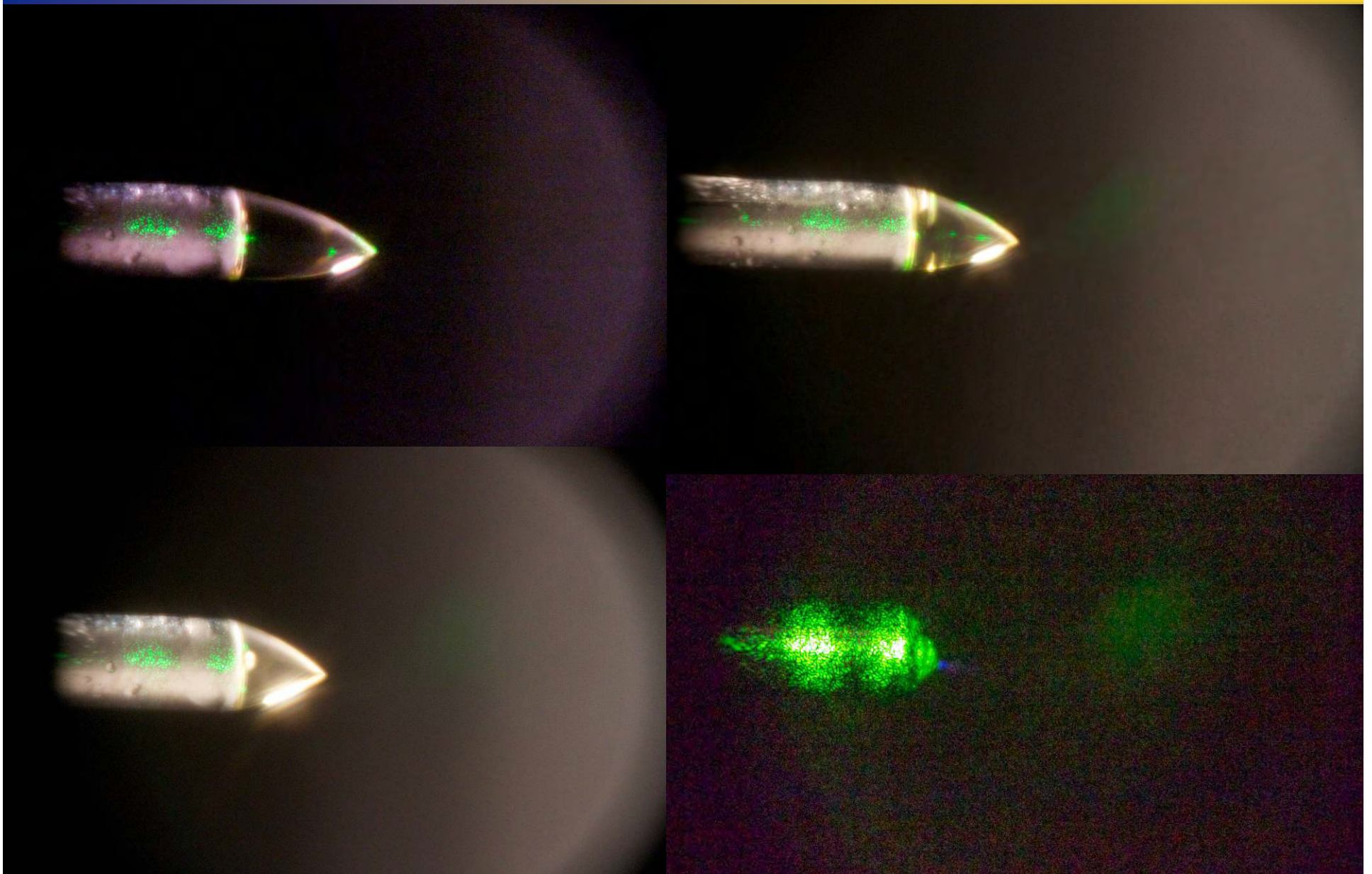


[Electrospray movie 1](#)

[Electrospray movie 2](#)



Taylor Cone modes



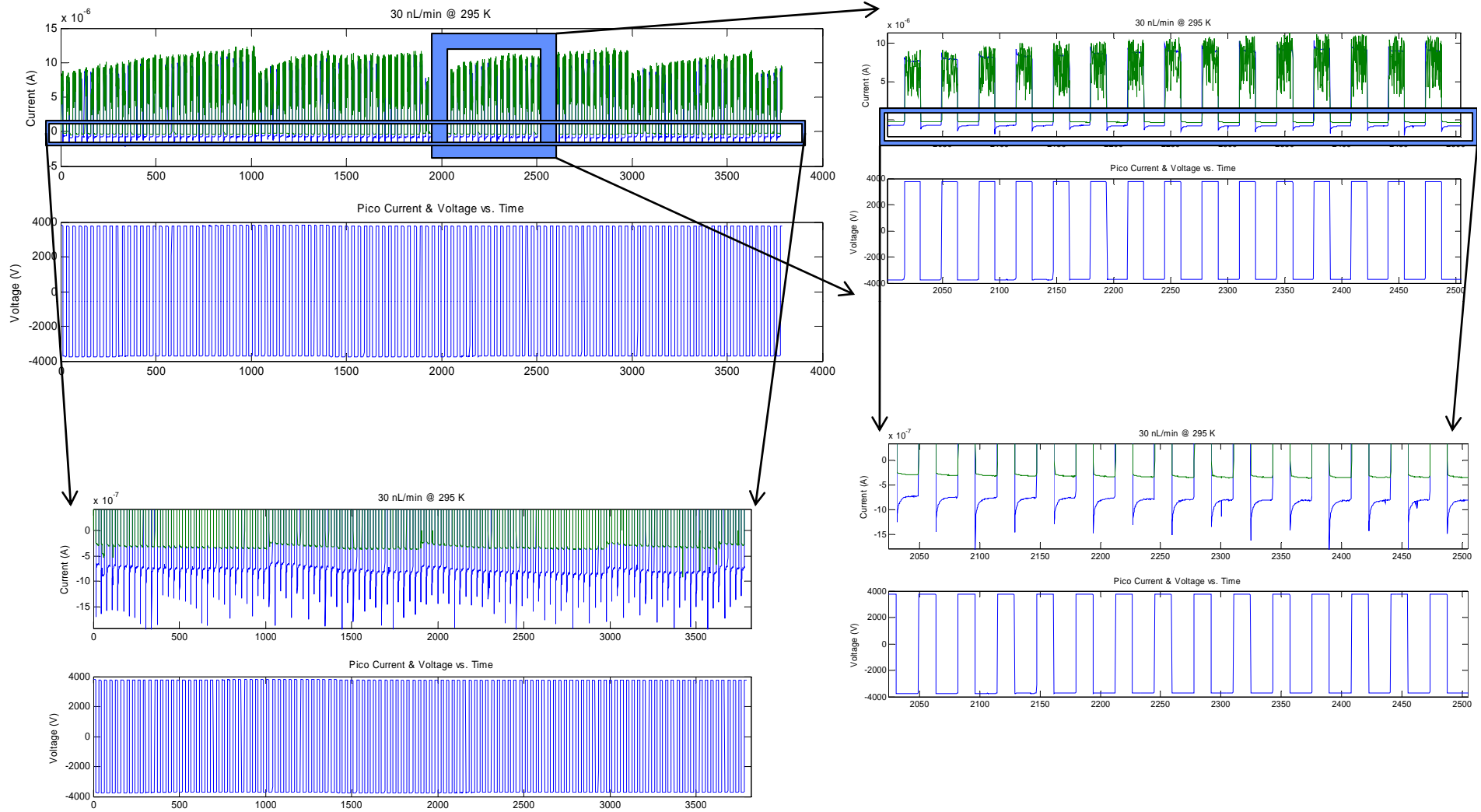


Glow Discharge



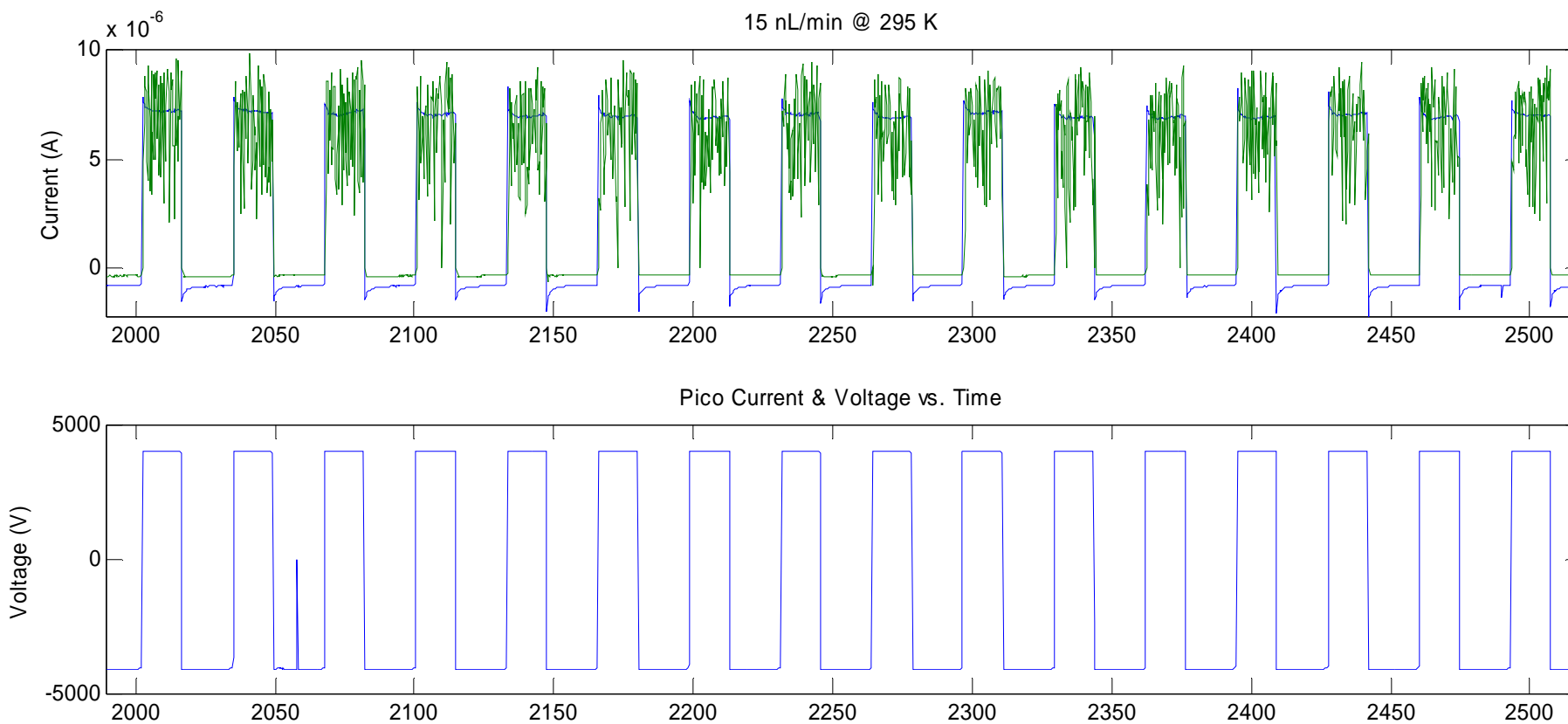


Graph Overview





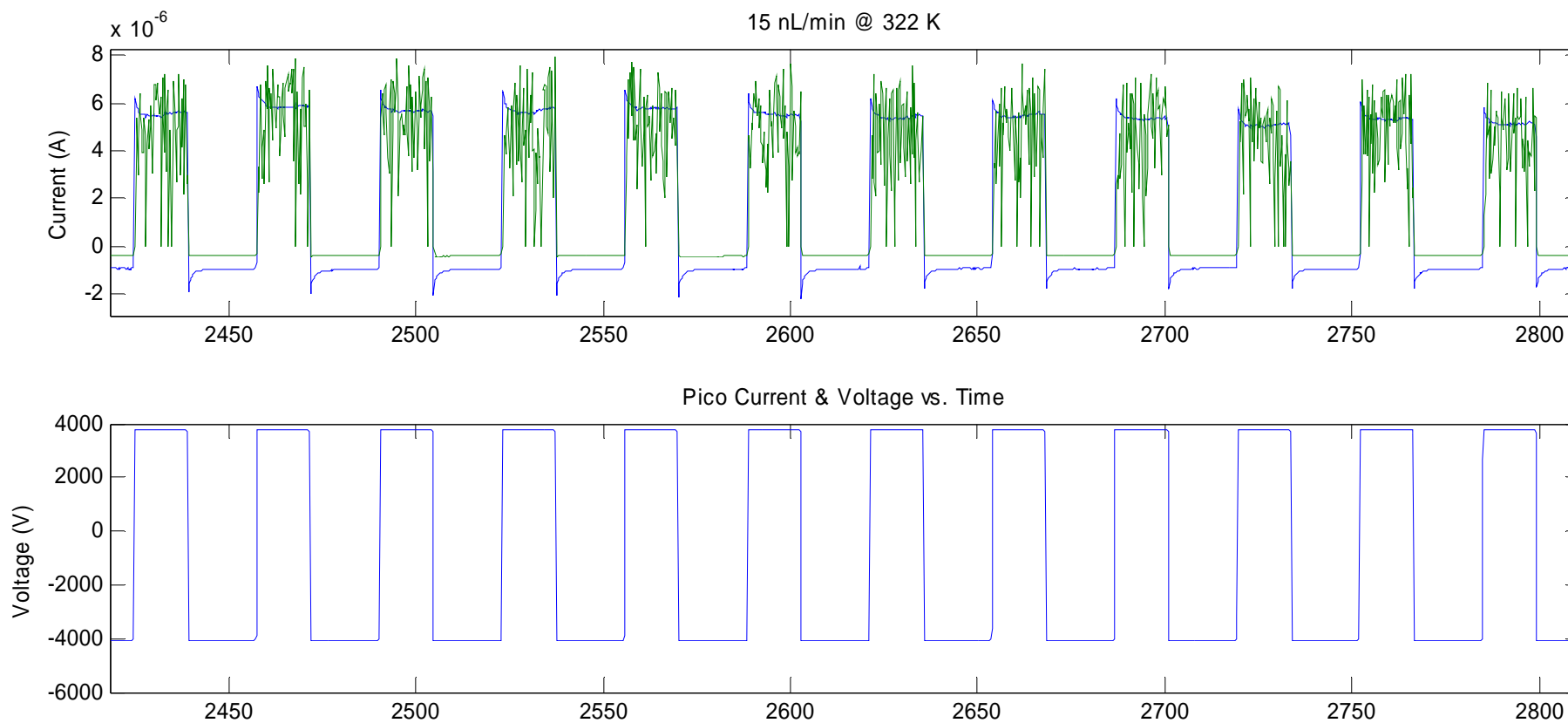
15 nL/min @ 22 °C



DISTRIBUTION A. Approved for public release; distribution unlimited.



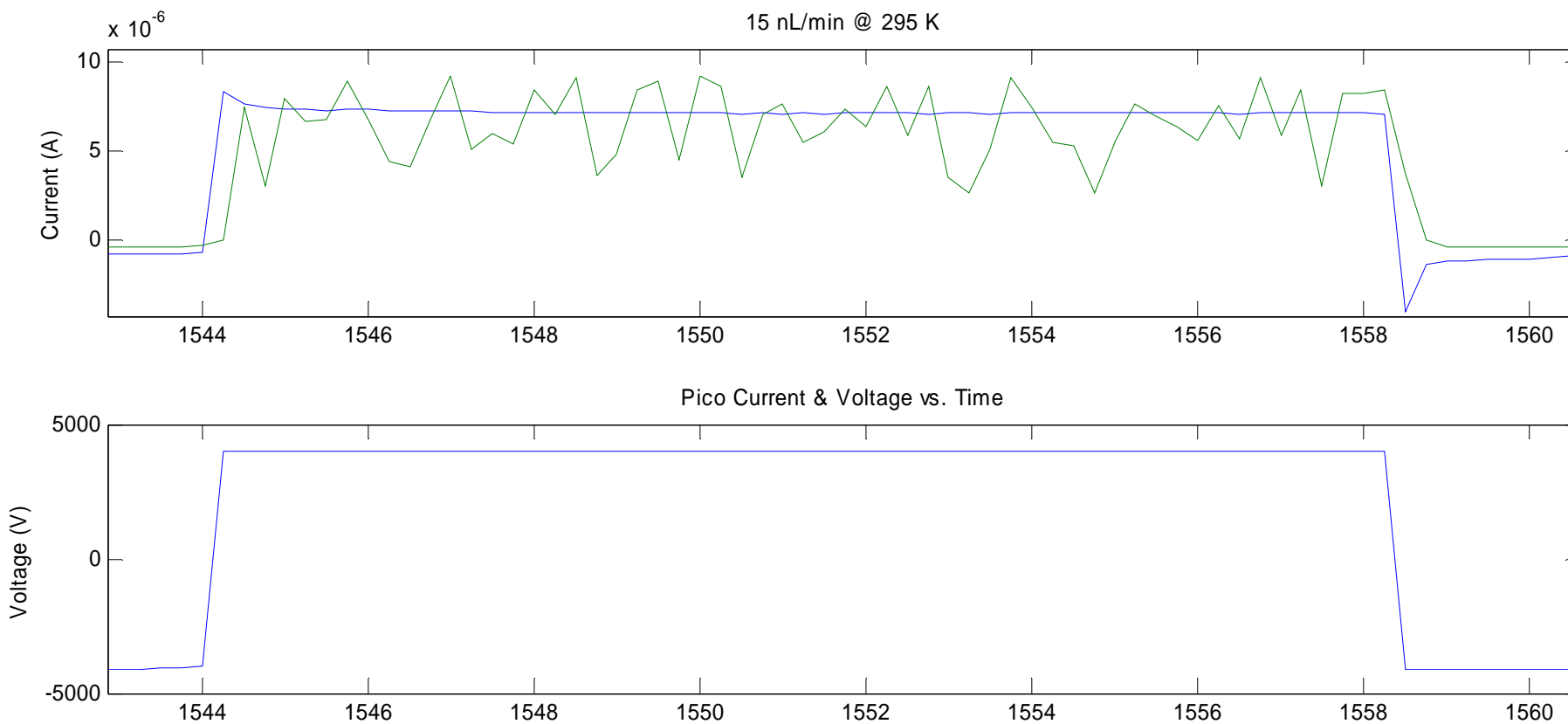
15 nL/min @ 49 °C



DISTRIBUTION A. Approved for public release; distribution unlimited.

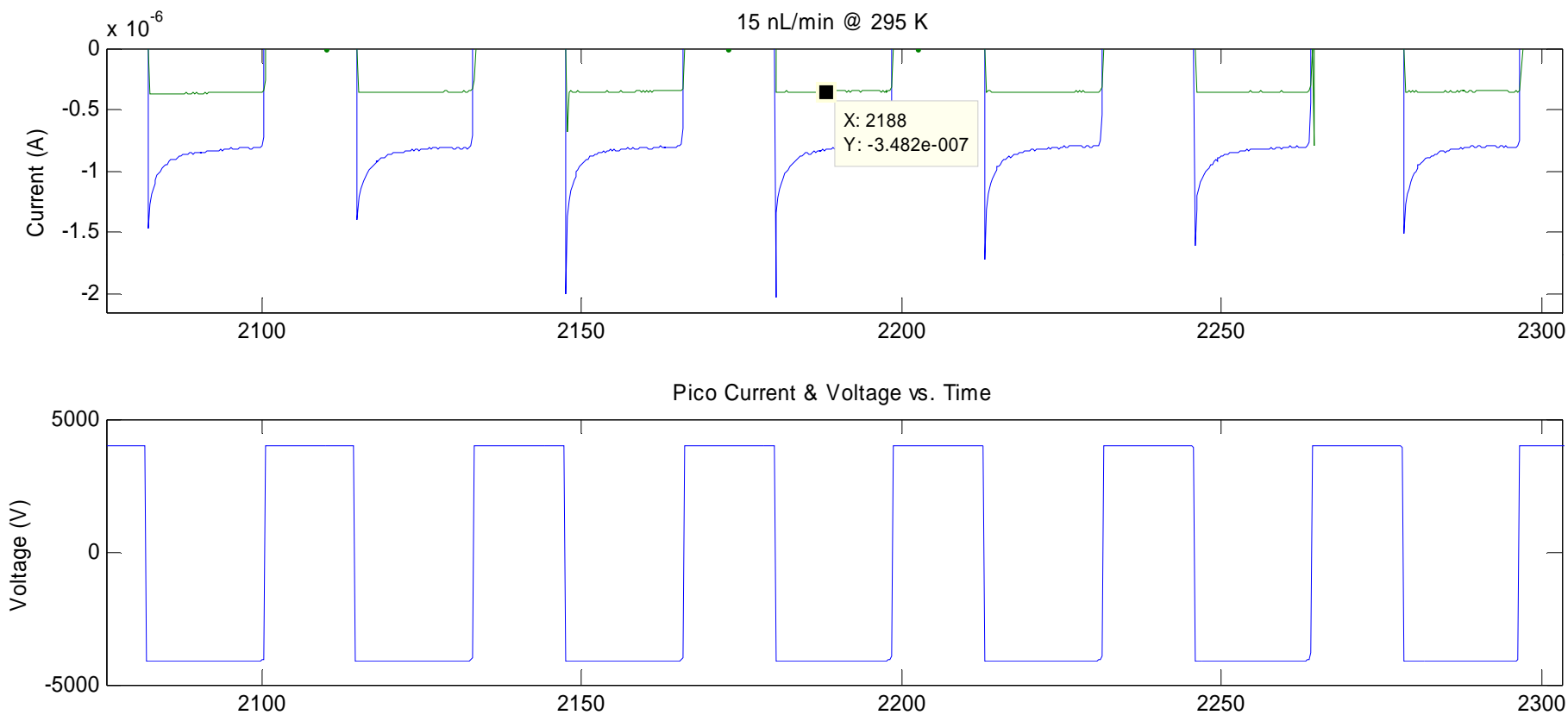


Oscillations



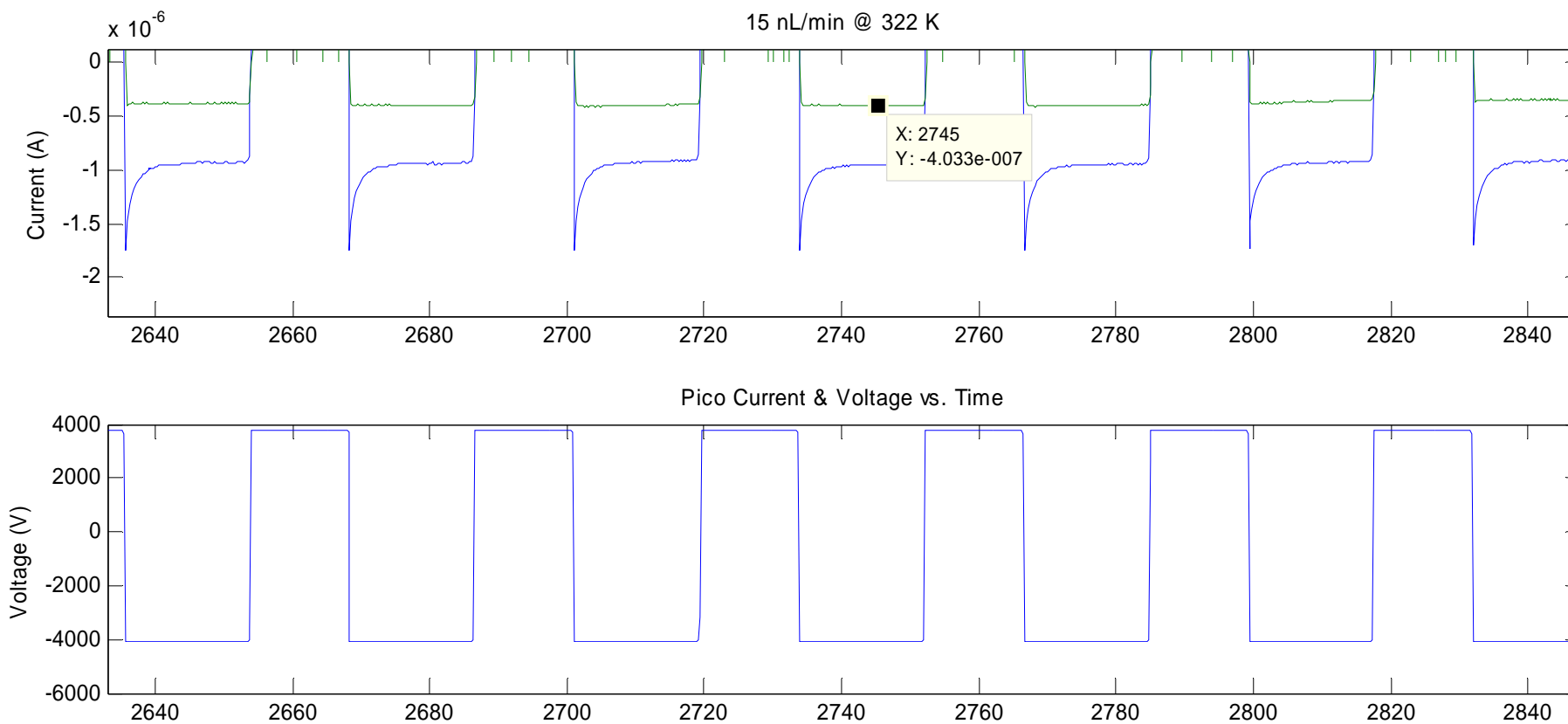


15 nL/min @ 22 °C



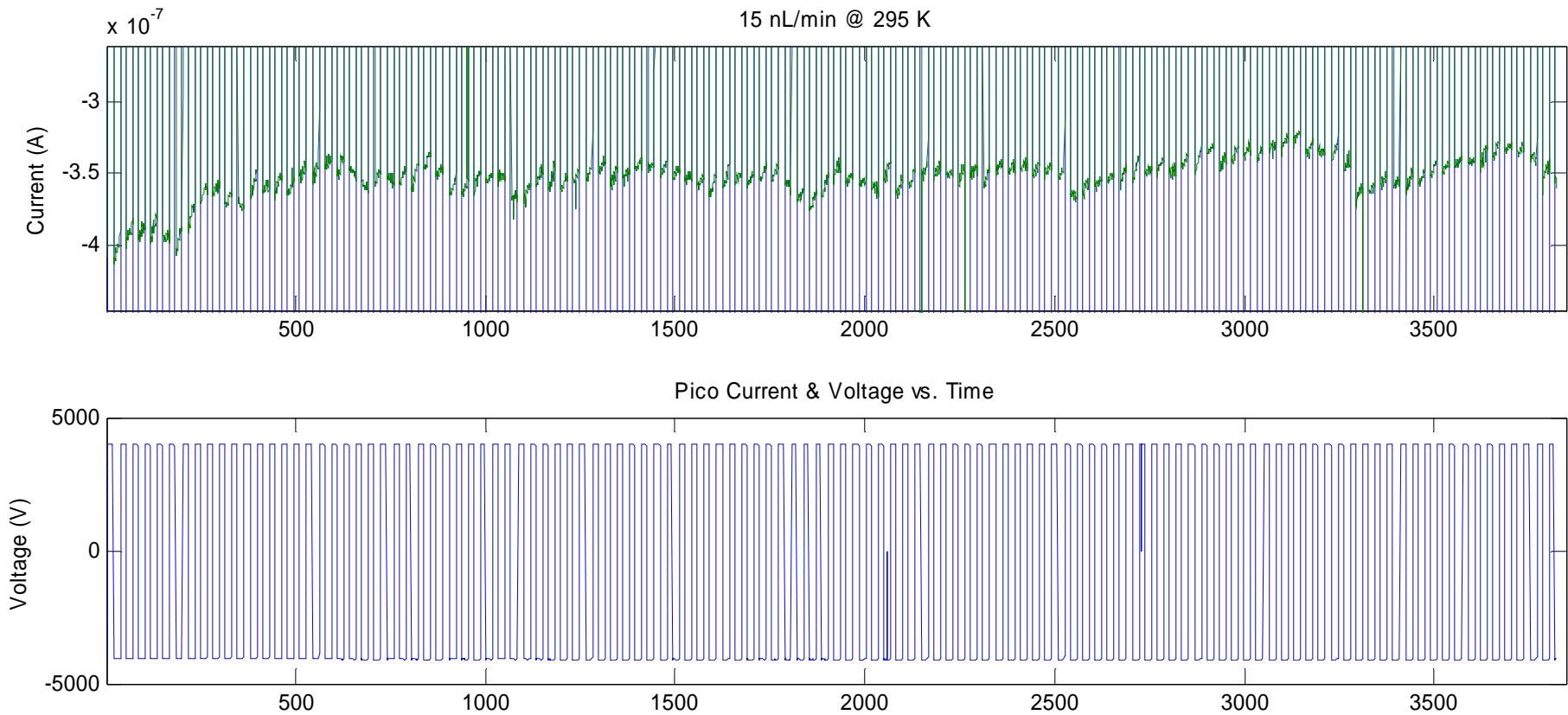


15 nL/min @ 49 °C



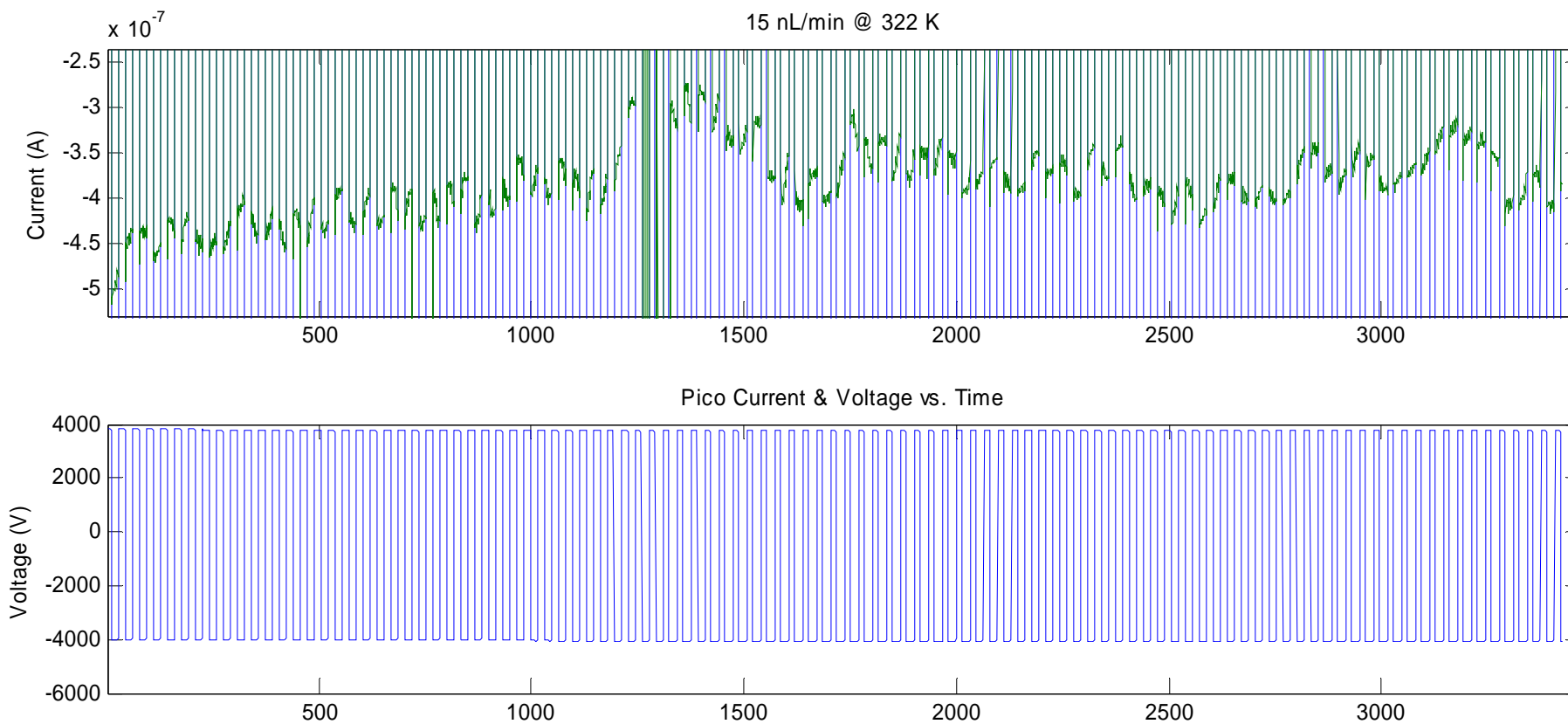


15 nL/min @ 22 °C





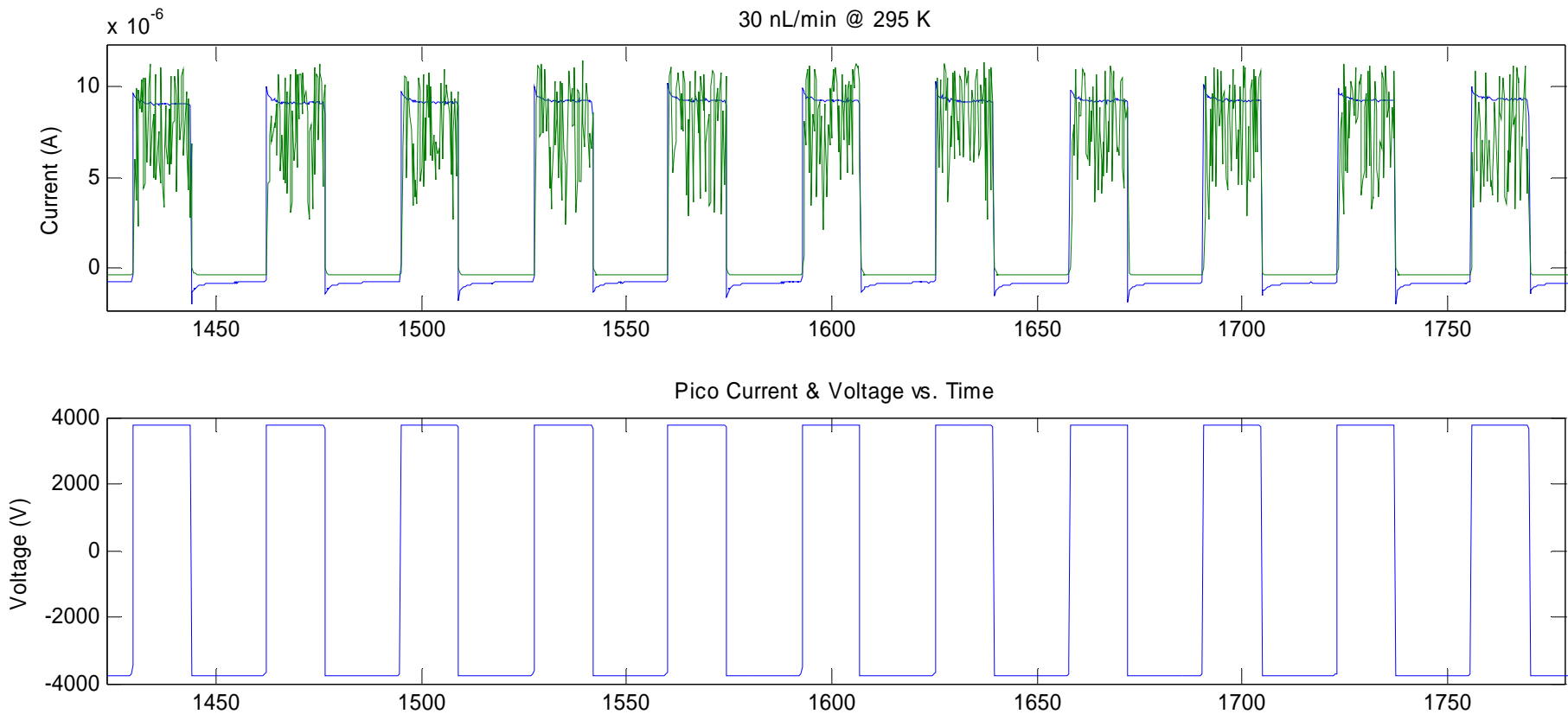
15 nL/min @ 49 °C



DISTRIBUTION A. Approved for public release; distribution unlimited.

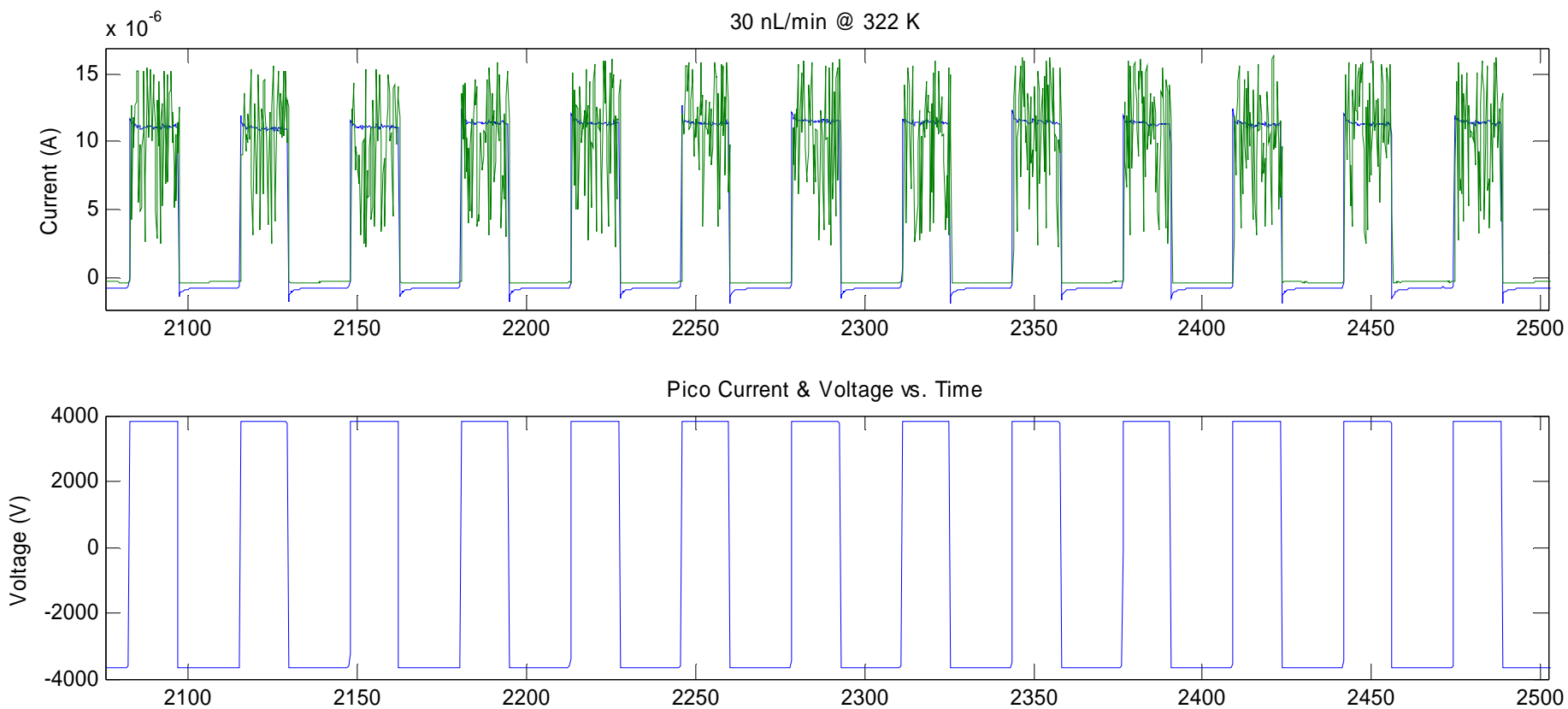


30 nL/min @ 22 °C





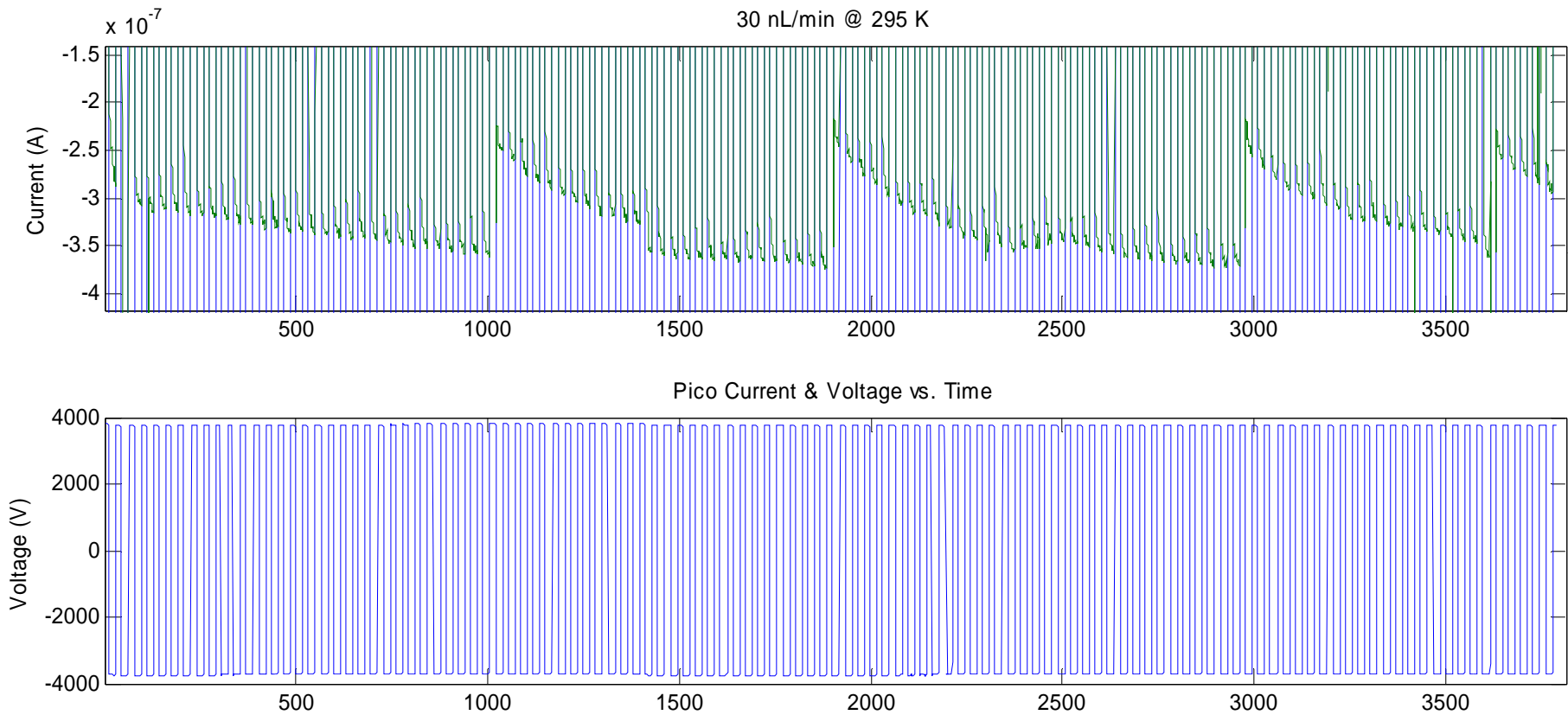
30 nL/min @ 49 °C



DISTRIBUTION A. Approved for public release; distribution unlimited.



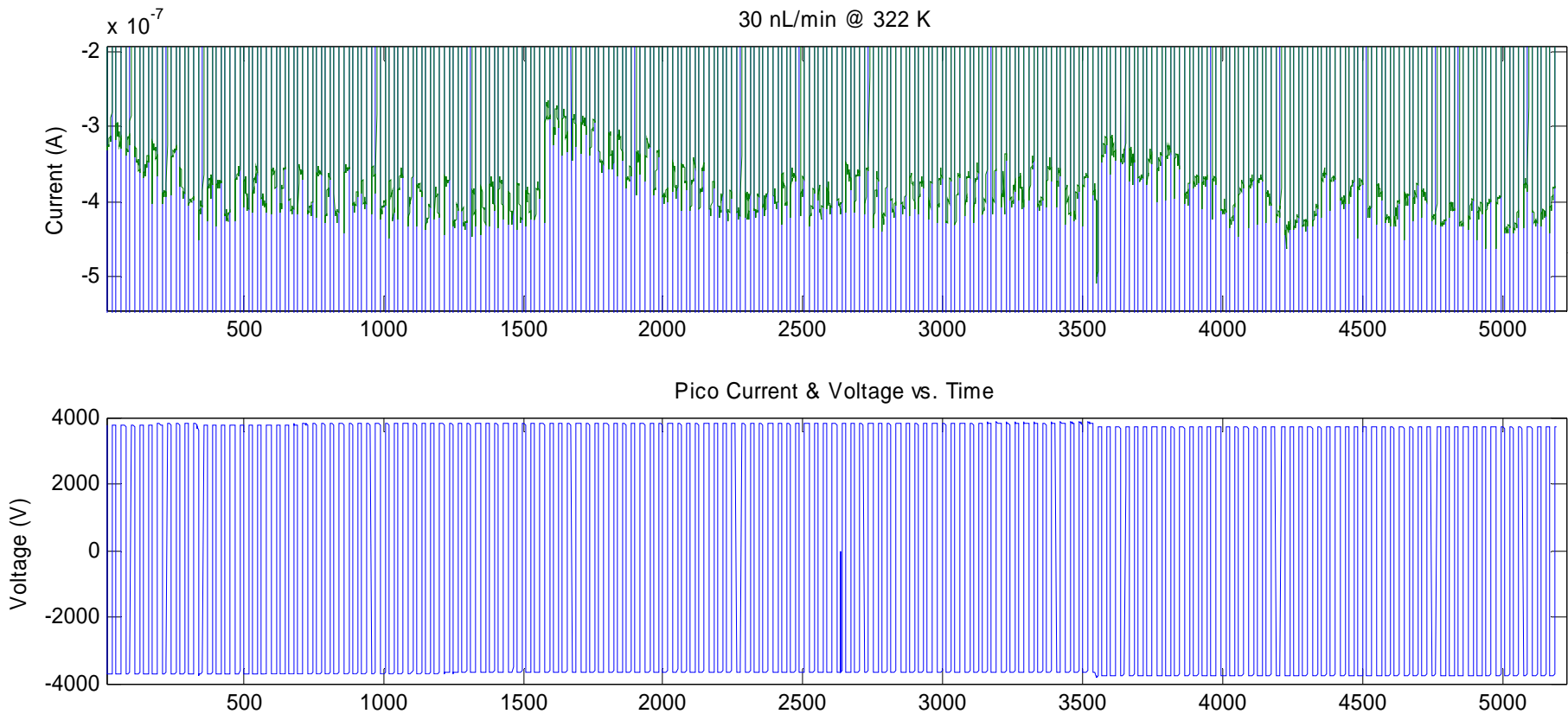
30 nL/min @ 22 °C



DISTRIBUTION A. Approved for public release; distribution unlimited.



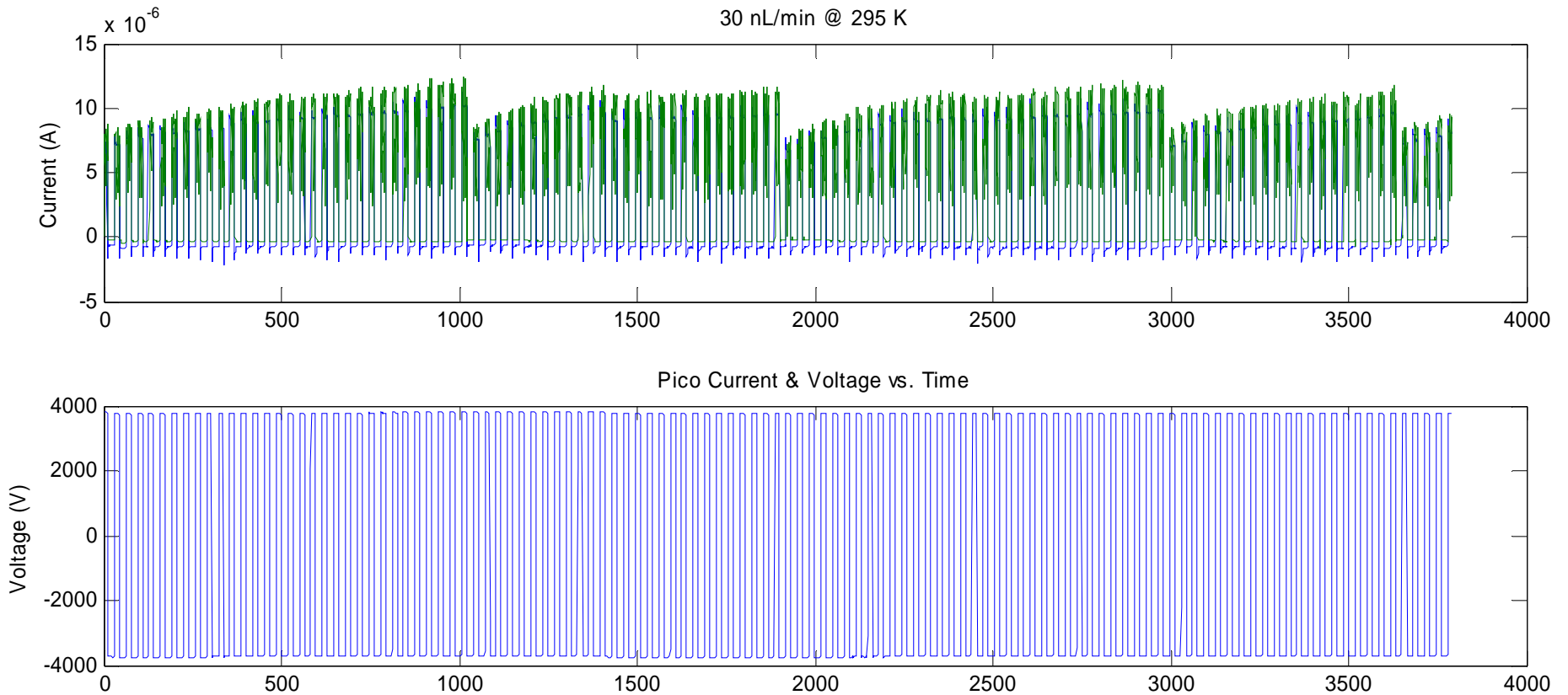
30 nL/min @ 49 °C



DISTRIBUTION A. Approved for public release; distribution unlimited.



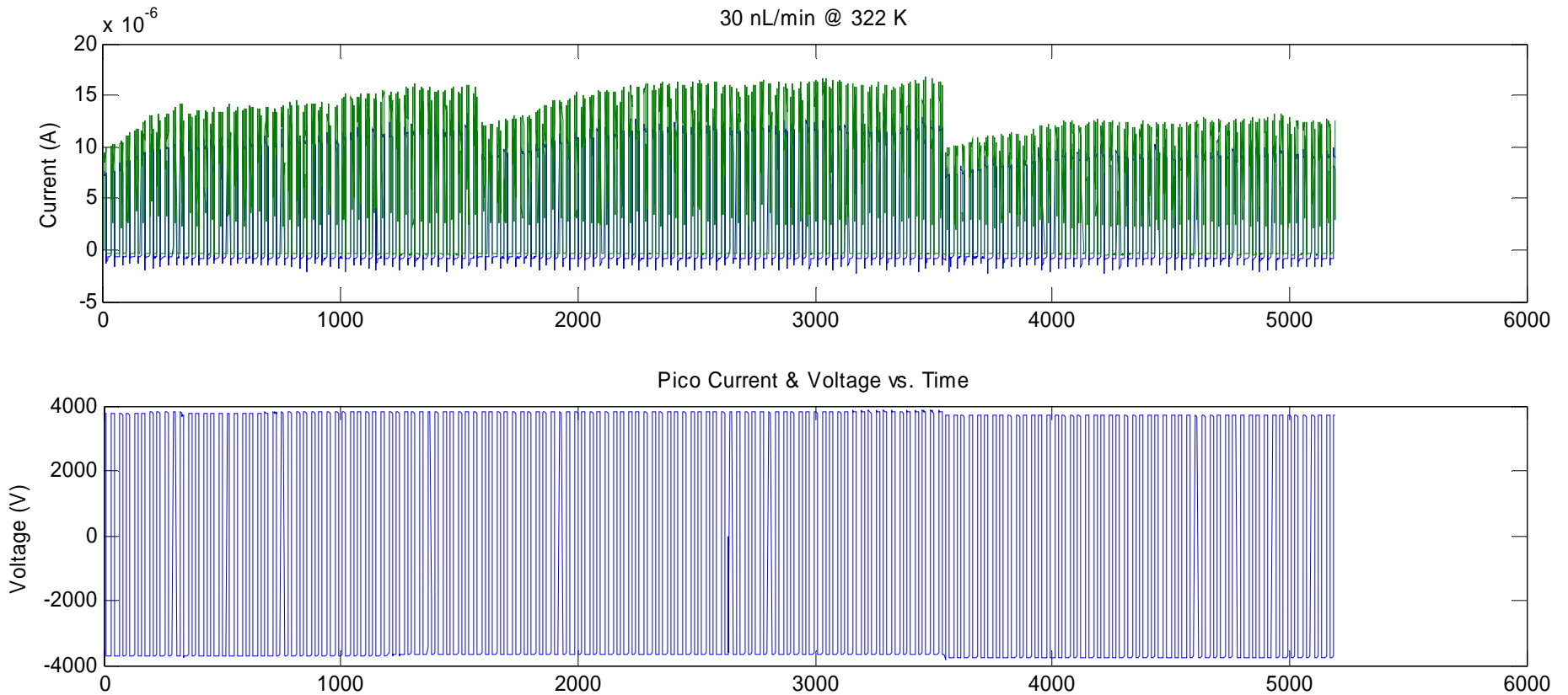
30 nL/min @ 22 °C



DISTRIBUTION A. Approved for public release; distribution unlimited.



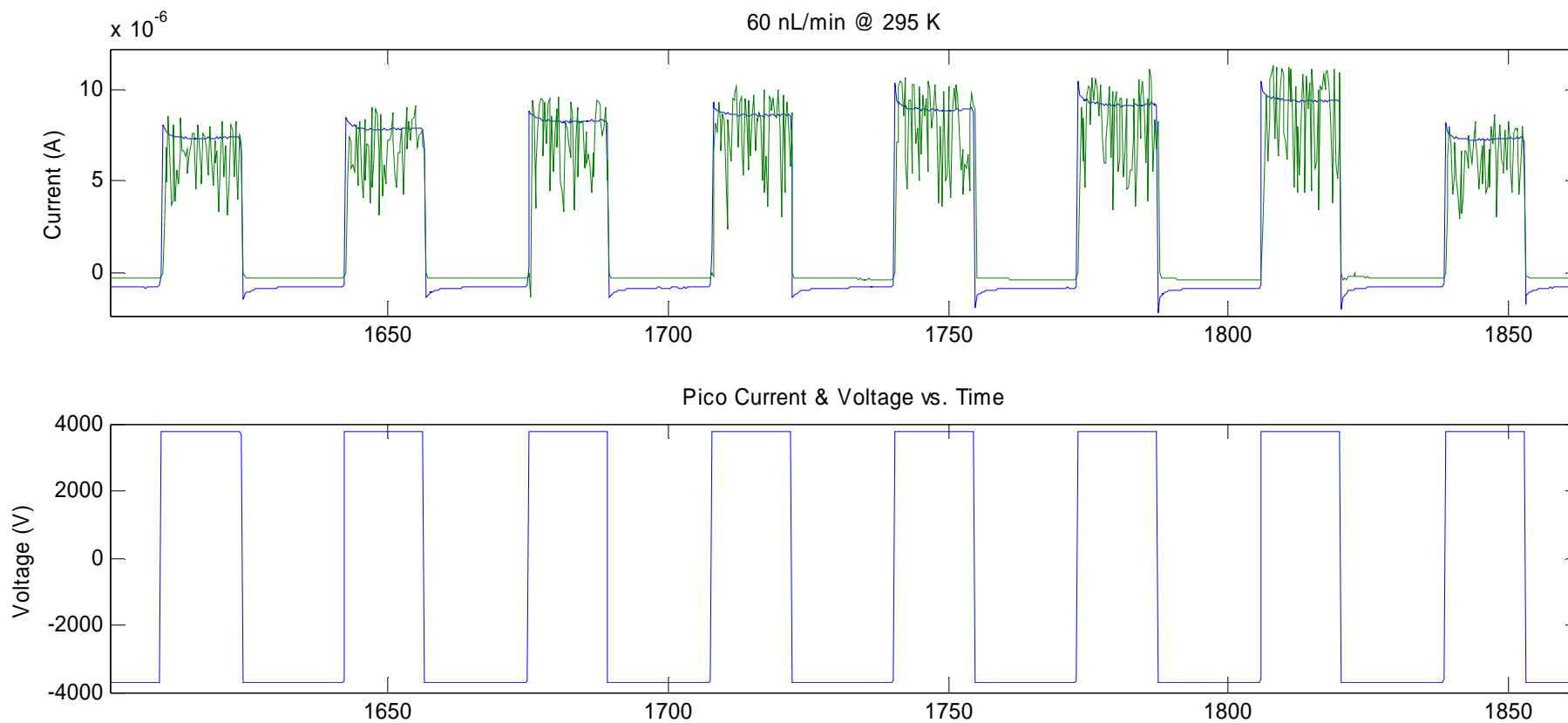
30 nL/min @ 49 °C



DISTRIBUTION A. Approved for public release; distribution unlimited.



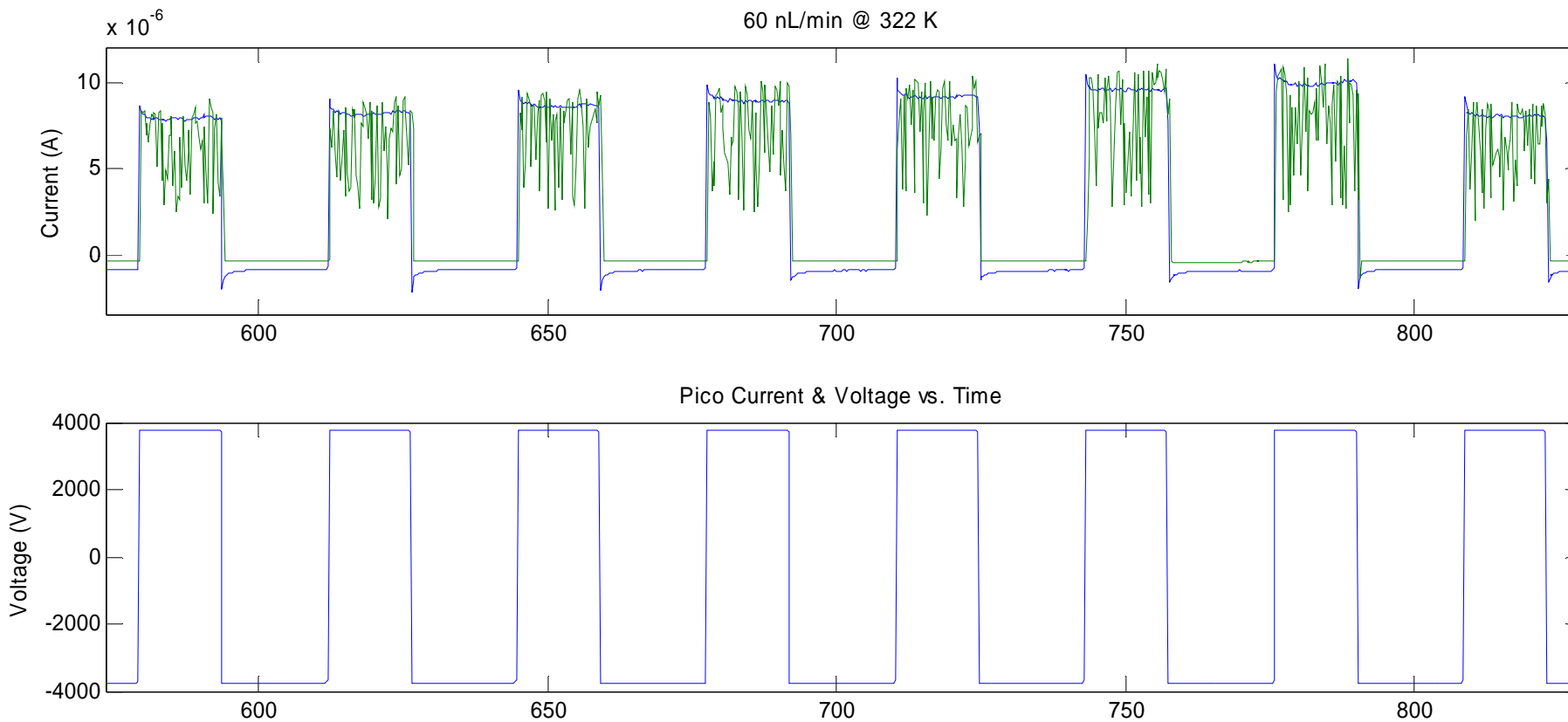
60 nL/min @ 22 °C



DISTRIBUTION A. Approved for public release; distribution unlimited.



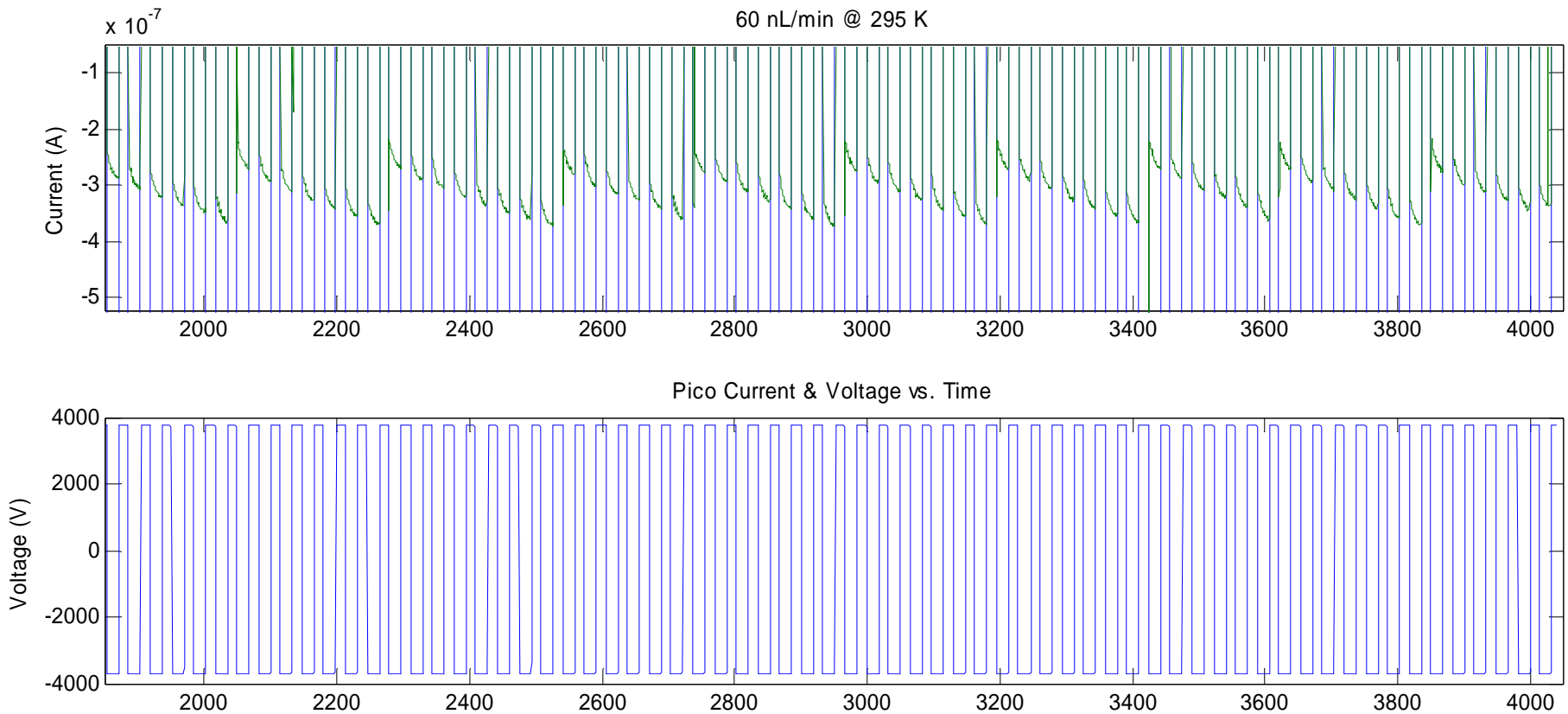
60 nL/min @ 49 °C



DISTRIBUTION A. Approved for public release; distribution unlimited.



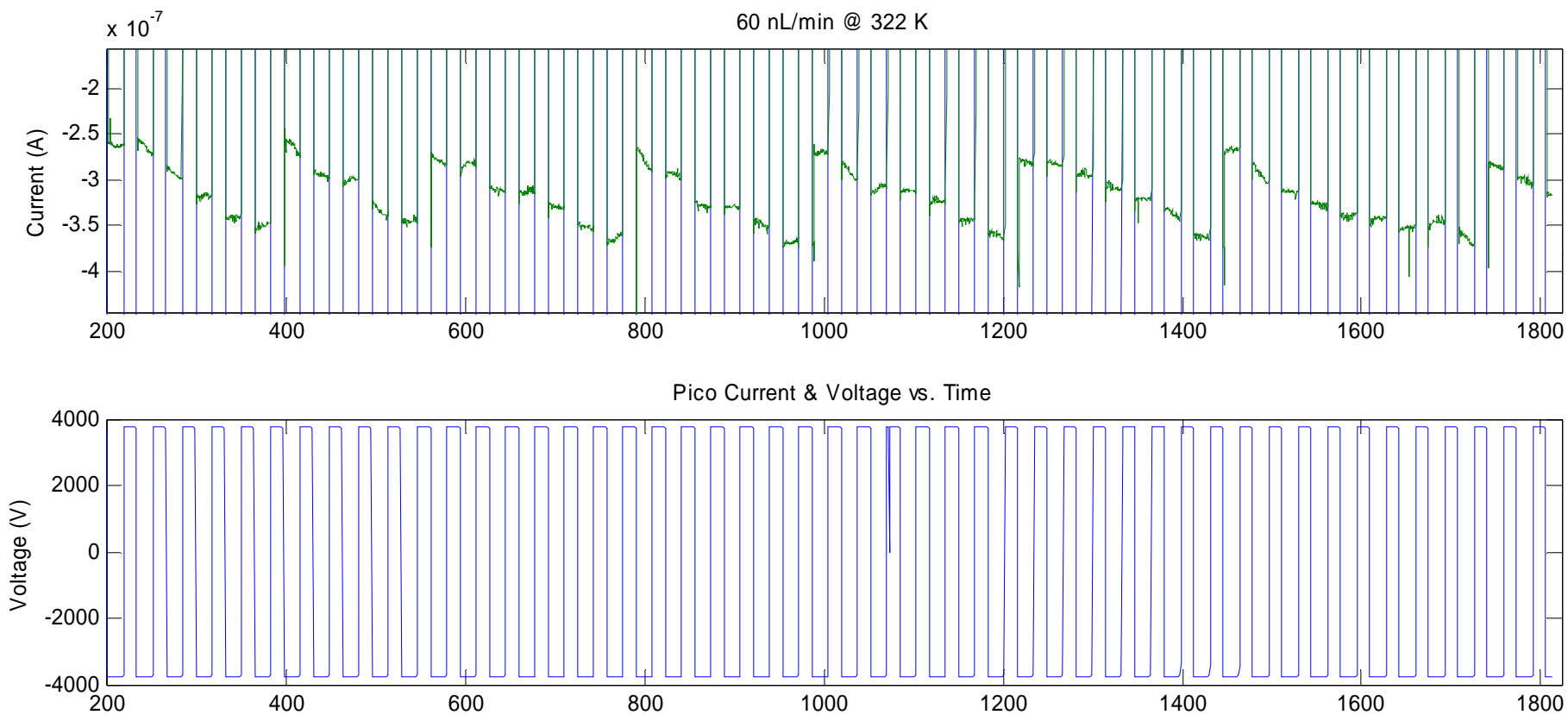
60 nL/min @ 22 °C



DISTRIBUTION A. Approved for public release; distribution unlimited.

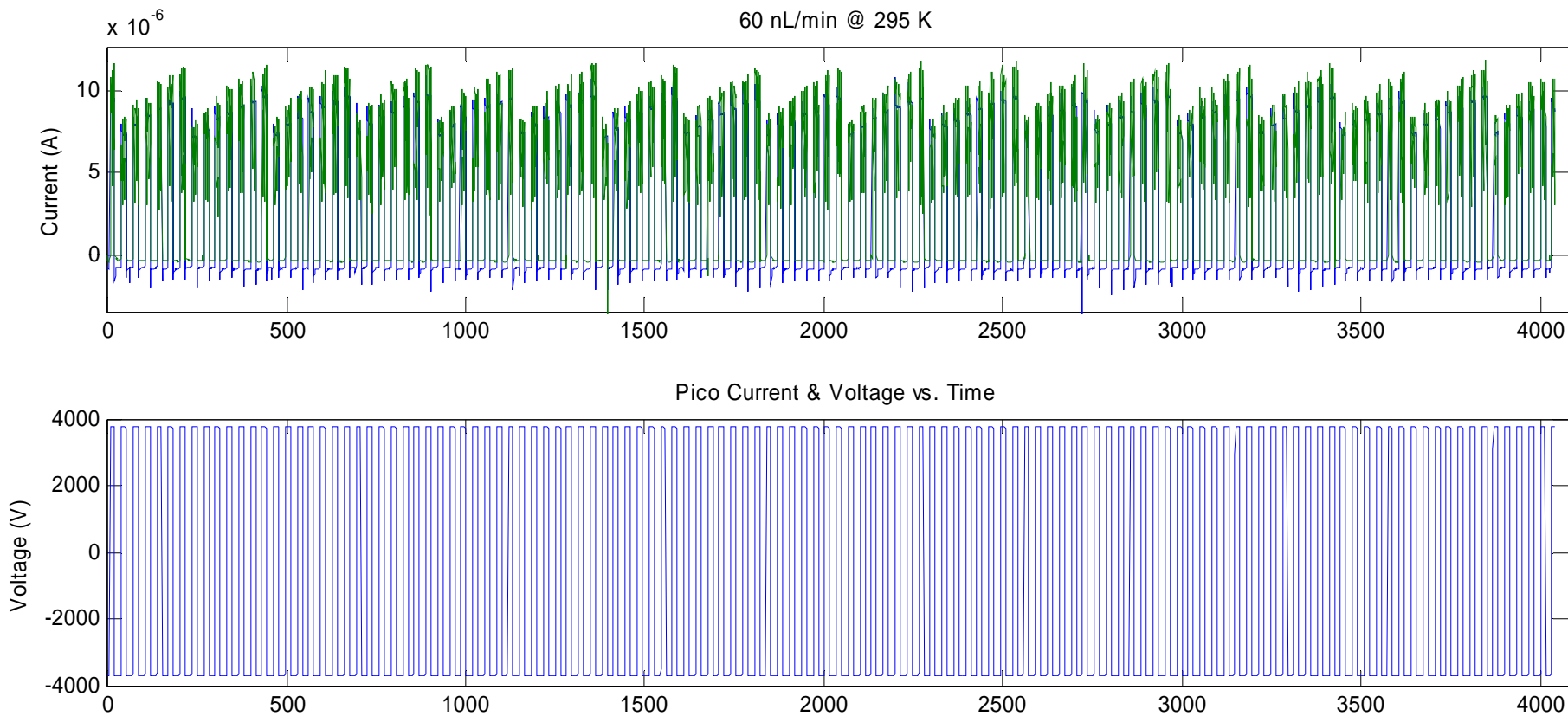


60 nL/min @ 49 °C





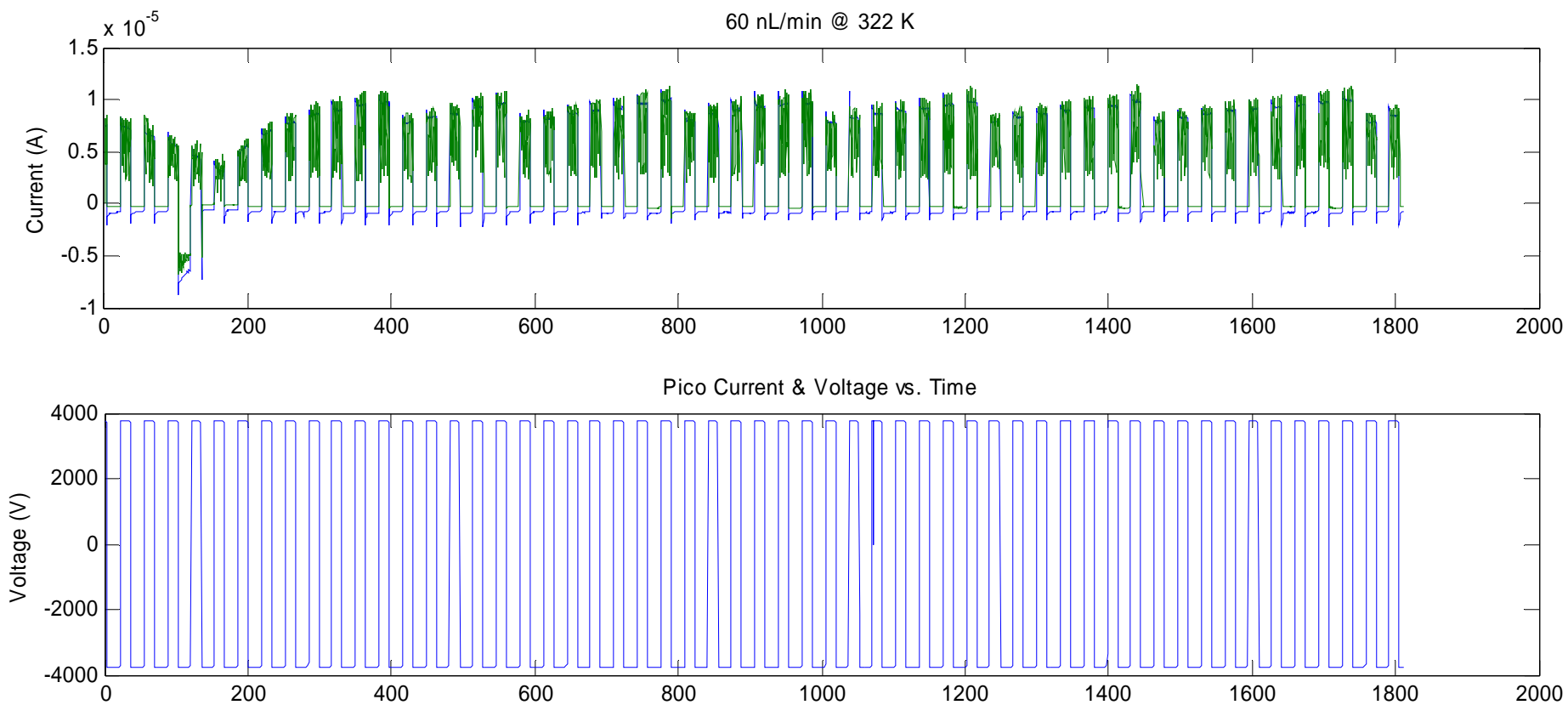
60 nL/min @ 22 °C



DISTRIBUTION A. Approved for public release; distribution unlimited.



60 nL/min @ 49 °C



DISTRIBUTION A. Approved for public release; distribution unlimited.

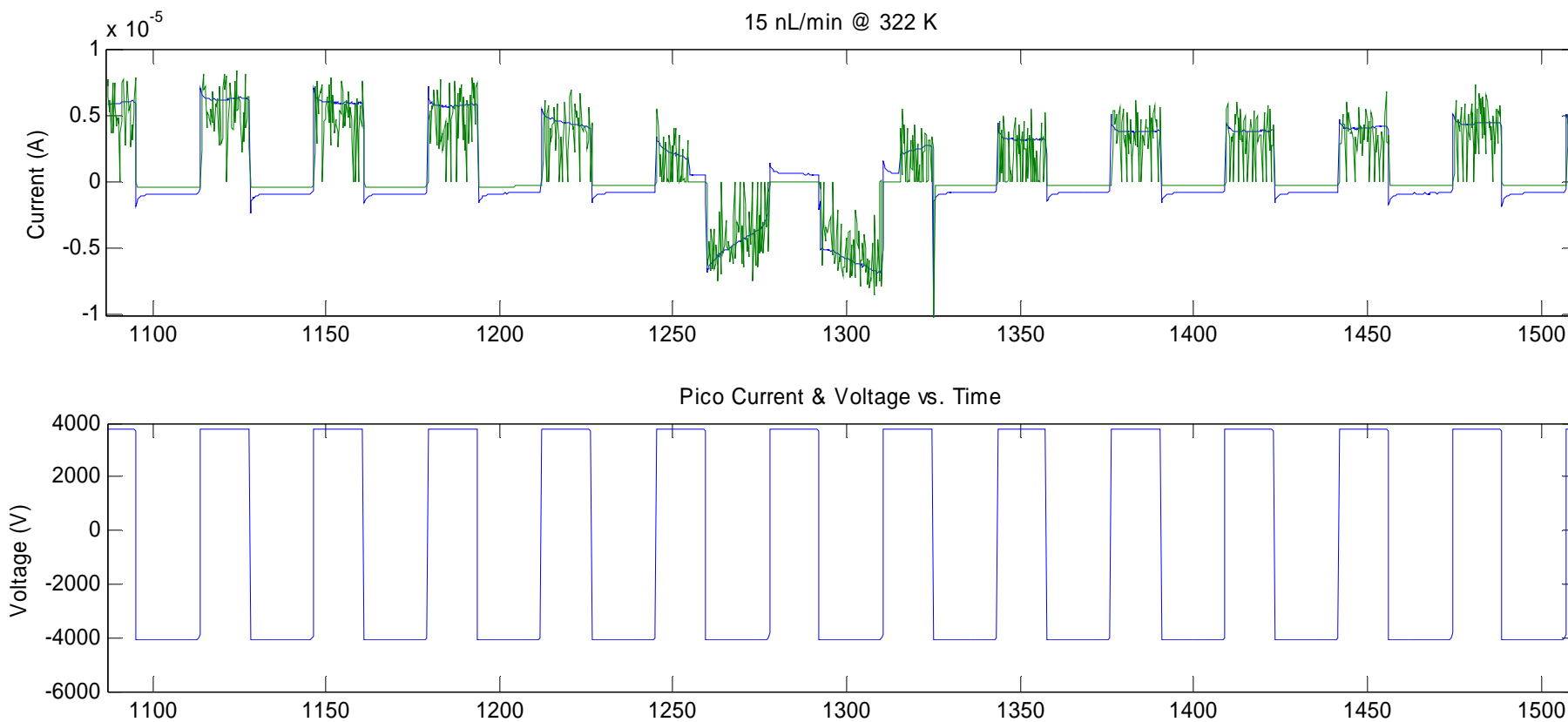


Observations

- Order of magnitude difference between positive and negative bias
- Electrospray droplets in negative bias
- Glow discharge
 - Positive bias, easily attained
 - Negative bias, HV or very low flow rate
- Order of magnitude difference between positive predictions and data
- Length of Taylor cone effects current

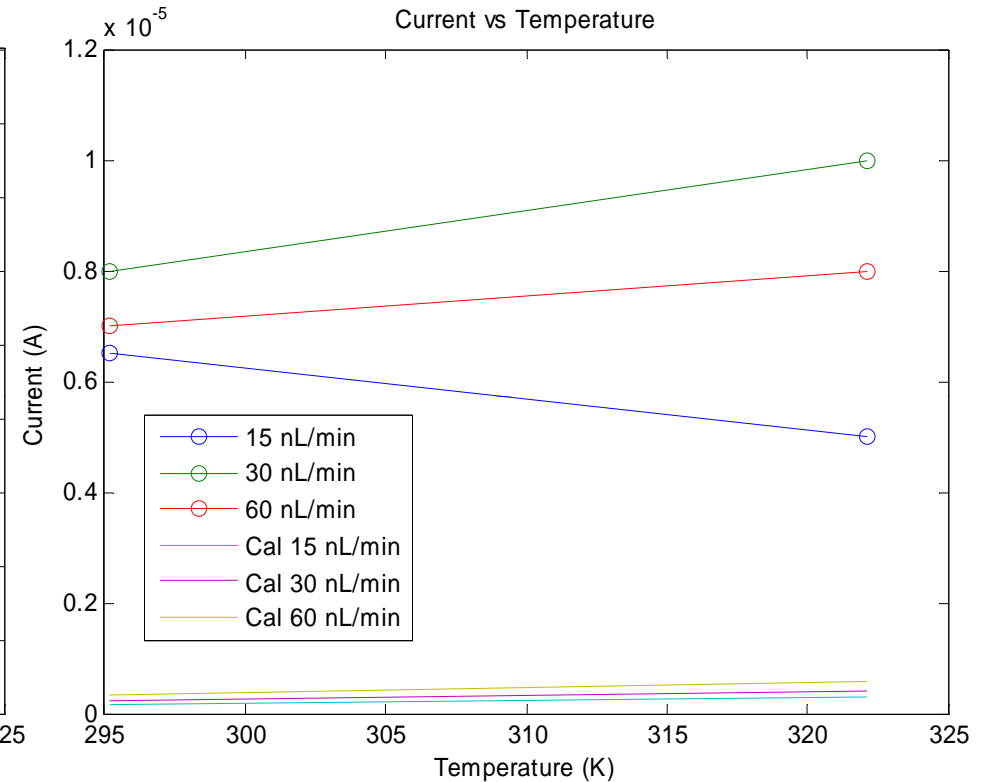
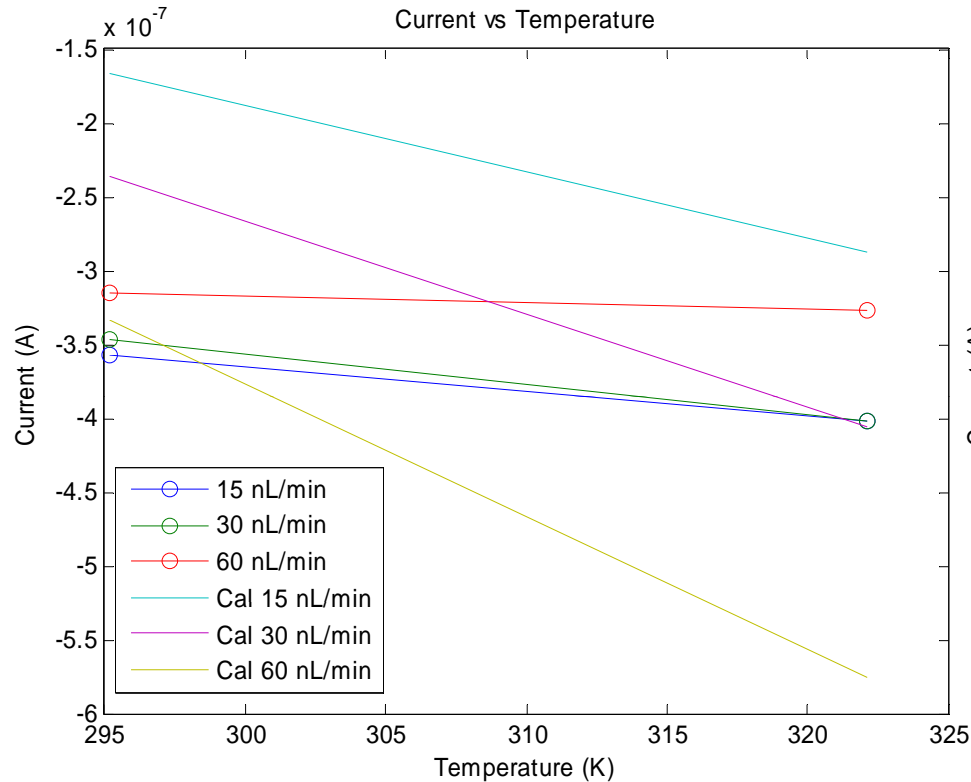


Lamp off





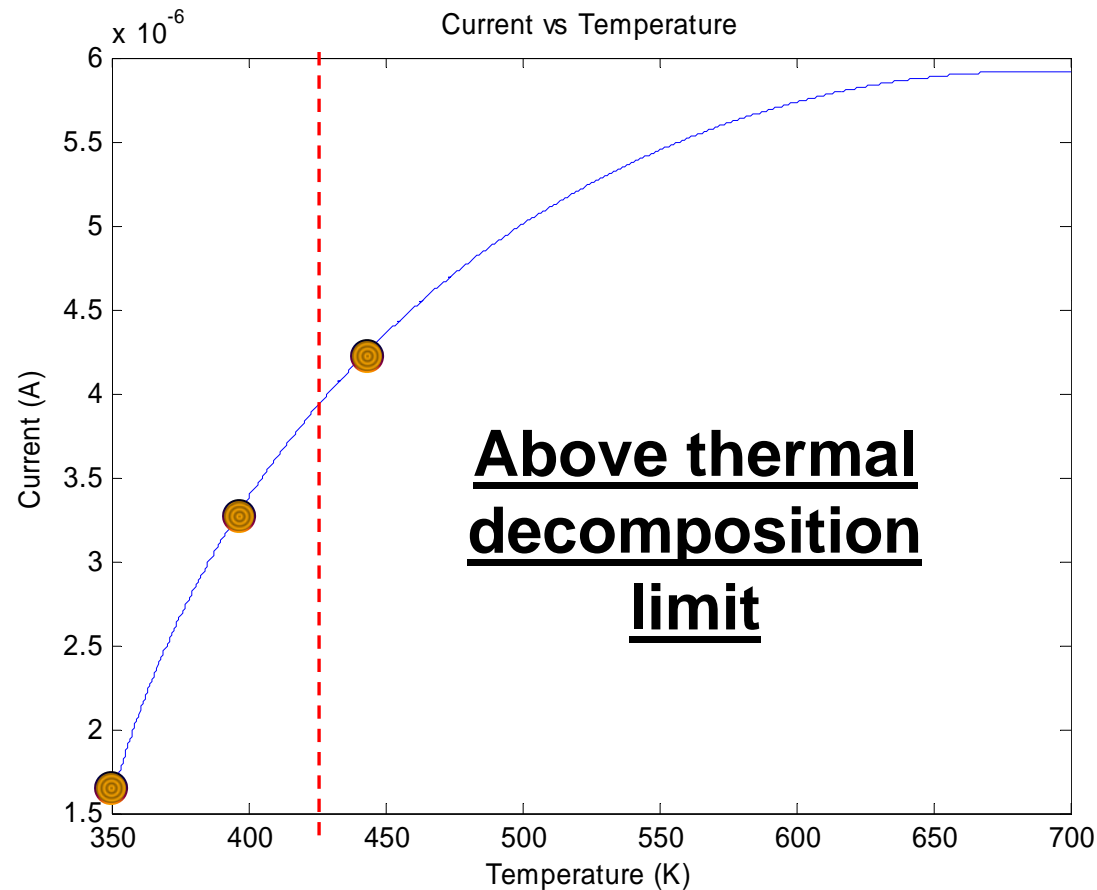
Current Comparison



15 nL/min (295 K)	Prediction	Actual	% increase
q/m (C/kg)	555.4336	23,2317.8	41,826.57
Isp (Calculated)	215	1392	647.5
T (Calculated)	6.3405 X 10 ⁻⁷	1.018 X 10 ⁻⁶	160.5



BMIM BF₄ Theoretical Limit





Thruster Design Considerations



- Geometric design of emitters
- Thermal conduction of emitters
- Mission requirements



Future Work

- Expand Temperature range
- Repeat tests under vacuum
- Implement faster sampling
- Better predictive tools encoded



Conclusions

- Stable electrospray cones achieved
- Showed current very sensitive to temperature
- Model did not match data
 - Future work to identify why
- Better predictions needed in model
- Showed unexpected ionic emission
 - This is good for improved performance
 - This is not what I predicted



Summary



- **Introduction to Electrospray Thrusters**
- **Model Development**
- **Code Results**
- **Experiment Setup**
- **Experiment Results**
- **Future work**
- **Conclusion**



Questions



???



References

- Taylor cone pictures:
- <http://www.dataweb.clrc.ac.uk/Activity/CCLRCAnnualReport0203;SECTION=4560;>
- http://www.flow3d.com/apps/micro/app_micro_elecphor.html, retrieved 16 Sep 08
- <http://www.gwu.edu/~vertes/News.html>, retrieved 16 Sep 08
- BmiBF4 properties: <http://ilthermo.boulder.nist.gov/ILThermo/pureprp.uix.do>, 20 Jan 11
- Cole, R. B. (2000). Some tenets pertaining to electrospray. *JOURNAL OF MASS SPECTROMETRY* , 763-772.
- James A. Nabity, G. M. (2006). *Studies of MEMS Colloid Thrusters*. Boulder, CO: American Institute of Aeronautics and Astronautics.
- Jijun Xiong, D. S. (2006). Investigation of the Onset Voltage for the Design of a. *IEEE/ASME TRANSACTIONS ON MECHATRONICS* , 66-74.
- Matthew S. Alexander, K. L. (September–October 2007). Voltage-Modulated Flow Rate for Precise Thrust Control. *JOURNAL OF PROPULSION AND POWER* , 1042-1048.
- Michael E. Van Valkenburg, R. L. (2003). Ionic Liquid Heat Transfer Fluids. *Fifteenth Symposium on Thermophysical Properties* .
- Mora, M. G.-C. (2000). Direct measurement of ion evaporation kinetics. *JOURNAL OF CHEMICAL PHYSICS* , 815-832.
- TRC/NIST/Boulder. (2006). *Ionic Liquids Database- IL Thermo*. Retrieved December 1, 2010, from Ionic Liquids Database:
- W.D. Luedtke, U. L.-H. (2008). Nanojets, Electrospray, and Ion Field Evaporation: Molecular Dynamics Simulations and Laboratory Experiments. *J. Phys. Chem.* , 9628-9648.